The Function of the Reflected Lamina in Therapsids and the Origin of the Mammalian Middle Ear

Savannah L. Olroyd

A dissertation

submitted in partial fulfillment of the

requirements for the degree of

Doctor of Philosophy

University of Washington

2022

Reading Committee:

Christian Sidor, Chair

Sharlene Santana

Gregory Wilson-Mantilla

Patricia Kramer

Program Authorized to Offer Degree:

Biology

University of Washington

Abstract

The Function of the Reflected Lamina in Therapsids
and the Origin of the Mammalian Middle Ear

Savannah L. Olroyd

Chair of the Supervisory Committee:
Christian Sidor
Department of Biology

The selective pressures that drove the remarkable transition of the postdentary and jaw hinge bones of non-mammalian synapsids into the mammalian middle ear are uncertain because the hearing capability of early synapsids is poorly understood. This work investigates the hypothesis that non-mammalian therapsids used their reflected lamina, a plate of bone on the mandible, for sound reception. A systematic survey of reflected lamina anatomy is conducted to assess evolutionary patterns across Therapsida, and a consistent arrangement of ridges and fossae on the angular surface is observed, suggesting a shared ancestral pattern for therapsids. The pterygoid of chameleons is chosen as a modern analogue for a sound-receptive therapsid reflected lamina, and the distribution of pterygoid-based hearing across Chamaeleonidae is assessed via dissections. Finally, the allometry of the pterygoid in chameleons is examined, as the scaling of a sound receptor is likely important for its function. Chameleons with a pterygoid ear show signs of stabilizing selection around a specific allometric coefficient compared to chameleons without this ear. Similarly constricted allometry is also found in the reflected

lamina of therocephalian and basal anomodont therapsids, suggesting that selective pressures consistent with sound reception were present long before the origin of the mammalian ear.

The Function of the Reflected Lamina in Therapsids and the Origin of the Mammalian Middle Ear

Savannah L. Olroyd

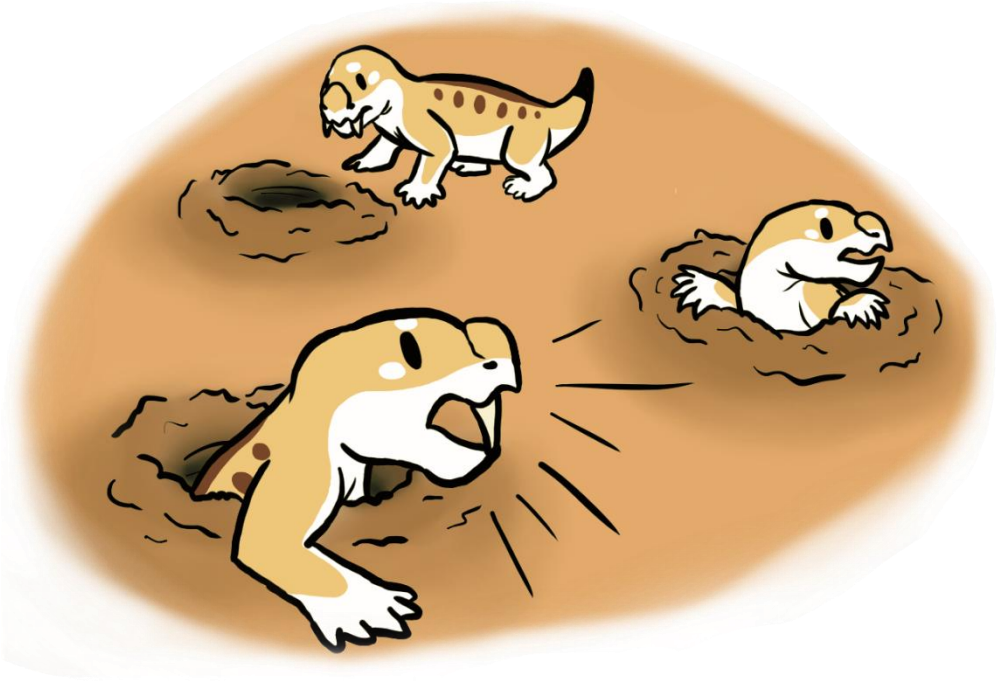

This work is dedicated to my rabbits Dilly and Ender, whose magnificent ears have been a surprising source of inspiration.

Table of Contents

INSTITUTIONAL ABBREVIATIONS

AMNH, American Museum of Natural History, New York, U.S.A.; **BP**, Evolutionary Studies Institute, Johannesburg, South Africa; **CGP**, Council for Geosciences, Pretoria, South Africa; **CM**, Carnegie Museum of Natural History, Pittsburgh, PA, U.S.A; **FMNH**, Field Museum of Natural History, Chicago, U.S.A.; **LACM**, Natural History Museum of Los Angeles County, Los Angeles, CA, U.S.A.; **MB.R.**, Museum für Naturkunde, Fossil Reptile Collection, Berlin, Germany; **MCZ**, Museum of Comparative Zoology, Harvard University; **ML**, Museu da Lourinhã, Lourinhã, Portugal; **NHCC**, National Heritage Conservation Commission, Lusaka, Zambia; **NMQR**, National Museum, Bloemfontein, South Africa; **PIN**, Paleontological Institute of the Russian Academy of Sciences, Moscow; **SAM**, Iziko Museums of South Africa, Cape Town, South Africa; **TM**, Ditsong Museum of Natural History, Pretoria, South Africa; **UCMP**, University of California Berkeley Museum of Paleontology, Berkeley, U.S.A.; **UCMVZ**, University of California Berkeley Museum of Vertebrate Zoology, Berkeley, CA, U.S.A.; **UF**, Florida Museum of Natural History, Gainesville, FL, U.S.A.; **UWBM**, University of Washington Burke Museum of Natural and Cultural History, Seattle, WA, U.S.A.; **VTPE**, Virginia Polytechnic Institute and State University, Blacksburg, VA, U.S.A.; **YPM**, Yale Peabody Museum, New Haven, CT, U.S.A.

1. Introduction

1.1 BACKGROUND

Sensory systems are remarkably complex and often finely tuned to their specific function. The study of sensory evolution offers a unique glimpse at how highly specialized features originate. The vertebrate ear is an especially interesting case of sensory evolution because, despite its complexity, it is incredibly labile evolutionarily. Methods of sound reception vary widely across vertebrates (Fay and Popper, 1974; Wever, 1978; Boistel et al., 2013; Capshaw and Soares, 2016; Ladich and Schulz-Mirbach, 2016), clades independently converge on similar sound conduction pathways (Clack, 1993; Martin and Luo, 2005), and the loss of specialized hearing structures occurs frequently (Toerien, 1963; Hetherington, 1992). The complicated evolutionary history of the vertebrate ear makes it a rich study system for understanding co-option and the origin of complex features. Additionally, the ear relies on several bony components, so its evolution can be traced through the fossil record.

The best-documented case of vertebrate ear evolution in the fossil record is that of early mammals and their non-mammalian synapsid relatives. The synapsid fossil record illustrates a myriad of changes that gradually led to the assembly of a characteristic mammalian body plan from a superficially reptile-like ancestor (Kemp, 1982; Sidor and Hopson, 1998; Lautenschlager et al., 2017; Jones et al., 2018). One unique mammalian trait captured in the synapsid fossil record is the arrangement of the mandible and middle ear bones (Allin and Hopson, 1992). Extant mammals are unique in having a mandible made up of a single bone, the dentary. Their middle ear, on the other hand, is made up of three ossicles, while most tetrapods have only one middle ear bone. The earliest synapsids had a mandible made up of multiple bones, and the synapsid fossil record documents the shrinking of the postdentary bones until they were eventually displaced from the mandible and incorporated into the middle ear, along with the quadrate and stapes.

The leading hypothesis for why these bizarre changes occurred is that the postdentary bones of early synapsids were used for rudimentary sound reception, which would have been transferred to the quadrate, stapes, and finally the inner ear (Tumarkin, 1968; Allin, 1975; Allin and Hopson, 1992). Under this hypothesis, the earliest synapsids, a paraphyletic grade referred to as "pelycosaurs" (Figure 1.1), may have sensed substrate-borne vibrations via their mandible, jaw hinge, and stapes. In the most crownward group of "pelycosaurs", the early sphenacodontians, a part of the angular bone separated laterally from the body of the angular to form a small reflected lamina with a cleft medial to it. The angular cleft then expanded anteriorly in therapsids, a subclade of Sphenacodontia that includes mammals, to produce an expanded reflected lamina. This plate of bone was extremely thin in some taxa, and the surface bore a pattern of ridges and fossae in the majority of non-mammalian therapsids. A widely accepted idea is that the reflected lamina acted as a sound receiver in early therapsids, vibrating over an air-filled angular cleft in response to substrate- or airborne sound. The reflected lamina is homologous with the ectotympanic bone of extant mammals, so an early role in sound reception would explain the eventual association between this structure and the tympanic membrane. However, there is also the possibility that the changes in the synapsid mandible were driven exclusively by selection pressure for a larger dentary to withstand higher bite forces, and the reduction of the postdentary bones was simply a side-effect of that. Distinguishing between these hypotheses relies on assessment of the proposed hearing function for the postdentary bones of non-mammalian synapsids.

A few studies have attempted to characterize the capability of the synapsid postdentary bones in serving some hearing function. Several authors have voiced that these bones would be too bulky to transfer detectable vibrations to the inner ear in response to airborne sound (King, 1981). However, mechanical modeling and simple calculations have indicated that the postdentary bones, quadrate, and stapes could have received and transmitted low frequency vibrations (Hotton, 1959; Kemp, 2007; Laaß, 2016), although it is generally understood that

they would do so poorly, and these studies give no indication that the amplitude of such vibrations would be detectable to the inner ear. Several authors have compared the area ratio between the reflected lamina (and/or a hypothetical tympanic membrane associated with it) and the stapes footplate to demonstrate that a mandibular therapsid ear would have been capable of impedance matching, the amplification of airborne sound to elicit detectable vibrations in the fluid of the inner ear (Kermack et al., 1981; Kermack and Mussett, 1983; Kemp, 2007; Laaß, 2016). Many therapsids exhibit a general trend towards the reduction of the postdentary bones, which is consistent with selection for lighter bones that may vibrate more efficiently (Sidor, 2003). CT data has revealed that the orientation of the stapes differs between therapsids with reconstructed terrestrial and subterranean lifestyles, suggesting specializations for sound transfer related to life habit (Laaß, 2015, 2016). Several therapsids also have a cochlear recess, which could indicate a heightened sense of hearing in these species (Castanhinha et al., 2013; Laaß, 2016; Benoit et al., 2017). Overall, there is evidence that the reflected lamina could have been used as a sound receptor in non-mammalian therapsids.

Much of the existing research focuses on cynodonts, and the diversity in hearing function in non-cynodont therapsids has only recently been investigated in detail, so the early evolution of this hypothesized mandibular ear is still poorly understood. Additionally, these studies are almost exclusively concerned with whether the reflected lamina could function as a sound receiver, not whether it was indeed used in this way. Finally, a feature that has been almost entirely overlooked in discussions of the hearing function of the reflected lamina is the complex series of ridges and fossae present on its surface. The present work employs a multi-faceted approach to understanding the evolution of bony sound reception structures in general and an evaluation of the hypothesized hearing function of the reflected lamina in non-mammalian synapsids.

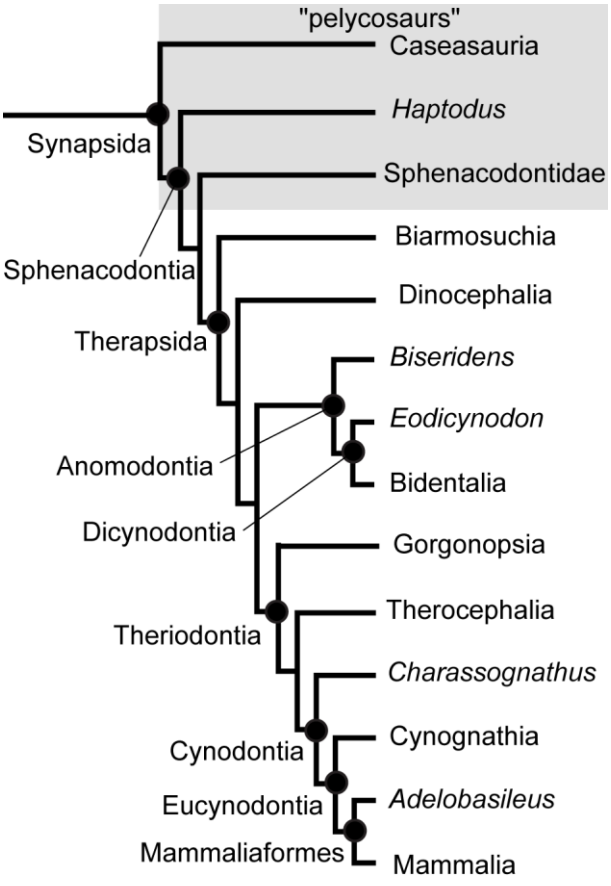

FIGURE 1.1. Cladogram with relevant synapsid groups. Topology from Rubidge and Sidor (2001) and Abdala (2021).

1.2 SYNAPSID PHYLOGENY

Early synapsids constitute a paraphyletic grade referred to as “pelycosaurs” (Fig. 1.1). The reflected lamina of the angular first appeared in the Sphenacodontia, which includes therapsids, sphenacodontids, and “haptodonts”. In the earliest sphenacodonts, the small reflected lamina is inferred to have aided in the attachment of jaw adductor muscles. In therapsids, the reflected lamina became further separated from the body of the angular, and the lateral face of the angular was ornamented by a characteristic pattern of ridges and fossae. The relationships between the major therapsid subclades are supported by relatively few characters (Rowe, 1988; Rubidge and Sidor, 2001; Sidor and Rubidge, 2006; Kemp, 2009), but it is generally considered that gorgonopsians, therocephalians, and cynodonts form a monophyletic group termed Theriodontia. Dramatic changes in jaw morphology occurred within Cynodontia. The postdentary series, including the reflected lamina, became notably smaller, and in the derived eucynodonts the reflected lamina was reduced to a delicate hook of bone. The dentary-squamosal jaw joint first appeared in Mammaliaformes, and it coexisted with the primitive quadrate-articular jaw joint until the postdentary bones detached from the dentary, which occurred independently multiple times within crown Mammalia (Martin and Luo, 2005).

1.3 DISSERTATION OVERVIEW

The first chapter is a comparison of reflected lamina surface features and angular cleft morphology across Synapsida. A detailed, systematic survey of reflected lamina topology has never been undertaken, which hinders research on the evolution of the angular complex. A large sample of fossils from each major therapsid clade was examined, and specimens were surface scanned for visualization of the topology. Existing CT data was also used to map the extent of the angular cleft in most therapsid clades. The results of this survey facilitate inferences about the function of the angular complex in synapsids.

The second chapter describes a modern analogue for the hypothesized reflected lamina sound receiver: the pterygoid plate in chameleons. Chameleons lack a tympanum, but some species have co-opted their expanded pterygoid for hearing by connecting it to the columella via a process of the extracolumella (Wever, 1968, 1978). The distribution of this feature within Chamaeleonidae is unknown, so dissections were performed on a variety of species to reconstruct the evolutionary history of this trait. Enhanced contrast CT scans were also done to explore the tissues surrounding the middle ear cavity in these chameleons.

The third chapter involves the development of a proxy for hearing use in the chameleon study system and the application of that proxy to the synapsid fossil record. The proxy that was investigated was allometry of a sound reception structure with head size, as the size of an object influences the frequency and amplitude at which it vibrates. Allometry of the pterygoid plate was compared between chameleon species that use this structure as a sound receptor and those that do not. Allometry of the reflected lamina was then compared between synapsid clades.

2. Reflections on the Reflected Lamina of the Angular in Nonmammalian Synapsids: Nomenclature, Comparative Anatomy, and Evolution

2.1 ABSTRACT

The reflected lamina of the angular has long been portrayed as a key component in understanding the evolution of the mammalian mandible and middle ear, yet the function of this structure in non-mammalian therapsids remains uncertain. We undertake a broad scale survey of two aspects of the reflected lamina that have been poorly characterized: the ridges and fossae on its lateral surface and the extent of the underlying angular cleft. These two features were visualized in a wide range of therapsids using CT data from the literature and blue light surface scanning. Most species exhibit a clade-specific pattern of surface topography, although dicynodonts are highly variable. A striking similarity in the general number and orientation of fossae and ridges is seen between the otherwise disparate therapsid clades, and we propose homologies in these surface features across Therapsida. These features may serve as useful phylogenetic characters in analyses of the relationships between the major therapsid clades. The angular cleft does not underlie all of what is often referred to as the 'reflected lamina' in the literature, and an updated definition of this term is provided. Several therapsid groups independently expanded the angular cleft to further separate the reflected lamina from the angular body. We discuss some functional consequences of our findings and note inconsistency between proposed clade-specific muscle attachment sites and the presence of homologous fossae and ridges across much of Therapsida.

2.2 INTRODUCTION

Some of the most dramatic morphological changes that occurred during the evolution of non-mammalian synapsids were the transformations of the mandible: the coronoid eminence heightened into a tall coronoid process, the quadrate-articular jaw joint was replaced by a dentary-squamosal joint, muscle insertions on the postdentary bones shifted onto the dentary, and the postdentary bones completely separated from the dentary to become incorporated into the mammalian middle ear (Crompton, 1963; Barghusen, 1968; Kermack et al., 1973; Meng et al., 2018). These changes allowed synapsids to process food more efficiently, which was crucial to support the high-energy lifestyle that eventually became a hallmark feature of mammals (Crompton and Parker, 1978; Farmer, 2000; Kemp, 2007; Hopson, 2012). Because of its importance in understanding the assembly of the mammalian body plan, and therefore major evolutionary transitions and the origin of higher taxa, the functional morphology of the synapsid mandible has received detailed attention for over a century (Watson, 1912; Adams, 1919; Crompton, 1963, 1972; DeMar and Barghusen, 1972; Kermack et al., 1973; Bramble, 1978; King et al., 1989; Lautenschlager et al., 2017). Despite this extensive research, the function of the reflected lamina of the angular in the mandible of non-mammalian therapsids remains a glaring paleobiological mystery.

The reflected lamina of the angular is a plate of bone separated medially from the body of the angular by a thin space called the angular cleft. This structure is found in sphenacodontids and therapsids, and the fossil record clearly documents its homology with the ectotympanic bone of mammals (Palmer, 1913). In most non-eucynodont therapsids, the surface of the reflected lamina features a radiating pattern of ridges and fossae. Despite its distinctiveness and potential importance for the study of the mammalian feeding system and middle ear, the function of the reflected lamina, including its surface topography and associated angular cleft, has never been decisively determined.

Several functions have been proposed for this suite of structures. Some have suggested that the angular cleft may have housed a gland (Broom, 1932; Watson, 1953), but glands rarely occupy bony recesses and likely would not require a dedicated space in which to reside (Janensch, 1952; Allin, 1975). Several authors have placed an insertion for the pterygoideus (Romer and Price, 1940; Watson, 1953; Barghusen, 1968) or pseudotemporalis (Westoll, 1943) muscles within the angular cleft, supposing that these muscles wrapped around the ventral edge of the mandible to reach insertion points on the ventrolateral surface of the angular body, as in the pterygoideus of extant reptiles. Others have placed attachments for various jaw adductor or throat muscles in the fossae on the lateral face of the reflected lamina (Janensch, 1952; Barghusen, 1968; Kemp, 1969, 1982; King, 1981). The alternating ridges and fossae have also been proposed to strengthen the reflected lamina against muscle strain (Parrington, 1955). The angular cleft could represent an air-filled diverticulum of the pharynx that may have been used as a resonating chamber for vocalization (Westoll, 1943). A widely accepted idea is that the reflected lamina of non-mammalian therapsids had some role in a rudimentary airborne- or substrate-borne sound reception system involving the postdentary bones, quadrate, and stapes (Allin, 1975; Allin and Hopson, 1992; Laaß, 2016). If the reflected lamina was indeed involved in sound reception in early therapsids, then the evolution of the mammalian middle ear was likely the consequence of sustained selection for improved hearing ability rather than simply a side effect of the appearance of the dentary-squamosal joint (Allin, 1975; Crompton and Parker, 1978). Assessing function in the fossil record is notoriously difficult and, unfortunately, there is little direct evidence supportive of one hypothesis for the function of the angular complex in non-mammalian therapsids. In sum, it is premature to assume the validity of any of these proposed functions.

It is difficult to assess the competing hypotheses for the function of the reflected lamina because potentially important systematic variation in this structure remains poorly documented. The external topography of the angular is rarely described in detail in the literature, and there

are likely several reasons for this. First, because the reflected lamina is extremely fragile, with sub-millimeter thickness in many specimens, it is often absent or heavily damaged, especially in historic specimens that have not benefitted from modern preparation techniques. The rarity of specimens with a relatively complete, undeformed reflected lamina hinders comparative descriptions of the structure. A second potential reason for the lack of detail in descriptions of the reflected lamina is that its surface topography is highly stereotyped within some clades, meaning that researchers rarely feel the need to do more than affirm that a newly described fossil conforms to the expected morphology of its clade. Descriptions of these stereotyped arrangements have been made for a few clades, which we review below, but comparisons between clades have not been made because the patterns of ridges and fossae in each clade are often so complex and different that it is difficult to recognize homologous features that could be reasonably compared. Solving these problems requires surveying a large number of specimens and making comparisons across a wide taxonomic sample, which has not been undertaken across all of non-mammalian Synapsida.

The angular cleft is also rarely described in detail, as it is largely obscured by the reflected lamina laterally. Intricate fossil preparation can occasionally reveal the morphology of the angular cleft, but in many cases the cleft is deep and thin enough that it can only be visualized by serial sectioning or computed tomographic (CT) scanning. Serial sections have occasionally been used to describe the angular cleft, but this method is limited in the amount of detail that can be reasonably obtained for a sectioned structure (Maier and van den Heever, 2002). As a result, it is unclear how much of what has been called the ‘reflected lamina’ in the literature is actually separated from the angular body. Further, substantive comparisons of angular cleft morphology have not been made between therapsid clades, which further hinders our understanding of how this feature evolved and its potential function.

Here we describe in detail the surface features on the angular across non-mammalian synapsids and make comparisons between the major therapsid clades in order to identify

potential homologies. Such homologies provide a framework to examine the evolution of the reflected lamina. The features we identify may also prove useful in future phylogenetic analyses of therapsids, which historically have suffered from a dearth of characters that can be applied across the highly distinct clades (Sidor and Hopson, 1998; Rubidge and Sidor, 2001; Kemp, 2009). We propose a set of anatomical terms to help identify homologous features on the reflected lamina, which should facilitate informative descriptions of angular topography in the future. We use CT data to map the extent of the angular cleft in several therapsids to clarify how much of what has been called the 'reflected lamina' is indeed physically separated from the body of the angular. Finally, we discuss some implications of our findings for hypothesized functions of the angular complex.

2.3 MATERIALS AND METHODS

2.3.1 Digitization Methods

Specimens across all major synapsid clades were surface scanned using an Artec Space Spider blue light scanner with a voxel size of 0.3 mm. Detailed sketches were also made for each specimen, including notes on the relevant morphology and the position of cracks, glue, matrix, etc. on the fossil. These extraneous objects were digitally removed using the smoothing functions in Meshmixer V3.5.474 (©Autodesk, San Rafael, CA, U.S.A) to produce clean meshes of the mandible. The scans were also retrodeformed using Landmark Editor V3.0 (©IDAV) to minimize the effects of diagenetic deformation on the orientation and position of relevant surface features.

The extent of the angular cleft was determined by segmenting CT scans of therapsid mandibles. Surface scans of specimens in which the angular cleft was fully prepared out were also used for this purpose. The CT data was previously published and made available by the authors of their respective studies (Castanhinha et al., 2013; Benoit et al., 2017; Bendel et al.,

2018a; Pusch et al., 2019a; Huttenlocker and Sidor, 2020). The raw CT image stacks for *Cynariops* and *Lycosuchus* were downloaded from the Data Repository of the Museum für Naturkunde Berlin (Bendel et al., 2018b; Pusch et al., 2019b), and the raw image stack for *Probainognathus* was downloaded from DigiMorph.org. The part of the angular cleft that lies between the reflected lamina and the body of the angular was segmented in the CT scans using Avizo V9.2.0 (© FEI VSG, Hillsboro OR, USA), as this portion was the easiest to delineate using surrounding anatomical structures and is the most relevant to visualizing the extent of the reflected lamina. For the surface scans, a mesh of this part of the angular cleft was built manually using the "draw" sculpting tool in Meshmixer to fill in the space between the reflected lamina and medial lamina.

2.3.2 Specimens Examined

A total of 56 fossil synapsid genera were digitized for this study, spanning a wide phylogenetic and temporal range: three pelycosaur-grade genera, four biarmosuchians, six dinocephalians, 23 anomodonts, eight gorgonopsians, 14 therocephalians, and five non-mammalian cynodonts. Specimens that were figured or mentioned directly in the text are listed in Table 2.1. Additional specimens supporting the distribution of surface features described here are listed in Appendix 1.

2.4 DESCRIPTION

2.4.1 Anatomical Terms

We follow Allin's (1975) detailed terminology of the angular complex and propose a series of new terms to describe the fossae on its external surface (Figure 2.1A). The angular keel is a thin projection of bone extending ventral to the margin of the lower jaw. Posterodorsally, the keel is continuous with a sheet of bone that is mediolaterally separated from the body of the

angular. This sheet of bone is the reflected lamina, and the portion of the angular body that lies directly medial to it to is termed the medial lamina. At its dorsalmost contact with the angular body, the reflected lamina generally curves slightly posteriorly or dorsally, forming a dorsal notch. Posterior to the angular body is a curved rim of bone formed by the surangular and articular. The space between this rim and the posterior edge of the reflected lamina is called the angular gap, and the wide, gentle concavity on the angular body in this area is the external fossa of the angular. The angular gap and the space between the reflected and medial laminae make

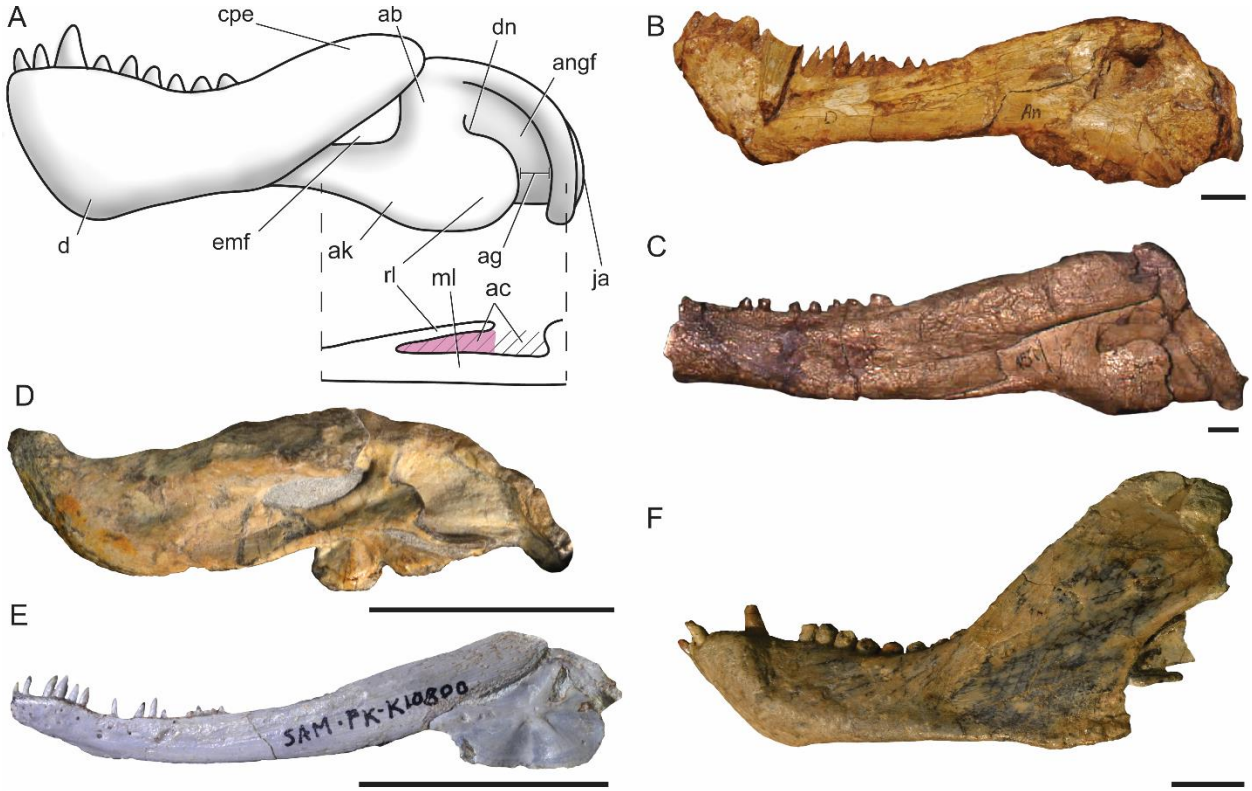

FIGURE 2.1. Photographs and line drawings illustrating therapsid mandible anatomy. **A)** Line drawing of a generalized therapsid jaw illustrating terminology of the angular complex and other relevant structures (anterior is to the left) with horizontal section taken between dotted lines; **B)** photo of Biarmosuchus tener (PIN 1758/2); **C)** photo of Syodon biarmicum (PIN 157/2); **D)** photo of Emydops arctatus (BP/1/1307, mirrored); **E)** photo of Tetracynodon darti (SAM-PK-K10800); **F)** photo of Trirachodon berryi (BP/1/4658). Scale bars 1 cm. **Abbreviations**: **ab** = body of the angular; **ac =** angular cleft; **ag** = angular gap; **ak** = angular keel; **cpe**, =coronoid process/eminence; **d** = dentary; **dn** = dorsal notch; **emf** = external mandibular fenestra; **ja** = jaw articulation surface; **ml** = medial lamina of the angular; **rl** = reflected lamina of the angular.

up the angular cleft, although our description focuses mainly on the latter portion (Fig. 2.1A), as its bony medial and lateral boundaries provide ready landmarks during segmentation of the CT scans. Some therapsids also have an oval or triangular space between the dentary and the body of the angular called the external mandibular fenestra (Fig. 2.1).

2.4.2 Systematic Review

Pelycosaur-grade synapsids— The lateral surface of the angular lacks ridges and fossae in all non-therapsid synapsids (Fig. 2.2). Moreover, in the earliest-diverging forms (e.g., caseasaurs, varanopids, ophiacodontids) the ventral surface of the angular is broadly rounded (Reisz, 1986). A subtle angular keel is first seen in edaphosaurids, and in later-diverging "haptodonts", the posterior edge of the keel becomes mediolaterally separated from the angular body, resulting in a reflected lamina of the angular that is separated from the body of the angular by a small angular cleft. The relationship of "haptodonts" to other synapsids is unclear (Spindler, 2016; Angielczyk and Kammerer, 2018), but they are likely basal sphenacodontians (Huttenlocker et al., 2021). The reflected lamina of the angular

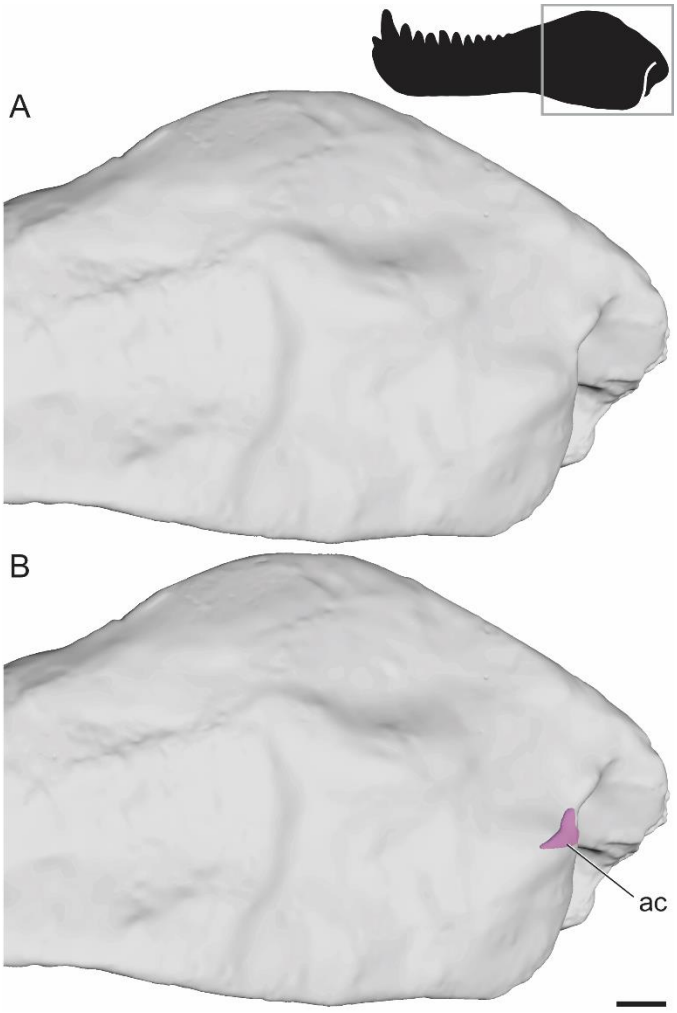

FIGURE 2.2. Surface scan of the angular region in the sphenacodontid *Dimetrodon limbatus* (FMNH UC 1001) in lateral view. **A)** model showing surface features; **B)** model from A with angular cleft overlay. Box on silhouette illustrates location of images. Scale bar 1 cm.

Abbreviations: **ac** = angular cleft.

is present in all members of Sphenacodontidae, the sister group of Therapsida (Reisz et al., 1992; Sidor and Hopson, 1998). In sphenacodontids, the angular keel is separated from the body of the angular only at its most posterior edge, and this emargination does not extend very far dorsally from the ventral margin of the jaw, so the effective reflected lamina is relatively small (Fig. 2.2B). It should be noted that Figure 2.2 is based on a surface scan in which matrix in the angular cleft was fully prepared out, so the angular cleft may be underestimated in this figure. Still, the space is distinctly smaller than that seen in therapsids. The anterodorsal edge of the cleft forms a straight line extending anteroventrally to the ventral margin of the jaw. The posterior edge of the reflected lamina curves anterodorsally where it meets the angular body, forming a slight dorsal notch (Fig. 2.2).

Biarmosuchia—The mandible is poorly known in biarmosuchians because these therapsids are relatively rare (Rubidge and Sidor, 2001; Sidor, 2015; Whitney and Sidor, 2016). Smith et al. (2006) noted a similar overall pattern of radiating ridges and fossae in four biarmosuchian genera (*Hipposaurus*, *Lemurosaurus*, *Lobalopex*, and *Paraburnetia*), but in-depth comparisons of angular surface features have not yet been made for this group. Here, we recognize four fossae that are present in nearly identical positions and orientations in every biarmosuchian specimen with a well-preserved angular (Fig. 2.3A, B). In lateral view, a horizontal ridge extending from the contact between the angular and dentary meets a near-vertical ridge near the middle of the angular. Together, these ridges meet at an approximately right angle to bound a triangular fossa facing anterodorsally from the center of the angular, here termed the anterodorsal fossa. The horizontal ridge also meets a posteroventrally-oriented ridge at an oblique angle in the center of the angular, forming a wide, triangular fossa facing anteroventrally and spanning much of the ventral portion of the angular. This posteroventrally-oriented ridge bounds a third fossa that faces posteriorly to posteroventrally. The shape of this third fossa is roughly triangular but varies in width among the species examined. In *Bullacephalus, Paraburnetia,* and *Lemurosaurus,* the posteroventral fossa is bordered dorsally

by a wide, laterally convex area, dorsal to which is a small fourth fossa facing posterodorsally. This posterodorsal fossa has been figured in *Biarmosuchus* (Fig. 2.1B; Sigogneau-Russell and Tchudinov, 1972), *Proburnetia* (Sigogneau-Russell, 1989; Rubidge and Sidor, 2002), *Herpetoskylax* (Sidor and Rubidge, 2006) and possibly *Lobalopex* (Sidor et al., 2004). It is difficult to determine whether this fossa is present in *Hipposaurus*, as this area seems to be deformed in CGP/1/66, and the posterodorsal fossa is a subtle feature.

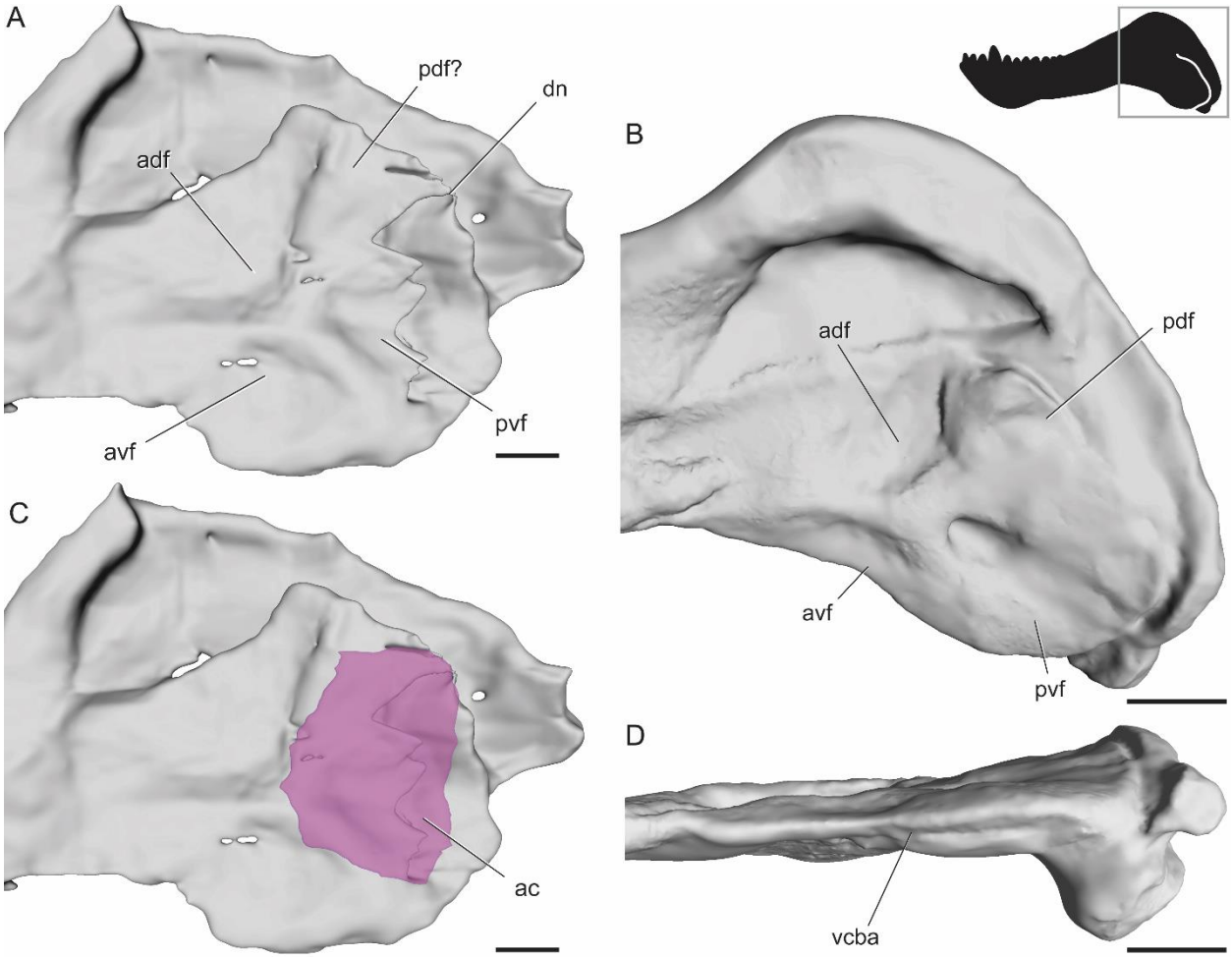

FIGURE 2.3. Surface and CT scans of the angular region in biarmosuchians. **A)** *Hipposaurus* sp. (CGP/1/66) in lateral view; **B)** *Paraburnetia sneeubergensis* (SAM-PK-K10037) in lateral view; **C)** *Hipposaurus* sp. (CGP/1/66) with angular cleft overlay; **D)** *Paraburnetia sneeubergensis* (SAM-PK-K10037) in ventral view showing anterior extent of the angular cleft. Box on silhouette illustrates location of images. Scale bars 1 cm. **Abbreviations**: **ac** = angular cleft; **adf** = anterodorsal fossa; **avf** = anteroventral fossa; **dn** = dorsal notch; **pdf** = posterodorsal fossa; **pvf** = posteroventral fossa; **vcba** = ventral connection to body of the angular.

The extent of the angular cleft, and therefore the overlying reflected lamina, can be seen in Figure 4C. It is expanded beyond the condition seen in sphenacodontids, but it is still restricted to the posterior portion of the angular. The dorsal notch is farther anterior than what is seen in sphenacodontids. The anterior extent of the angular cleft appears related to the position of the vertical ridge. In *Hipposaurus*, the cleft is deeply incised anteriorly into the angular, with the ventral contact between the reflected lamina and angular body located far posteriorly (Fig. 2.3A). In contrast, *Paraburnetia* shows a ventral connection farther anterior, at about the level of the posteroventral ridge, meaning that the angular cleft opens ventrally as well as posteriorly in this specimen (Fig. 2.3B). The discrepancy between the two specimens examined here likely indicates variation in the shape of the angular cleft among biarmosuchians, perhaps between basal members of the clade and its derived burnetiamorph subclade, although it should be noted that this morphology is somewhat unclear in the CT scan of CGP/1/66 and should be interpreted with caution.

The CT data indicates that the ridges and fossae on the reflected lamina is made up of corrugations in the thin bone rather than differences in thickness across the structure, which agrees with observations of serial sections in other therapsids (Maier and van den Heever, 2002). However, ridges on the angular body are formed by thickening of the bone.

Dinocephalia—The reflected lamina is thicker relative to its surface area in dinocephalians than in most other therapsids, although it is often only a few millimeters thick. Most dinocephalians lack ridges and fossae on the reflected lamina itself, although some anteosaurs have a thick bony boss on the angular just anterior to the reflected lamina. The size and shape of this boss is highly variable between species (Kammerer, 2011). The only dinocephalian with evidence for surface features on the reflected lamina itself is the holotype of '*Delphinognathus*' (SAM-PK-713), which has a posteriorly to posterodorsally-facing groove. The surface of this specimen does not appear to be broken, worn, or warped, so this is likely a real feature.

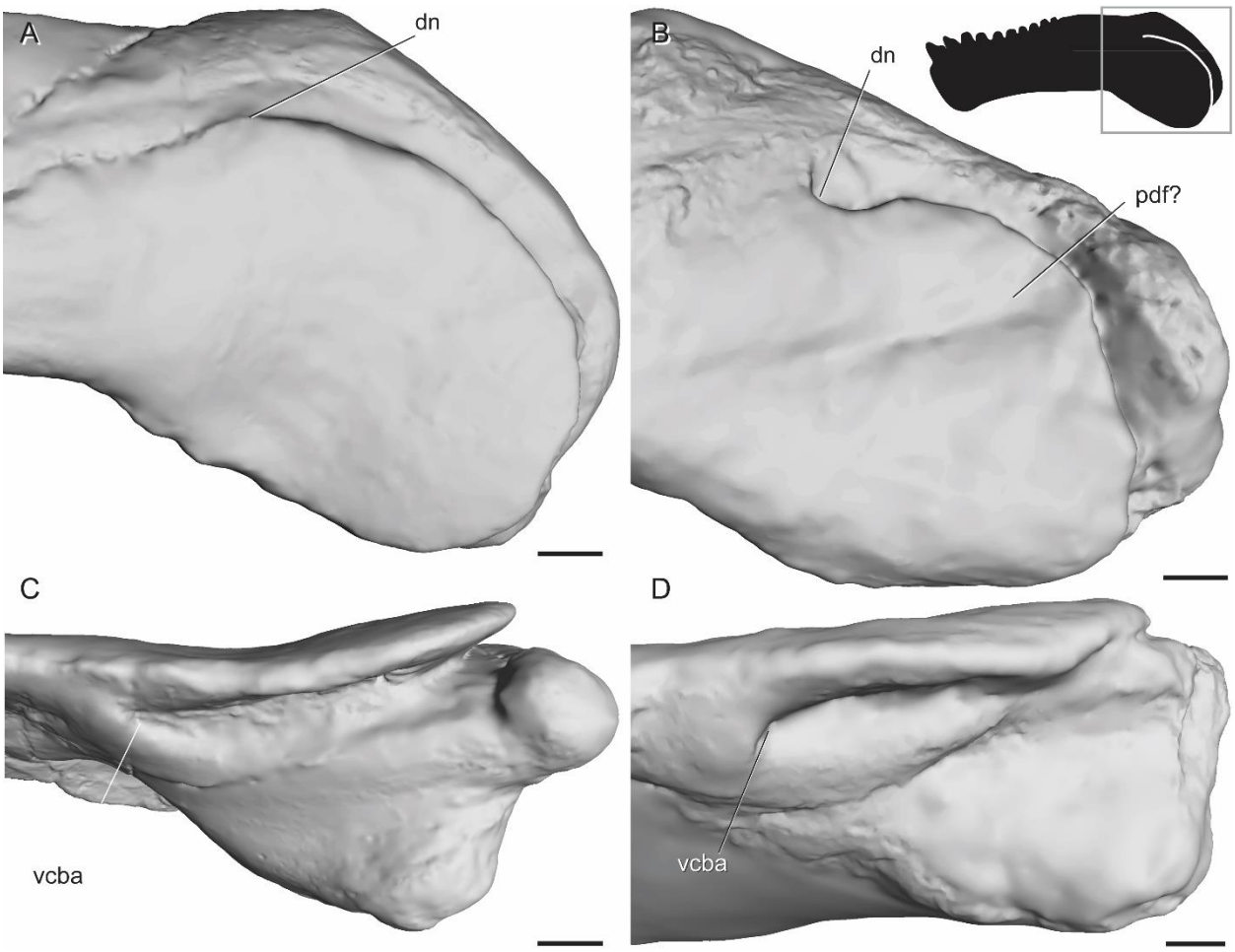

FIGURE 2.4. Surface scans of the angular region in tapinocephalian dinocephalians. **A)** *Moschops capensis* (AMNH FR5550) in lateral view; **B)** *"Delphinognathus" conocephalus* (SAM-PK-713) in lateral view; **C)** *Moschops capensis* (AMNH FR5550) in ventral view showing anterior extent of the angular cleft; **D)** *"Delphinognathus" conocephalus* (SAM-PK-713) in ventral view showing anterior extent of the angular cleft. Box on silhouette illustrates location of images. Scale bars 1 cm. **Abbreviations**: **dn** = dorsal notch; **pdf** = posterodorsal fossa; **vcba =** ventral connection to body of the angular.

Though we did not use CT data to determine the exact shape of the angular cleft, the extent of the cleft can be discerned from the dorsal and ventral connections between the reflected lamina and the angular body. In dinocephalians, both of these connection points are located far anteriorly, resulting in a large reflected lamina relative to the angular keel (Fig. 2.4C, D). The ventral connection is at a level slightly anterior to that of the dorsal connection.

Anomodontia—Anomodonts evolved jaw morphologies that were highly disparate from those seen in other early therapsids or in mammals (Sidor, 2003) and, unsurprisingly, this diverse and geologically long-lived group had the highest variability in angular anatomy. Overall, the reflected lamina is relatively large in anomodonts, extending farther below the ventral margin of the jaw than in other therapsids. The dorsal notch is located anteriorly near the dentary, and a vertical ridge extends dorsally from this notch, sometimes reaching the surangular (Angielczyk et al., 2021). The Triassic kannemeyeriids have often been described as having a uniquely large reflected lamina that nearly reaches the articular posteriorly (Janensch, 1952; Keyser, 1974; Keyser and Cruickshank, 1979), although this feature can also be seen in some specimens of earlier-diverging dicynodonts such as *Diictodon* (BP/1/356).

In all anomodonts except the early-diverging *Biseridens*, there is an oval or triangular external mandibular fenestra between the dentary and the angular. Posterior and ventral to this fenestra are two ridges, one vertical and one horizontal, that meet at a right angle, enclosing an anterodorsal fossa at the posterior and ventral edges of the external mandibular fenestra (Figs. 2.5, 2.6). Liu et al., (2010) reported two fossae facing posteriorly on the reflected lamina of *Biseridens*, and published figures of *Patranomodon* also seem to show this arrangement (Rubidge and Hopson, 1996). No non-dicynodont anomodonts were examined in person for this study, but photographs of *Ulemica* clearly show at least two fossae in addition to the anterodorsal one: a broad, triangular fossa facing anteroventrally and a thinner fossa facing posteriorly (Fig. 2.5A). The area around the dorsal notch appears to be broken in this specimen, but in *Suminia* (PIN 2212/62) there is a strong vertical ridge bordering a small fossa facing posterodorsally (Fig. 2.5B). Other surface features cannot be discerned in PIN 2212/62, as the rest of the reflected lamina seems to be heavily deformed.

There is extensive variation in the surface features of the angular among species of basal dicynodonts, ranging from three to five fossae separated by radiating ridges. Despite this variation, the fossae and ridges tend to have similar positions among taxa. The ridges radiate

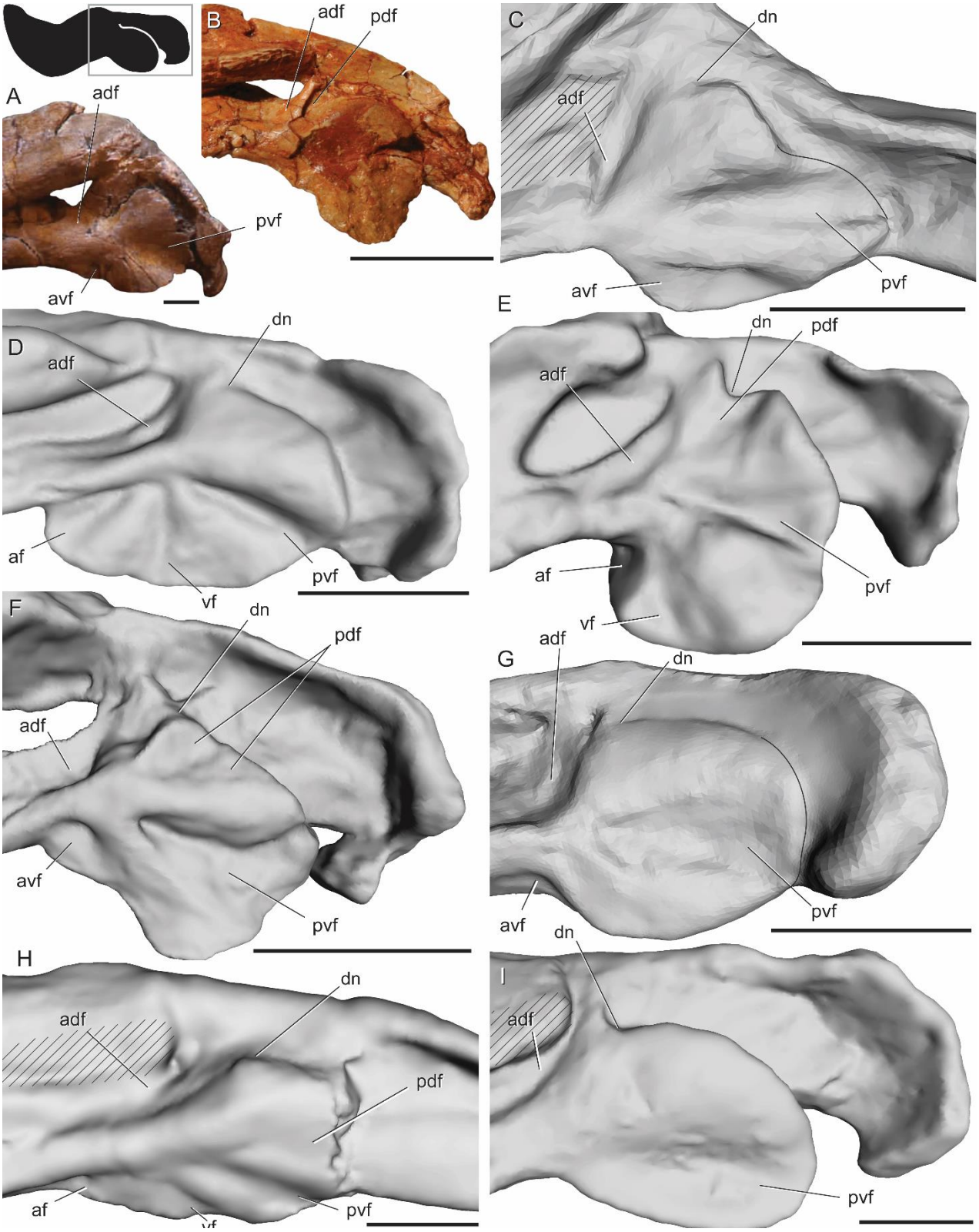

FIGURE 2.5. Surface scans and photos of the angular region in dicynodonts showing surface features in lateral view. **A)** photo of *Ulemica invisa* (PIN 157/1112); **B)** photo of *Suminia getmanovi* (PIN 2212/62); **C)** *Eodicynodon oosthuizeni* (BPI/1/6230); **D)** *Pristerodon mackayi* (BP/1/6685); **E)** *Emydops arctatus* (BP/1/1307); **F)**

Kembawacela kitchingi (NHCC LB18); **G)** *Cistecephalus microrhinus* (BP/1/253); **H)** *Tropidostoma microtrema* (SAM-PK-8633); **I)** *Lystrosaurus curvatus* (BP/1/5086). Box on silhouette illustrates location of images. Scale bars 1 cm. Areas filled with hashed lines indicate external mandibular fenestra. Solid, curved lines in C and G mark the posterior edge of the preserved reflected lamina. Photo in B courtesy of Brandon Peecook. **Abbreviations**: **adf =** anterodorsal fossa; **af** = anterior fossa; **avf =** anteroventral fossa; **dn** = dorsal notch; **pdf** = posterodorsal fossa; **pvf** = posteroventral fossa; **vf** = ventral fossa.

from a point just anterior to the center of the angular in lateral view. In addition to the anterodorsal fossa described above, all dicynodonts have a fossa facing posteriorly to posteroventrally, which is bounded dorsally by a ridge extending roughly posteriorly (Figs. 2.5, 2.6; Angielczyk and Rubidge, 2013; Angielczyk et al., 2016). In many dicynodonts, there is also a wide fossa facing anteroventrally just ventral to the horizontal ridge described above (Fig. 2.5F, G; 6). An additional ridge extending ventrally sometimes subdivides this fossa into two parts, a thin anterior component here termed the anterior fossa and a wider posterior component here termed the ventral fossa (2.5D, E, H). The anterior, ventral, and posteroventral fossae, along with their associated bounding ridges, have previously been described in dicynodonts (King, 1988; Sullivan and Reisz, 2005; Angielczyk and Rubidge, 2010). Occasionally, a small posterodorsal fossa is also present (Fig. 2.5B, D, E; Angielczyk et al., 2016). Angielczyk et al. (2021) reported an additional ridge splitting the posterodorsal fossa into two in *Kembawacela*, and this subtle feature is also visible in our scan (Fig. 2.5F). *Niassodon* has a unique morphology in which the reflected lamina balloons out laterally to enclose a mediolaterally-expanded angular cleft (Fig. 2.6A). In the closely-related *Endothiodon bathystoma*, the reflected lamina is thickened into a dorsoventrally elongate boss at its anteroventral end (Fig. 2.6B). This thickening is absent in *Endothiodon tolani* (Cox and Angielczyk, 2015).

In general, surface features on the angular are simplified in derived dicynodonts. For example, in cryptodonts, the angular has fewer ridges and fossae than in more basal forms, though *Tropidostoma* does have a complex topography (Fig. 2.5H). *Geikia* and the large-bodied

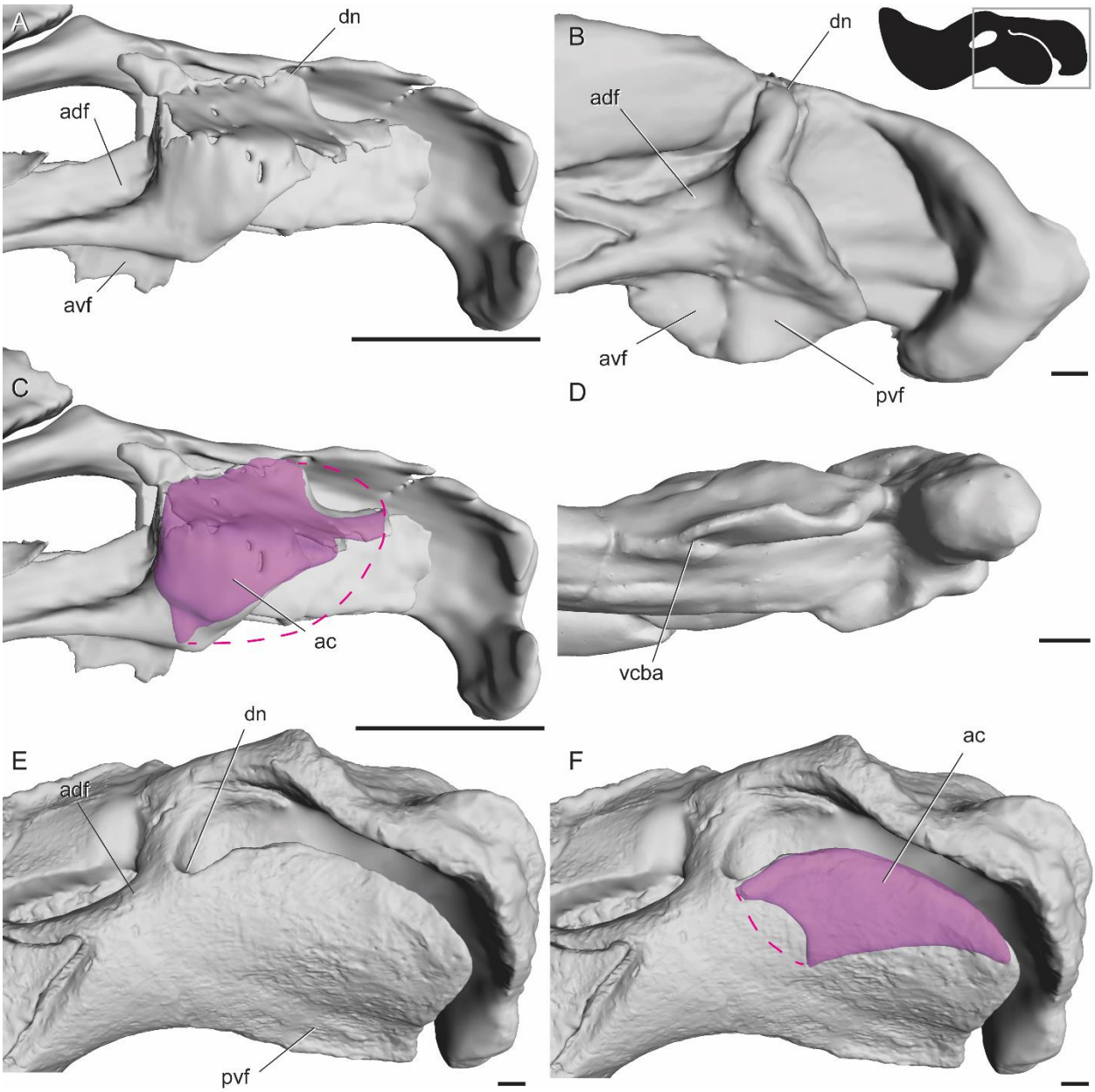

FIGURE 2.6. Surface and CT scans of the angular region in dicynodonts. **A)** *Niassodon mfumukasi* (ML1620); **B)** *Endothiodon bathystoma* (SAM-PK-K11031, mirrored) in lateral view; **C)** *Niassodon mfumukasi* (ML1620) with angular cleft overlay; **D)** *Endothiodon bathystoma* (SAM-PK-K11034) in ventral view showing anterior extent of the angular cleft; **E)** *Stahleckeria potens* (AMNH FR3857) in lateral view; **F)** *Stahleckeria potens* (AMNH FR3857) with angular cleft overlay. Box on silhouette illustrates location of images. Dotted line indicates approximated minimum extent of missing reflected lamina in C and approximated minimum extent of unprepared angular cleft in F. Scale bars 1 cm. **Abbreviations**: **ac** = angular cleft; **adf** = anterodorsal fossa; **avf** = anteroventral fossa; **dn** = dorsal notch; **pvf** = posteroventral fossa; **vcba =** ventral connection to body of the angular.

Aulacephalodon have only the anterodorsal fossa and the posteroventral fossa, and this pattern found in all dicynodontoids, making it the most common topographic pattern found in dicynodonts (Fig. 2.5I, 2.6E; Janensch, 1952; Rowe, 1980; Liu, 2020). In these forms, the posteroventral fossa is bounded dorsally by a wide, convex area spanning the dorsal half of the reflected lamina.

The extent of the angular cleft is somewhat variable within Dicynodontia, but the dorsal notch is consistently placed far anteriorly. The early-diverging *Niassodon* has an angular cleft that extends anteriorly to just beneath the vertical ridge bordering the anterodorsal fossa (Fig. 2.6C). The anterior edge of the angular cleft follows a straight line ventrally from this area. The ventral edge of the angular keel and reflected lamina is missing in this specimen, so it is uncertain whether the location of the cleft coincides with any surface features in this region. In *Pristerodon* (SAM-PK-K10153)*, Endothiodon* (SAM-PK-K11034)*,* and *Tropidostoma* (SAM-PK-8633) the ventral connection between the reflected lamina and the angular body occurs at the level of the ridge between the anteroventral and posteroventral fossae (Fig. 2.6D). This is also true in more derived dicynodonts, although in some of these taxa the posteroventral fossa is located farther posteriorly relative to the dorsal notch, resulting in an angular cleft whose anterior margin is angled posteroventrally (Fig. 2.6F). As in CGP/1/66, the surface features overlying the angular cleft are formed by corrugations in the bone, while ridges on the angular body are formed by thickening of the bone.

Gorgonopsia—Gorgonopsians have a stereotyped pattern of four fossae on their reflected lamina facing anterodorsally, posterodorsally, posteroventrally, and anteroventrally (Kemp, 1969; Sigogneau-Russell, 1989; Kammerer, 2016; Fig. 2.7). The ridges between the fossae form a cross-like shape with a strong vertical ridge and a weaker horizontal one. The vertical ridge tends to run in a slightly posteroventral direction. The anterior end of the horizontal ridge is at about the level of the ventral margin of the dentary, but its posterior end is near the dorsal notch. The horizontal ridge is often broader, less pronounced, and greatly

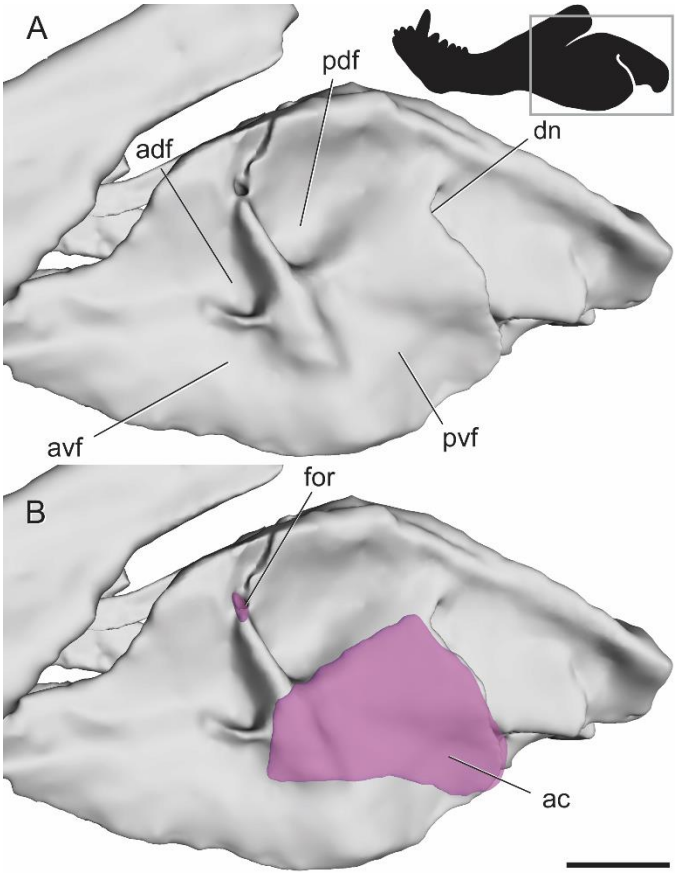

FIGURE 2.7. CT scan of the angular region in the gorgonopsian *Cynariops robustus* (MB.R.999). **A)** model showing surface features; **B)** model from A with angular cleft overlay. Box on silhouette illustrates location of images. Scale bar 1 cm. **Abbreviations**: **ac =** angular cleft; **adf =** anterodorsal fossa; **avf** = anteroventral fossa; **dn** = dorsal notch; **for** = foramen; **pdf** = posterodorsal fossa; **pvf** = posteroventral fossa.

attenuated in length compared to the vertical ridge (Fig. 2.7). As a result, the horizontal ridge is occasionally masked by specimen deformation, leading some authors to interpret the angular as lacking it (e.g., Barghusen, 1968). The horizontal ridge was reported to be absent in *Nochnitsa*, which has been proposed to be the basalmost gorgonopsian (Kammerer and Masyutin, 2018). While it is possible that this specimen has been deformed in a way that erased the subtle horizontal ridge, the absence of the ridge in this specimen may be a genuine feature indicating the plesiomorphic condition for Gorgonopsia. The horizontal ridge ranges from being straight to having dorsal concavities which produce small, blind-ended pockets, near where it crosses the vertical ridge (Fig. 2.7). Its anterior and posterior ends generally flare out into broad convex surfaces.

The posterior margin of the reflected lamina barely extends beyond the level of the dorsal notch, exposing a wider portion of the angular body laterally in the angular gap than in other therapsids (Fig. 2.7B). The horizontal ridge marks the dorsal boundary of the angular cleft. The anterior boundary of the cleft is slightly anterior to the level of the vertical ridge, a feature

also visible in a specimen of *Cyonosaurus* (BP/1/2598) and previously reported by Kemp (1969). The dorsal half of the vertical ridge and the anterior half of the horizontal ridge are formed by thickening of the bone, while the parts of these ridges that overlie the angular cleft are formed by corrugations in the bone.

We observed a foramen at the dorsal tip of the vertical ridge in well-preserved specimens of *Aelurognathus*, *Arctops*, *Cynariops*, *Lycaenops*, and *Scylacocephalus* (Fig. 2.7B). Kemp (1969) figured the foramen, as well as three others along the dentary-angular contact, in an acid-prepared specimen of *Arctognathus*, but did not comment on their significance. Segmentation of the dorsal foramen in the scan of *Cynariops* reveals that it penetrates ventromedially from its appearance on the lateral surface of the angular and emerges on the medial side of the angular. The vertical ridge is otherwise formed by solid bone in *Cynariops* (and all the other therapsids for which we had CT data). A similar foramen is unknown in other therapsids and its function in gorgonopsians remains obscure.

Therocephalia— The angular of therocephalians has a well-developed ridge at the anterior edge of the dorsal notch that runs posterodorsally, sometimes reaching or even slightly overlapping the surangular (Fig. 2.8). This ridge has been termed the angular crest (Barghusen, 1968), and its position is consistent with that of the dorsal ridge seen in other therapsids, especially the dorsally far-reaching ridge seen in many anomodonts (Angielczyk et al., 2021). Some authors have mistakenly considered the bone surface between the angular crest and the convex surface posteroventral to it as part of the reflected lamina (Barghusen, 1968), but it is actually the angular body visible in a large dorsal notch (Fig. 2.8E, G). This surface can appear to be part of the reflected lamina in specimens where the lamina is tightly pressed against the angular body. In eutherocephalians, an external mandibular fenestra is present between the angular and dentary, as in most anomodonts (Fig. 2.8A–C; Huttenlocker, 2009).

Therocephalians have a stereotyped pattern of four fossae radiating from a point just anterior to the center of the angular in lateral view (Fig. 2.8; Huttenlocker, 2009). Barghusen

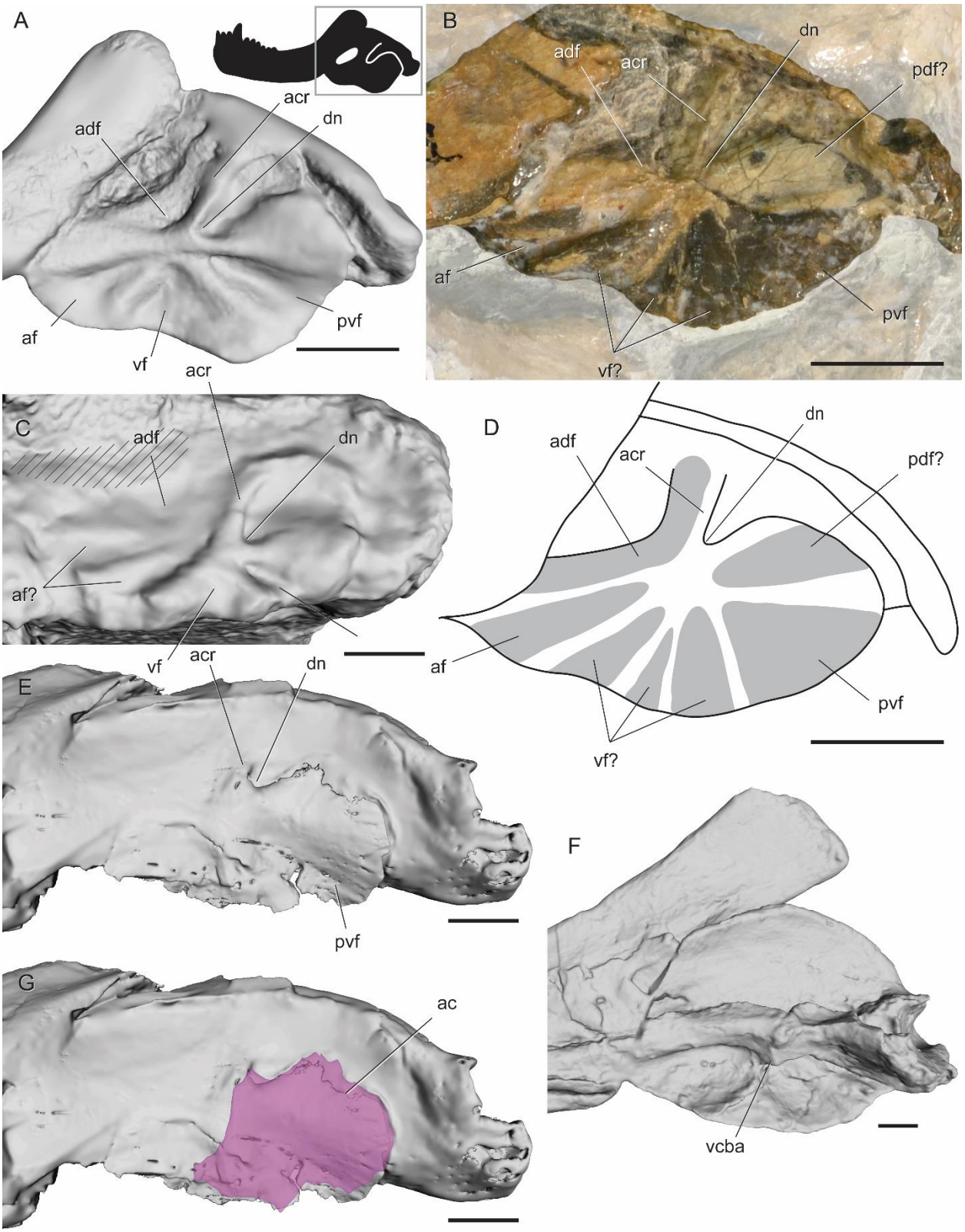

FIGURE 2.8. Surface and CT scans and photos of the angular region in therocephalians. **A)** *Hofmeyria atavus* (TM 254) in lateral view; **B)** photo of *cf. Ictidostoma* sp. (BP/1/3155, mirrored) in lateral view; **C)** pristerognathid therocephalian CGP RMS 1185 in lateral view; **D)** interpretive drawing of *cf. Ictidostoma* sp. (BP/1/3155,

mirrored); **E)** *Lycosuchus vanderrieti* (MB.R.995) in lateral view; **F)** *Pristerognathus polyodon* (SAM-PK-11942) in medial view; **G)** *Lycosuchus vanderrieti* (MB.R.995) with angular cleft overlay. Box on silhouette illustrates location of images. Scale bars 1 cm. Areas filled with hashed lines indicate external mandibular fenestra. **Abbreviations**: **ac** = angular cleft; **adf** = anterodorsal fossa; **af** = anterior fossa; **dn** = dorsal notch; **pvf** = posteroventral fossa; **vcba** = ventral connection to body of the angular; **vf** = ventral fossa.

(1968) described and numbered three of these fossae and the ridges bounding them, though these names were never broadly adopted in the therapsid literature. Interestingly, the arrangement of the fossae in therocephalians is nearly identical to that seen in some basal dicynodonts (Fig. 2.5C, E, H). The angular crest meets a horizontal ridge on the body of the angular at a slightly oblique angle. Together, these ridges border the anterodorsal fossa. When present, the external mandibular fenestra is surrounded by this fossa on its ventral and posterior edges, as in dicynodonts. Ventral to the horizontal ridge is the thin anterior fossa (C1 of Barghusen, 1968), which is angled slightly ventrally. A gentle ridge bounds this fossa posteriorly, separating it from the wide ventral fossa (C2 of Barghusen, 1968). Further posterior is another gentle ridge and a posteroventral fossa (C3 of Barghusen, 1968), which is bordered dorsally by a wide, convex area spanning the dorsal half of the reflected lamina. The ridges and convexities described above radiate outwardly from roughly the same point just anterior to the middle of the angular, as in some dicynodonts (Figs. 2.5, 2.8).

This stereotyped topographic pattern is present across nearly all therocephalians, with differences confirmed in only a few specimens. BP/1/3155, which is likely referrable to the hofmeyriid *Ictidostoma*, exhibits three additional ridges splitting the typical therocephalian fossae (Fig. 2.8B, D). Based on their position, two of the extra ridges seem to split the ventral fossa into three smaller fossae, and the third ridge extends along the free dorsal edge of the reflected lamina, bounding a posterodorsal fossa. An additional ridge is also seen in the pristerognathid therocephalian specimen CGP RMS 1185 from the *Tapinocephalus* Assemblage Zone of South Africa, in which the anterior fossa seems to be split in two (Fig. 2.8C). Liu and

Abdala (2017) reported only two fossae in the holotype of *Dalongkoua fuae*, the ventral and posteroventral fossae, though it is possible that other fossae were either overlooked or not well preserved in that specimen.

The dorsal notch is placed far anteriorly in therocephalians, resulting in an extensive free dorsal edge of the reflected lamina (Huttenlocker, 2009). The anterior edge of the angular cleft follows a fairly straight path ventrally near the point where the ridges meet. At its ventral end, the angular cleft curves anteriorly (Fig. 2.8G). Much of the ventral portion of the angular is missing in the specimen of *Lycosuchus* examined, so this may be an incomplete picture of the extent of the angular cleft. However, the specimen of *Pristerognathus* (SAM-PK-11942) has the medial face of the reflected lamina partially prepared and seems to show that the ventral connection with the angular body occurs along the edge of the posteroventral fossa near the point from which the surface ridges radiate, which seems consistent with CT scan data for *Lycosuchus* and descriptions in the literature (Fig. 2.8F; Barghusen, 1968).

Cynodontia— The reflected lamina is reduced in cynodonts so that the lateral surface of the angular body is broadly exposed. The topography of the angular is simplified in basal cynodonts compared to most other nonmammalian therapsids. At least two fossae are generally present, one facing posteriorly to posteroventrally and another ventral to that which faces antero- to posteroventrally (Fig. 2.9A-C). These two fossae are present in *Thrinaxodon*; descriptions of a simple, splint-like reflected lamina in this genus (summarized by Parrington, 1979) were based on specimens missing much of the dorsal portion of the reflected lamina. Figures of the basal cynodont *Charassognathus* seem to indicate that the anteroventral fossa is divided into anterior and ventral components by a ridge, as in therocephalians and some dicynodonts (Botha et al., 2007). A posterodorsal fossa is also present in *Galesaurus* (Fig. 2.9B) and possibly *Charassognathus* (Botha et al., 2007). Eucynodonts completely lack ridges and fossae on the angular, where the bone is substantially reduced into a hook-shaped structure in lateral view (Allin and Hopson, 1992).

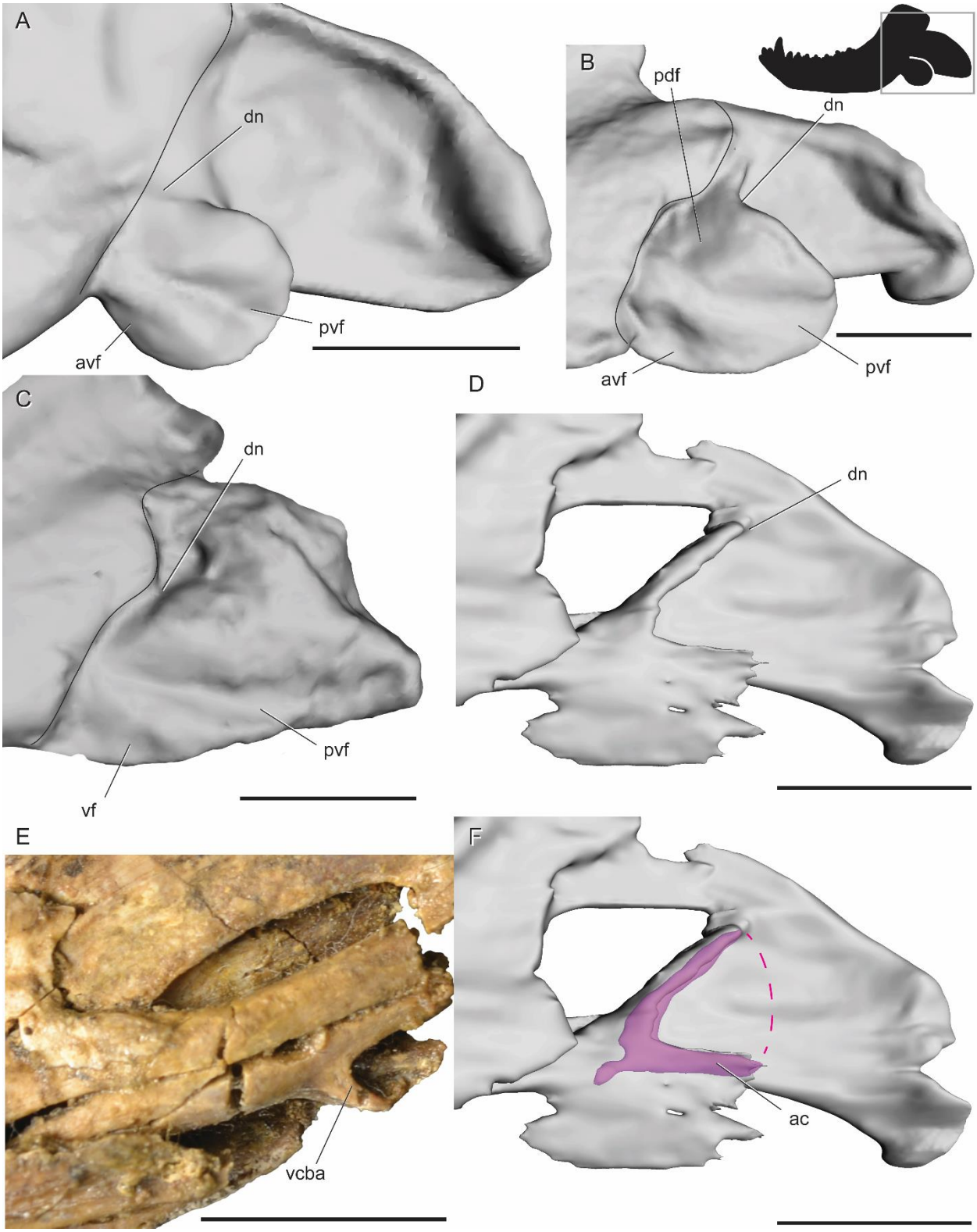

FIGURE 2.9. Surface and CT scans and photos of the angular region in non-eucynodont cynodonts. **A)** *Procynosuchus delaharpeae* (BP/1/226) in lateral view; **B)** *Galesaurus planiceps* (BP/1/5064) in lateral view; **C)** *Thrinaxodon liorhinus* (BP/1/2513) in lateral view; **D)** *Nshimbodon muchingaensis* (NHCC LB277, mirrored) in

lateral view; **E)** *Thrinaxodon liorhinus* (TM81, mirrored) in medial view; **F)** *Nshimbodon muchingaensis* (NHCC LB277, mirrored) with angular cleft overlay. Box on silhouette illustrates location of images. Dotted line indicates approximated minimum extent of missing reflected lamina. Scale bars 1 cm. Curved, solid lines indicate posterior edge of preserved dentary. **Abbreviations**: **ac** = angular cleft; **avf** = anteroventral fossa; **dn =** dorsal notch; **pdf** = posterodorsal fossa; **pvf** = posteroventral fossa; **vcba** = ventral connection to body of the angular.

There is no substantial angular keel in cynodonts, so the whole lateral portion of the angular is a free-hanging reflected lamina with an angular cleft separating it from the angular body (Fig. 2.9E, F; 10B). In non-eucynodont cynodonts, the sole remnant of an angular keel is a small finger of bone curving along the anteroventral edge of the medial face of the reflected lamina (Fig. 2.9E). Eucynodonts show no evidence of an angular keel; their reflected lamina becomes a thin, simple splint of bone (Hopson and Kitching, 2001). The reflected lamina dips below the ventral margin of the jaw in *Trirachodon berryi* (Fig. 2.10A), but it overlaps the body of the angular in *Probainognathus* (Fig. 2.10B).

2.5 DISCUSSION

2.5.1 Comparative Anatomy of the Angular Complex

Revised Definition of the Reflected Lamina—The reflected lamina has been traditionally defined as the part of the angular that is mediolaterally separated from the angular body (Allin, 1975). Under this definition, the reflected lamina is restricted to the portion of the angular that overlies the angular cleft, but some authors have also included the ventrally-hanging angular keel as part of the reflected lamina (King, 1981). It is also common in the literature to describe all surface features on the lateral surface of the angular as occurring on the reflected lamina, but our results indicate that much of this topography is more precisely understood to be located on the body of the angular, not its reflected lamina. Given the varied use of this term and the data presented here, we propose an updated definition of the term

'reflected lamina': the part of the angular bounding the angular cleft laterally, and the ventral continuation of this sheet of bone below the body of the angular. The more anterior part of the angular that hangs ventral to the jaw margin but is not separated mediolaterally from the body of the angular is the angular keel. Our revised definition has the benefit of relying on specific landmarks (i.e., the angular cleft and the ventral jaw margin) that allow for a precise delineation of each part of the angular. It is also useful because the reflected lamina and the part of the angular body with surface features would undoubtedly have different biomechanical properties (e.g., vibration quality or resistance to muscle strain), suggesting they should be considered separate functional units. The main downside to our proposed definition of the reflected lamina is that it is defined based on an internal structure (the angular cleft) that cannot be easily visualized in every fossil. Fortunately, there is a degree of correspondence between the external

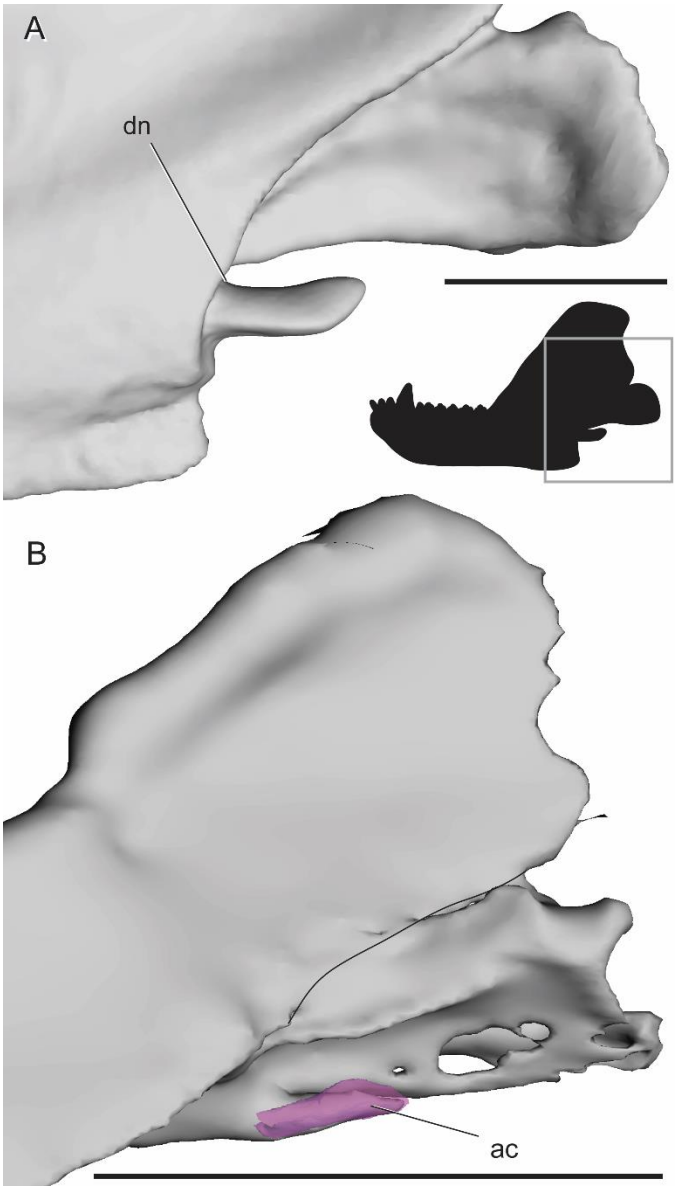

FIGURE 2.10. Surface and CT scans of the angular region in non-mammalian eucynodonts in lateral view. **A)** *Trirachodon berryi* (BP/1/4658); **B)** *Probainognathus jenseni* (PVSJ 410) with angular cleft overlay. Box on silhouette illustrates location of images. Scale bars 1 cm. Curved, solid line in B indicates posterior edge of preserved dentary. **Abbreviations**: **ac** = angular cleft; **dn** = dorsal notch.

morphology and the extent of the underlying angular cleft: in every therapsid with angular ridges and fossae that we examined, the anterior extent of the angular cleft roughly coincides with the ridge bounding the posteroventral fossa anteriorly. This fossa is present in nearly all therapsids, so delineating the extent of the reflected lamina with only an exterior view of a given fossil should be feasible. The correspondence between the angular cleft and the overlying topography across therapsid clades also implies some degree of homology between reflected laminae under our definition, which is another reason this definition is biologically meaningful.

Systematic Review—Stereotyped patterns of ridges and fossae on the angular have long been recognized in gorgonopsians and therocephalians (Barghusen, 1968; Sigogneau-Russell, 1989; Huttenlocker, 2009), but they have been more difficult to appreciate in other therapsid clades. Here we outline broad scale patterns of angular topography that are common within biarmosuchians, anomodonts, and cynodonts.

Biarmosuchians have a pattern of four radiating ridges, three of which are sharply defined while the posterior ridge is a broader, convex area (Fig. 2.3). These ridges bound four fossae, three of which are large and triangular whereas the posterodorsal fossa is smaller and more U-shaped. Anomodonts are diverse and thus highly variable, but general patterns can be seen in each subclade. We were unable to examine non-dicynodont anomodont material in person for this study, but photographs and published reports seem to agree that these taxa generally have an anterodorsal fossa shaped like a right triangle, a wide anteroventral fossa, a posterior to posteroventral fossa, and a small posterodorsal fossa (Fig. 2.5A, B; Rubidge and Hopson, 1996; Rybczynski, 2000; Liu et al., 2010). Non-bidentalian dicynodonts exhibit remarkable variability in topography, but they often have four or five radiating fossae, sometimes missing the posterodorsal fossa and/or the ventral ridge subdividing the anteroventral fossa (Fig. 2.11). Most bidentalian dicynodonts only have the anterodorsal and posteroventral fossae, although some cryptodonts retain more complex angular topography.

Non-eucynodont cynodonts are also variable, but they typically have at least the anteroventral and posteroventral fossae.

Recognition of these within-clade patterns will hopefully provide a baseline for future descriptive work, giving researchers a better idea of what to expect when examining a new specimen. This is especially important because the ridges and fossae on the angular are often subtle and easily masked by deformation, resulting in specimen descriptions that can inadvertently oversimplify the morphology present. For example, descriptions of non-bidentalian dicynodonts often miss subtle surface features on the angular that were recognized here (e.g., Crompton and Hotton, 1967; Sullivan and Reisz, 2005; Angielczyk and Rubidge, 2010), which is unsurprising given the overwhelming variability in this group and the lack of thorough comparisons of this morphology across taxa. We also encourage the use of the fossa names introduced here, as a consistent naming scheme will facilitate comparisons between taxa.

2.5.2 Evolution and Homologies of the Angular Complex

Figure 11 depicts the phylogenetic sequence of anatomical modifications to the angular region suggested by the systematic review discussed above. The cladistic relationships used are primarily those discussed by Rubidge and Sidor (2001), with the dicynodont part of the tree based on Olroyd et al. (2018) and Kammerer and Ordoñez (2021). However, it should be noted that several studies have suggested alternative arrangements, and most agree that character support for the higher level clades is weak (Rowe, 1988; Sidor and Rubidge, 2006; Kemp, 2009).

A substantial morphological gap exists between sphenacodontids and the earliest therapsids, with Sidor and Hopson (1998) noting that at least 36 character changes separate the two. We reconstruct three angular features as first evolving in therapsids: the angular notch being located more anteriorly (leading to a longer free dorsal margin of the reflected lamina), enlargement of the angular cleft, and the development of a quadripartite ridge system with

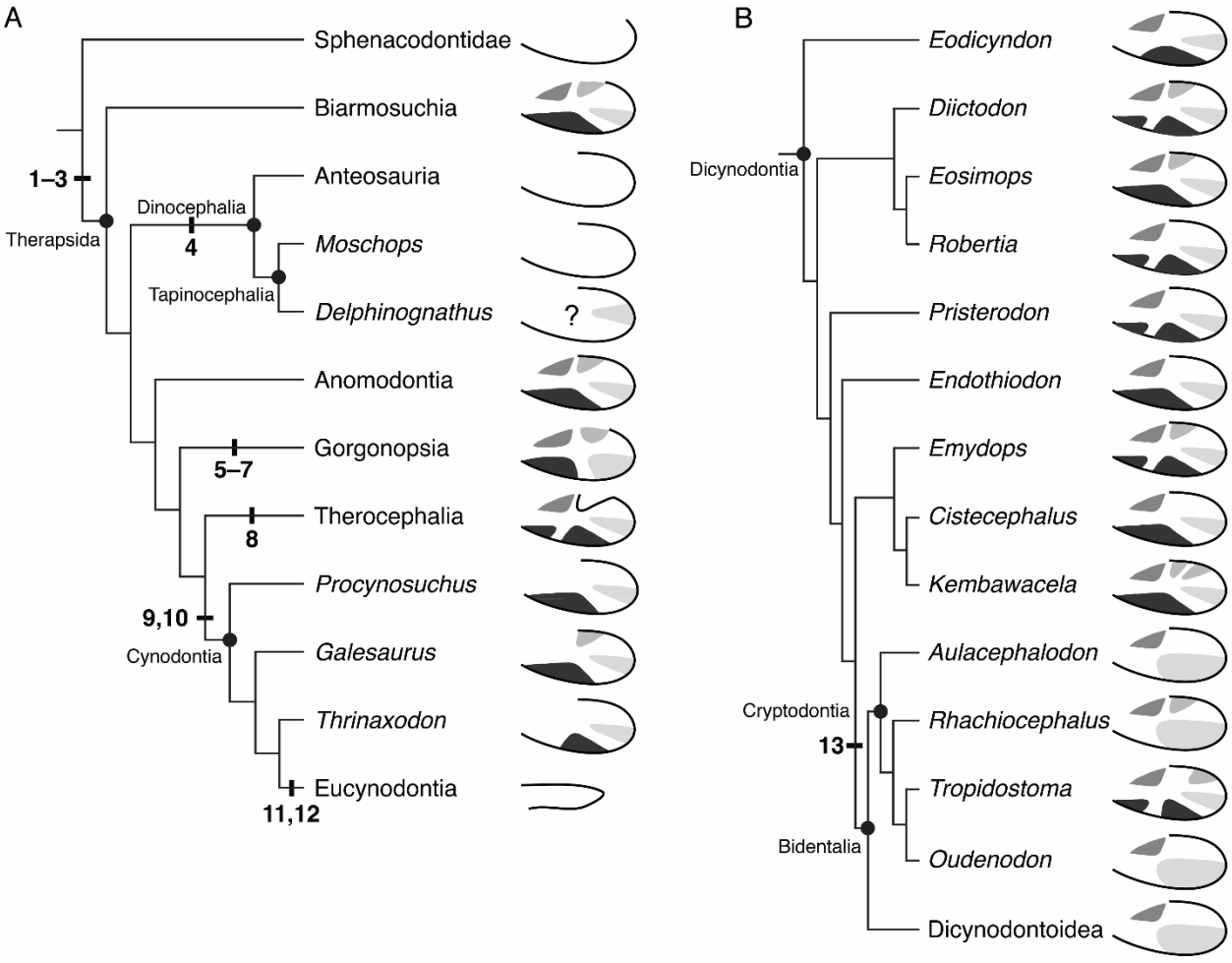

FIGURE 2.11. The evolution of angular traits within non-mammalian synapsids. **A)** cladogram showing relationships of the major synapsid subclades, with schematic angulars depicting the condition for each group; **B)** expanded cladogram illustrating the diversity of angular topography in Dicynodontia. The following synapomorphies are noted: 1) angular notch located more anteriorly, thus creating a long dorsal free margin of the reflected lamina; 2) angular cleft enlarged; 3) reflected lamina has quadripartite ridge system with attendant fossae; 4) loss of ridges and fossae on reflected lamina; 5) pronounced vertical ridge on reflected lamina; 6) angular notch position more posteriorly, reducing free edge of the reflected lamina; 7) presence of one of more foramina at dorsal end of vertical ridge; 8) angular crest present; 9) external topography of angular reduced to two fossae; 10) reflected lamina fully separated, with angular cleft open dorsally and ventrally; 11) reflected lamina reduced to small, curved element; 12) external ridges and fossae of angular absent; 13) external angular ridges and fossae reduced. See Table 1.1 for voucher specimens for each taxon. Higher level cladistic topology based on Sidor and Hopson (1998), with dicynodont topology based on Olroyd et al. (2018) and Kammerer and Ordoñez (2021).

attendant fossae. The consistency of the positions and orientations of the individual fossae and ridges on the angular across highly disparate therapsid clades strongly suggests that at least some of these structures are homologous. The posteroventral fossa is nearly ubiquitous, absent only in dinocephalians (Fig. 2.11), and is thus highly likely to be homologous between therapsids. Almost every therapsid with angular surface features also has an anterodorsal fossa, with only cynodonts lacking this feature, presumably as a result of the enlarged dentary overlapping the angular in this area. The anteroventral fossa and its presumed derivatives (the anterior and ventral fossae of therocephalians and some dicynodonts) are found in all therapsids with ridges and fossae on the reflected lamina except most of the bidentalian dicynodonts. The presence of an anteroventral fossa in basal anomodonts (Fig. 2.5A) suggests that this feature is homologous among major therapsid groups and was lost in some dicynodonts. The presence of an additional ridge subdividing the anteroventral fossa in therocephalians and basal dicynodonts is interesting but unlikely to represent a direct homology, as this feature is sporadically present in dicynodonts, absent in *Eodicynodon*, and unreported for any non-dicynodont anomodont. The posterodorsal fossa is also variably present in early-diverging dicynodonts, but it is present in many other therapsids. The distinctive shape of the dorsal notch in therocephalians may even be a derivative of this posterodorsal fossa, as the tissue between the ridges normally bounding this fossa in other taxa may not have ossified in therocephalians. This hypothesis is supported by the fact that the shape and relative position is consistent between the therocephalian dorsal notch and the posterodorsal fossa of other therapsids (Fig. 2.11). Barghusen (1968) recognized the similarity between these two structures in therocephalians and gorgonopsians and proposed a functional link between them. A fossa in this position is also seen in several non-dicynodont anomodonts (Fig. 2.5B; Rubidge and Hopson, 1996; Rybczynski, 2000; Liu et al., 2010), which supports the possibility that it is homologous across therapsids and was lost in some cynodonts and dicynodonts. The homology of the specific fossae and ridges among therapsids is also supported by their consistent spatial relationship to the angular cleft.

The anterior extent of the cleft seems to roughly coincide with the ridge that bounds the posteroventral fossa anteriorly, as does the ventral connection with the angular body. This suggests that the ridge between the posteroventral and anteroventral/ventral fossae is homologous across therapsids.

Under the relationships shown in Figure 11, the loss of an external ridge system would be a reversal for dinocephalians and, indeed, their lack has previously been considered a dinocephalian synapomorphy under some phylogenetic topologies (Sidor, 2000). This may be related to the agonistic headbutting behavior that has been inferred for dinocephalians based on pachyostosis in the skull (Barghusen, 1975; Benoit et al., 2016). A thin reflected lamina may be vulnerable to damage during fights, so this structure may have thickened in dinocephalians, masking the fine surface details seen in other therapsids (J. A. Hopson, pers. comm.). However, it should be noted that the phylogenetic position of dinocephalians is debatable. Sidor and Rubidge (2006) placed a monophyletic Dinocephalia (Anteosauria+Tapinocephalia) as the earliest diverging group of therapsids in their majority rule tree, in which case the lack of ridges would be retained plesiomorphically. Alternatively, Watson and Romer (1956) suggested that dinocephalians and anomodonts were close relatives, which was emphasized by King (1988), and more recently by Liu et al. (2010), which would likely only reinforce the character optimization outlined in Figure 11A. The apparent presence of a fossa in '*Delphinognathus*' is puzzling. It is important to note that '*Delphinognathus*' is likely a nomen dubium, possibly representing a young individual of a known genus (Atayman-Güven et al., 2009). Though this fossa could be an ontogenetically variable feature in dinocephalians, small individuals of the anteosaurian dinocephalian *Sinophoneus* lack surface features (Liu, 2013), so ontogeny alone cannot account for the morphology seen in '*Delphinognathus*'. Further research on dinocephalian jaws with well-preserved surface features may help clarify whether the reflected lamina is truly devoid of surface features in this clade. Ultimately, the phylogenetic arrangement

of non-theriodont therapsids lacks stability and must be readdressed with improved character data.

The ancestral condition for anomodonts is unclear because we were unable to directly examine any non-dicynodont anomodonts where the angular was sufficiently well preserved for this study. However, the condition described for *Biseridens* (Liu et al., 2010) and evident in photographs of *Ulemica* and *Suminia* (Fig. 2.5A, B) is very similar to what we show for *Eosimops*, and so this reflects our best understanding (Fig. 2.11). As noted above, dicynodonts are taxonomically diverse and show a corresponding diversity in their angular morphology. Bidentalian dicynodonts reduced complexity of the ridge system, but better sampling is needed to explain the re-occurrence of these ridges in *Tropidostoma*.

The morphology of the angular in gorgonopsians has long been recognized as diagnostic for the group (Kemp, 1969, 1982; Sigogneau-Russell, 1989) and we identify three features as likely synapomorphies of this clade. The first feature is the pronounced vertical ridge on the external surface of the angular. This feature is very well known, but our analysis suggests that it is best understood as a modified version of therapsid quadripartite morphology, with the horizontal rami reduced substantially, and not an independent evolution of angular topography. Second, the angular notch is positioned relatively posteroventrally, reducing the free edge of the reflected lamina to only its more posterior portion. Third, the presence of one or more foramina at the dorsal end of the vertical ridge is a feature that we have seen only in gorgonopsians among taxa with a reflected lamina. A systematic appraisal of this feature might be useful for within-clade relationships.

It should be noted that the earliest-diverging gorgonopsian *Nochnitsa* apparently lacks a horizontal ridge separating the two dorsal fossae from their ventral counterparts (Kammerer and Masyutin, 2018). This has been interpreted as the ancestral condition for Gorgonopsia. The horizontal ridge is subtle and often obscured by deformation in gorgonopsian specimens, so additional specimens of early gorgonopsians will aid in our understanding of the ancestral

condition in this clade. Given the distribution and similarities of the fossae across therapsids, we propose that a topographic pattern of four fossae separated by four ridges was present in the common ancestor of all known therapsids and was inherited by most of its descendants.

Therocephalian relationships have received renewed scrutiny over the past decade, including Kemp's (1972) hypothesis that this group is better understood as paraphyletic relative to cynodonts (Abdala et al., 2008). Recent work has advocated for the traditional hypothesis of therocephalian monophyly (Hopson and Barghusen, 1986; Huttenlocker 2009), which agrees with the elongated angular crest being unique to therocephalians and best considered a synapomorphy of the group.

The fossil record of non-mammalian cynodonts is well known to record a pronounced reduction in the size reflected lamina of the angular, and this transformation is often captured in cladistic data sets (Sidor and Hopson, 1998). Our review suggests that a reduction in the surface features of the angular can be considered a cynodont synapomorphy, even though the overall size of the reflected lamina was only slightly reduced compared to the condition in other theriodonts. In addition, the ventral connection between the reflected and medial laminae shifted anteriorly in cynodonts, resulting in a fully separated reflected lamina with an angular cleft that was open both dorsally and ventrally. In eucynodonts, the reflected lamina was reduced to a small, curved element and the angular lacked all surface features.

2.5.3 Function of the Angular Complex

Our systematic review reveals a few clues that help to narrow down the potential functions of the angular complex in non-mammalian therapsids. Many authors have considered the angular cleft as an area for the insertion of the posterior pterygoideus muscle (Romer and Price, 1940; Watson, 1953; Barghusen, 1968), although King (1981) favored the attachment of throat muscles here and others have suggested that the other jaw adductors might partially insert in the dorsal region of the cleft (Westoll, 1943; Kemp, 1982). Under this scenario, the cleft

would be filled with muscle attached to the medial lamina and/or the medial face of the reflected lamina. Keyser (1974) attributed increased robusticity of the reflected lamina in kannemeyeriid dicynodonts to a change in diet and roughly correlated it with the reduction or loss of the quadrate foramen. King et al. (1989) noted striations on the medial lamina and medial face of the reflected lamina in dicynodonts that they interpreted as muscle scars. This hypothesis is also consistent with our findings that a trend towards the simplification of angular topography is seen in both dicynodonts and cynodonts (Fig. 2.11), two clades in which the pterygoideus musculature was likely reduced over time (Kemp, 1982; King et al., 1989).

However, the shape and orientation of the angular cleft make it unlikely that the cleft was solely a site for muscle attachment in all non-eucynodont therapsids. The cleft is so deeply incised and bounded by bone at its ventral edge in some taxa (e.g., *Hipposaurus* and some dicynodonts; Fig. 2.3C, 6F) that any muscle originating from the quadrate ramus of the pterygoid must take an indirect path across the thin edges of the medial lamina to access the deeper parts of the cleft. If this structure was only involved in muscular attachment, one would expect the angular cleft to exist only where the posterior pterygoideus could easily reach it. While there could be structural or developmental reasons that this additional space existed, it seems likely that there was another function for the angular cleft, even if this function was secondary to a function in muscle attachment. The posterior pterygoideus is also expected to insert near the articular (Barghusen, 1973), so the anterior extension of the angular cleft in therapsids is inconsistent with a purely muscular interpretation of the structure. It is also important to consider that the angular cleft is quite narrow in many therapsids (e.g., 2–10 mm), even in large dinocephalians and dicynodonts, which makes it unlikely that a large jaw adductor would be able to contract in this space (Camp, 1948; Allin, 1975; Barghusen, 1976), although a tendinous insertion is another possibility. Corrugations on the medial surface of the reflected lamina would make this an uneven surface, which would be difficult for a muscle to insert onto from a ventral direction.

Several authors have also proposed that the fossae and ridges on the lateral face of the angular served as muscle attachment sites, and that the reflected lamina was largely useful in providing additional area for the attachment of multiple muscles in this region of the jaw. The fossae on the ventral half of the angular have been reconstructed as sites for the attachment of throat constrictor, tongue, and hyoid muscles, usually in therocephalians (Janensch, 1952; Barghusen, 1968; Kemp, 1982). Various branches of the external jaw adductors are often considered to insert on the more dorsal portion of the reflected lamina, specifically in the posterodorsal fossa in gorgonopsians and the dorsal notch in therocephalians (Barghusen, 1968; Kemp, 1969, 1982; King, 1981). Kemp (1982) proposed that a muscle similar in function to the mammalian digastric attached to the reflected lamina and pulled posteroventrally, interpreting thin striations on the surface of the reflected lamina in dinocephalians and dicynodonts as muscle scars associated with his suggested jaw opening function.

The hypothesis that each fossa was a site for the attachment of a specific muscle offers a satisfying explanation for the mostly conserved orientation of the fossae across Therapsida. That said, the existing propositions for the identity of those muscles all suffer from the same shortcoming: a lack of comparison of topographic patterns between therapsid clades. Oftentimes the same fossa is proposed to have different muscular associations in different taxa. For example, Barghusen (1968) placed the insertion for his zygomaticomandibularis muscle in the posterodorsal fossa in gorgonopsians and the possibly homologous U-shaped dorsal notch in therocephalians. He claimed that a reflected lamina with an extensive free dorsal margin could not withstand the tension exerted by this muscle, yet many anomodonts have both a posterodorsal fossa and a free dorsal margin. It is unlikely that these fossae would have retained their orientation if they served as attachments for different muscles between therapsid clades, so any muscles proposed to attach to the angular ridges and fossae should be accounted for in the majority of therapsids. The overall similarity between basal anomodonts and other therapsids is difficult to explain if the ridges and fossae relate to musculature, as anomodonts are the only

non-eucynodont therapsids in which mastication has been inferred, and their jaw musculature was accordingly unique (King, 1988). The repeated loss of fossae is also surprising if each fossa housed a muscle attachment, especially given the high degree of variation in the presence and absence of fossae among some closely-related taxa (Fig. 2.11). Some of this variation may be attributable to differences in preservation, but it is unlikely to explain all of the observed variation. Another issue with this hypothesis is that some of the fossae have shapes or orientations that would likely not serve as useful attachments for any known muscle. The anterodorsal fossa is seen in most non-eucynodont therapsids, but the only muscle that would attach to the mandible from an anterodorsal direction would be the specialized jaw adductor of dicynodonts (analogous with the mammalian masseter; King et al., 1989). This fossa is absent in cynodonts, so even the masseter itself could not have inserted here. Similarly, the anteroventral fossa(e) would only provide a small area of attachment for the usually wide intermandibularis muscles that have been proposed to reside here (Janensch, 1952; Barghusen, 1968). Our systematic survey across Therapsida complicates the hypothesis that the external angular fossae served as sites for muscle attachment.

There are conflicting views on whether the thin reflected lamina could withstand the forces that would be applied to it by muscle action. Some authors assert that this structure was too thin and poorly supported in many therapsids to serve as a muscle attachment site (Maier and Ruf, 2016), although others consider it suitable for smaller throat muscles (Barghusen, 1968). However, some authors have suggested that the corrugations strengthen the reflected lamina against strain from attached muscles (Parrington, 1955), while others favor a more general strengthening function that is not necessarily related to muscle attachments (Allin, 1975; Maier and van den Heever, 2002). However, it is striking that the basic pattern of four fossae and ridges in roughly the same orientations is found across clades with such broadly differing ecologies. The directionality of the fossae and ridges is probably important for their function if they are so highly conserved, which makes it unlikely that their only purpose was to provide

general structural support to the reflected lamina. Importantly, a chief finding of this study is that much of this topography is not located on the reflected lamina itself; it is on the angular body or angular keel, which is often thicker than the reflected lamina and probably did not require the same amount of structural support. The ridges and fossae on the angular probably did not exist solely to strengthen the reflected lamina.

Adding to the confusion surrounding the angular complex is the foramen at the dorsal tip of the vertical ridge in gorgonopsians (Fig. 2.7). This foramen is visible in well-preserved specimens of both early- and late-diverging genera, so it is likely a common feature of Gorgonopsia as a whole. To our knowledge, the function of this foramen has never been addressed in the literature. Its absence in other therapsids suggests that its role in the function of the angular complex was unique to gorgonopsians. Scan data is not sufficient to determine if the impression of a blood vessel is present adjacent to the foramen medially, and so it is unclear if the foramen housed a nerve, blood vessel, or both. Future research on the contents of this foramen would likely further our understanding of the function of the angular complex in gorgonopsians.

Overall, muscle attachment seems incapable of explaining all of the features seen in the morphology of the angular in non-mammalian therapsids. There are areas of the angular cleft in some taxa that would be inaccessible to any known muscle. The four fossae and ridges that were probably plesiomorphic for Therapsida (although possibly excluding dinocephalians; see above) do not have known muscles that could have fit into each of them in every taxon. There is also variation in the presence or absence of the posterodorsal fossa and a subdivision of the anteroventral fossa, even between closely-related taxa. Structural support alone also cannot explain the consistent directionality of the fossae among therapsids. Even a combination of these two does not explain the consistent presence of the anterodorsal fossa on the body of the angular. There was probably an additional function for these structures. The deeply incised angular cleft could be explained by an auditory function, as this space may have been useful as a

resonating chamber for sounds collected by the overlying tissues. The trend towards expanding the angular cleft and freeing the reflected lamina from the angular body in multiple therapsid clades would support this hypothesis, as these changes would likely allow the reflected lamina to vibrate more effectively. However, King (1981) questioned whether the ridges and fossae on the angular would provide any function for a sound receiver, and an auditory function for these surface features has never been proposed to our knowledge. One potential auditory function for the corrugations could be in altering the vibrational qualities of the angular. The shape of an object affects both the way that it vibrates and the way that sound waves reflect off it. The folds of the mammalian pinna serve to alter the sound waves entering the external ear, amplifying biologically relevant frequencies and providing information about the direction of sound sources (Kahana and Nelson, 2006). A similar function could be conceived for the topography of the reflected lamina if it was indeed involved in sound reception, especially if the orientation of the fossae could somehow aid in the perception of directionality. Even the ridges and fossae on the angular body could potentially be useful in this way, depending on how exactly the structure and the tissue around it was vibrating. Similarly, if the resonator hypothesis of Westoll (1943) were true, the corrugations could alter the sounds produced by the angular cleft, although one might expect more interspecific variability if this structure was used in vocal communication with conspecifics. An auditory function for the ridges and fossae of the angular is highly speculative and would require confirmation from biomechanical modeling, but it is the only hypothesis proposed to our knowledge that could potentially explain all aspects of the angular complex. Therefore, it warrants further investigation.

2.6 CONCLUSIONS

The ancestral condition for the surface of the therapsid angular was likely a pattern of four fossae bounded by ridges radiating from a central point, with the position of each fossa

remaining fairly consistent across the major therapsid subclades. Individual fossae and ridges on the angular may be useful phylogenetic characters for assessing the relationships between the major therapsid clades. Alterations to the ancestral topographic pattern generally track phylogeny, with most therapsid subclades having a stereotyped variant of this topographic pattern. The recognition of similarities within and between therapsid clades will allow more informative descriptions of angular topography in new specimens. These similarities also imply functional similarity across non-eucynodont therapsids, and our findings pose several problems for reconstructed muscle attachments on the angular complex. A multi-functional role in hearing and muscular attachment may explain the anatomy of these features.

TABLE 1.1 Specimens figured and discussed in the text. Additional supporting specimens are listed in Appendix 1.

Clade	Identification	Specimen number	Stratigraphic position	Digitization method	Preservation notes
Anomodontia	*"Eodicynodon" oosthuizeni*	BP/1/6230	*Eodicynodon* Assemblage Zone, Karoo Basin, South Africa	Blue light	
	Aulacephalodon bainii	UCMP 42699	*Cistecephalus* Assemblage Zone, Karoo Basin, South Africa	Blue light	
	Cistecephalus microrhinus	BP/1/253	*Cistecephalus* Assemblage Zone, Karoo Basin, South Africa	Blue light	
	Diictodon feliceps	BP/1/356	*Endothiodon* Assemblage Zone, Karoo Basin, South Africa	photograph only	posterior edge of reflected lamina nearly reaches articular
	Diictodon feliceps	CGP/1/1234	*Cistecephalus* Assemblage Zone, Karoo Basin, South Africa	Blue light	
	Emydops arctatus	BP/1/1307	*Endothiodon* Assemblage Zone, Karoo Basin, South Africa		
	Endothiodon bathystoma	SAM-PK-K11131	*Endothiodon* Assemblage Zone, Karoo Basin, South Africa	Blue light	

	Endothiodon bathystoma	SAM-PK-K11134	*Endothiodon* Assemblage Zone, Karoo Basin, South Africa	Blue light	preserves ventral connection with angular body well. Angular keel and posterodorsal reflected lamina missing
	Eosimops newtoni	BP/1/6674	*Tapinocephalus* Assemblage Zone, Karoo Basin, South Africa	Blue light	only examined cast
	Kembawacela kitchingi	NHCC LB18	Upper Madumabisa Mudstone Formation, Luangwa Basin, Zambia	Blue light	
	Lystrosaurus curvatus	BP/1/5086	*Lystrosaurus declivis* Assemblage Zone, Karoo Basin, South Africa	Blue light	ventral edge chipped
	Niassodon mfumukasi	ML1620	K5 formation, Metangula Graben, Niassa Province, Mozambique	CT	not observed in person. Posterior and ventral edges missing
	Oudenodon bainii	BP/1/4260	*Daptocephalus* Assemblage Zone, Karoo Basin, South Africa	Blue light	
	Placerias hesternus	UCMP137369	Placerias Quarry, Chinle Formation, Arizona, USA	Blue light	middle section of reflected lamina is reconstructed
	Pristerodon mackayi	BP/1/6685	*Cistecephalus* Assemblage Zone, Karoo Basin, South Africa	Blue light	
	Pristerodon mackayi	SAM-PK-K10153	*Tropidostoma-Gorgonops* Subzone, Dunedin, Beaufort West, Karoo Basin, South Africa	Blue light	preserves ventral connection with angular body well
	Rhachiocephalus magnus	TM 4456	*Tropidostoma-Gorgonops* Subzone, Karoo Basin, South Africa	Blue light	posterior and dorsal surfaces of reflected lamina poorly preserved
	Robertia broomiana	BP/1/7614	*Endothiodon* Assemblage Zone, Karoo Basin, South Africa	Blue light	matrix in posteroventral fossa
	Stahleckeria potens	AMNH FR3857	Upper Rio do Rasto Formation, Paraná Basin, Brazil	Blue light	only observed cast

	Suminia getmanovi	PIN 2212-62	Kotel'nich locality, Kirov, Russia	photographed only	not observed in person
	Tropidostoma microtrema	SAM-PK-8633	Teekloof Formation, Karoo Basin, South Africa	Blue light	preserves ventral connection with angular body well
	Ulemica invisa	PIN157/1112	Isheevo Subassemblage, Cis-Urals region, Russia	photographed only	not observed in person
Biarmosuchia	*Biarmosuchus tener*	PIN1758/2	Ocher Subassemblage, Cis-Urals region, Russia	photographed only	not observed in person
	Bullacephalus jacksoni	BP/1/5387	*Tapinocephalus* Assemblage Zone, Karoo Basin, South Africa	Blue light	missing ventral edge
	Hipposaurus sp.	CGP/1/66	*Tapinocephalus* Assemblage Zone, Karoo Basin, South Africa	CT	not observed in person
	Lemurosaurus pricei	NMQR 1702	*Cistecephalus* Assemblage Zone, Karoo Basin, South Africa	Blue light	only examined cast
	Paraburnetia sneeubergensis	SAM-PK-K10037	Lowermost *Cistecephalus* Assemblage Zone, upper Teekloof Formation, Karoo Basin, South Africa	Blue light	
Cynodontia	*Galesaurus planiceps*	BP/1/5064	*Lystrosaurus declivis* Assemblage Zone, Karoo Basin, South Africa	Blue light	
	Nshimbodon muchingaensis	NHCC LB277	Upper Madumabisa Mudstone Formation, Luangwa Basin, Zambia	CT	posterior reflected lamina missing
	Probainognathus jenseni	PVSJ410	Ischigualasto Formation, San Juan Province, Argentina	CT	not observed in person
	Procynosuchus delaharpeae	BP/1/226	*Cistecephalus* Assemblage Zone, Karoo Basin, South Africa	Blue light	
	Thrinaxodon liorhinus	BP/1/2513	*Lystrosaurus declivis* Assemblage Zone, Karoo Basin, South Africa	Blue light	
	Thrinaxodon liorhinus	TM81	*Lystrosaurus declivis* Assemblage Zone, Karoo Basin, South Africa	Blue light	mostly broken, but medial view of reflected lamina is visible

	Trirachodon berryi	BP/1/4658	*Trirachodon-Kannemeyeria* Subzone, Karoo Basin, South Africa	Blue light	
Dinocephalia	*"Delphinognathus" conocephalus*	SAM-PK-713	unknown, Cape Province, Beaufort West	Blue light	
	Moschops capensis	AMNH FR5550	*Tapinocephalus* Assemblage Zone, Karoo Basin, South Africa	Blue light	
	Syodon biarmicum	PIN157/2	Isheevo Subassemblage, Cis-Urals region, Russia	photographed only	not observed in person
Gorgonopsia	*Aelurognathus tigriceps*	NHCC LB350	Upper Madumabisa Mudstone Formation, Luangwa Basin, Zambia	Blue light	ventral edge broken
	Arctops willistoni	NHCC LB396	Upper Madumabisa Mudstone Formation, Luangwa Basin, Zambia	Blue light	ventral portion broken and offset from dorsal portion
	Cynariops robustus	MB.R.999	*Tropidostoma/Gorgonops* Subzone, Biesiespoort locality, North Cape Province, Karoo Basin, South Africa	CT	not observed in person
	Cyonosaurus longiceps	BP/1/2598	*Cistecephalus* Assemblage Zone, Karoo Basin, South Africa	Blue light	ventral and posterior edges missing, but ventral connection between reflected lamina and angular body preserved
	Lycaenops n. sp.	NHCC LB178	Upper Madumabisa Mudstone Formation, Luangwa Basin, Zambia	Blue light	ventral edge missing
	Scylacocephalus sp.	NHCC LB177	Upper Madumabisa Mudstone Formation, Luangwa Basin, Zambia	Blue light	ventral edge missing
Sphenacodontidae	*Dimetrodon limbatus*	FMNH UC1001	Briar Creek Bonebed, Nocona Formation, Archer County, Texas, USA	Blue light	
Therocephalia	Pristerognathidae indet.	CGP RMS 1185	*Tapinocephalus* Assemblage Zone, Karoo Basin, South Africa	Blue light	
	Hofmeyria atavus	TM254	*Endothiodon* Assemblage Zone, Karoo Basin, South Africa	Blue light	

	cf. Ictidostoma sp.	BP/1/3155	*Endothiodon* Assemblage Zone, Karoo Basin, South Africa	Blue light	matrix filling some fossae
	Lycosuchus vanderrieti	MB.R.995	*Tapinocephalus* Assemblage Zone, Karoo Basin, South Africa	CT	not observed in person. Ventral edge missing
	Pristerognathus polyodon	SAM-PK-11942	*Diictodon/Styracocephalus* Subzone, Karoo Basin, South Africa	Blue light	posterior edge broken, medial view of reflected lamina visible
	Tetracynodon darti	SAM-PK-K10800	*Lystrosaurus declivis* Assemblage Zone, Karoo Basin, South Africa	Blue light	

3. Independent Origins of a Novel Atympanic Ear Within Chamaeleonidae

3.1 ABSTRACT

The evolution of the vertebrate ear is a complicated story of convergence, co-option, loss of function, and occasional regaining of said function. An incredible variety of structures have been adopted as sound receptors, but only chameleons are known to have a bony airborne sound receiver. In some chameleons, the pterygoid bone captures sound vibrations and relays them to the inner ear via a connection to the extracolumella. The distribution of this unique hearing system has not been examined across Chamaeleonidae. Here, I report on dissections on 12 species across four genera and describe their middle ear anatomy for the first time. Half of these species were found to have a link between their extracolumella and pterygoid, and ancestral state reconstruction supports four independent acquisitions of this novel sound conduction pathway. Species with this pathway tend to have a gular pouch, which seems to produce biotremors and possibly airborne sound, suggesting that this hearing system plays some role in intraspecific communication. Three species were also μ-CT scanned using enhanced contrast to investigate differences in the musculature surrounding the middle ear cavity. In species with a middle ear connected to the pterygoid, the muscles directly lateral to the pterygoid insert farther anterior onto the mandible, which may serve to minimize dampening of vibrations on the pterygoid. Together, these data suggest that the ear plays a more significant role in the lives of some chameleons than has been recognized, and that parallelism is common in the evolution of the ear.

3.2 INTRODUCTION

The ear is arguably the most evolutionarily labile of the vertebrate sensory systems. The sense of hearing can play an important role in navigation and orientation, localization of resources and habitat, detection of prey and predators, and intraspecific communication (Gans, 1992; Fay and Popper, 2000; Fay, 2009; Slabbekoorn, 2018), and this wide range of functions is reflected in its morphology. While the structure of the inner ear is relatively conserved (Popper and Fay, 1997), the pathway by which sound vibrations reach the inner ear from outside the body exhibits astounding variation among vertebrates. Specializations in this pathway typically serve to amplify sound vibrations as they pass to the inner ear (Wever and Lawrence, 1954). Though this amplification is less important for aquatic taxa, many of which lack a specialized pathway, the difference in acoustic impedance between air and water makes such amplification essential for a terrestrial tetrapod ear.

Vertebrates have evolved a myriad of ways to solve the problems of sound amplification and impedance matching. Several teleost lineages have independently evolved anterior extensions of their swim bladder, which amplify sound vibrations that can then spread to the nearby inner ear (Braun and Grande, 2008). In the Otophysi, vibrations in the swim bladder are transmitted to the inner ear via a set of highly specialized vertebrae termed the Weberian apparatus (Fay and Popper, 1974). Most tetrapod middle ears recruit the stapes or columella as a sound conductor, as this bone has a convenient articulation with the otic capsule (Westoll, 1943). Most tetrapods capture sound vibrations using a tympanum exposed to the air. This membrane transfers vibrations to the stapes/columella via the bony malleus and incus in extant mammals and the cartilaginous extracolumella in amphibians, reptiles, and birds. The ratio of the area of the tympanic membrane to that of the stapes/columella footplate is great enough to amplify vibrations and allow the detection of airborne sound (Wever and Lawrence, 1954). Evidence from embryonic development and the fossil record demonstrates that the tympanum

and its connection with the middle ear ossicle(s) has evolved multiple times throughout Tetrapoda (Lombard and Bolt, 1979; Clack, 1993; Martin and Luo, 2005; Kitazawa et al., 2015). However, many tetrapods do not rely solely on the tympanum for sound reception, and several clades have lost the tympanum entirely, sometimes replacing it with another means of sound reception. Frogs and salamanders have evolved the operecularis system, in which the operecularis muscle is hypothesized to communicate vibrations to the operculum and/or stapes to be relayed to the inner ear (Capshaw and Soares, 2016). This system is especially labile in taxa with relaxed selection for intraspecific communication. Some atympanic frogs use the resonant properties of their mouth to amplify mating call frequencies and divert those vibrations directly to the tissue surrounding the otic capsule (Boistel et al., 2013). Amphisbaenid lizards lack a tympanum, so the extracolumella instead extends into the skin of the lower jaw beneath a large, shield-like scale capable of transmitting airborne sound (Toerien, 1963; Wever, 1978). Odontocetes use fat masses around their mandible and throat to divert high-frequency echolocation signals to their inner ear (Cranford et al., 2008). The diverse structures that constitute the vertebrate ear provide a fascinating system for studying evolutionary processes like convergence, co-option, and novelty.

One of the most distinctive sound conduction pathways is found in several species of chameleon. The tympanum has been lost in all chameleons, possibly as a result of specializations in the feeding apparatus (Tucker, 2017), so the ears of most chameleons can only detect substrate vibrations through bone conduction (Wever, 1978). As a result, the middle ear is vestigial in many chameleons, its structures reduced or sometimes completely obliterated (Siebenrock, 1893; Brock, 1940; Engelbrecht, 1951; Frank, 1951; Toerien, 1963). However, early anatomical descriptions of *Chamaeleo chamaeleon* document a well-developed middle ear cavity and columella (Parker, 1881; Versluys, 1898), which prompted a series of dissections and physiological experiments by Wever (1968, 1969, 1978) that demonstrated that several chameleons have adopted alternate routes for sound transmission. Members of the genus

Chamaeleo were found to have an anterior process of the extracolumella that attaches to the quadrate ramus of the pterygoid, which in all chameleons is dorsoventrally expanded into a thin plate with an unossified membrane at the posterior end contacting the quadrate. His experiments showed that vibrations passing through the tissue of the side of the head are collected by the wide pterygoid plate and associated membrane and directed to the inner ear via the extracolumella and columella, which allows these animals to hear low frequency sounds (~200–600 Hz) almost as well as lizards with tympanic ears (Wever, 1968, 1978). Some members of the genera *Trioceros* and *Kinyongia* instead have an extracolumella that is partially embedded in the depressor mandibulae, which acts as a sound receiver in these species, albeit a less effective one than the pterygoid plate (Wever, 1969, 1978). This second pathway is partially present in *Chamaeleo*, as well, though the connection between the extracolumella and the depressor mandibulae is weaker and less useful for sound conduction (Wever, 1978).

Recent work has demonstrated that several species within the genera *Bradypodion*, *Chamaeleo*, *Furcifer*, and *Trioceros* use their gular pouch to produce vibrations to communicate with conspecifics (Huskey et al., 2020). Species in which Wever found a connection between the extracolumella and pterygoid plate were also shown to have a well-developed gular pouch. Species lacking this connection also lacked a gular pouch. The presence of a gular pouch in several genera other than *Chamaeleo* raises the possibility that the pterygoid ear is more widespread within Chamaeleonidae than previously thought. An expanded survey of chameleon middle ear anatomy is therefore timely, as it may reveal a complex evolutionary history of the chameleon ear and its role in social behavior.

I performed dissections on museum specimens of a wide array of chameleons to assess how widespread the pterygoid ear is within Chamaeleonidae. I also μ-CT scanned specimens of three species using the diffusible iodine-based contrast-enhanced computed tomography (diceCT) technique of Gignac et al. (Gignac and Kley, 2014; Gignac et al., 2016) to further investigate the morphology of the middle ear cavity. These scans were used to compare the

arrangements of jaw adductor muscles surrounding the pterygoid plate between species that are hypothesized to use this bone for hearing and those that are not.

3.3 MATERIALS AND METHODS

3.3.1 Materials

All specimens were from museums or university teaching collections. They were acquired by wild capture or donations from zoos or pet trade breeders. The following species were dissected: *Chamaeleo calyptratus, Ch. gracilis*, *Ch. gracilis* or *Ch. senegalensis*, *Ch. zeylanicus*, *Calumma brevicorne*, *Furcifer lateralis*, *F. oustaleti*, *F. pardalis*, *F. verrucosus*, *Kinyongia multituberculata*, *Trioceros cristatus*, *T. ellioti*, *T. jacksonii*, *T. johnstoni*, *T. melleri*, and *T. montium* (see Appendix 1 for details of each specimen). Most dissected specimens were formalin fixed and stored in alcohol, but the specimens at VTPE and UWBM were frozen and thawed.

The breeder from which VTPE acquired the *Kinyongia* specimen used in this study listed the species as *K. fischeri*. However, DNA evidence has revealed a multitude of species that were once lumped together under this species name, and it is unlikely that this specimen represents a true member of *K. fischeri* (Mariaux et al., 2008). Using the identification key provided by that study, the VTPE specimen is identified as *K. multituberculata* based on the posterior extent of the dorsal crest and the presence of horns in a female.

3.3.2 Methods

This work will follow terminology used by Wever (1978) for chameleon ear structures and Anderson and Higham (2013) for muscles.

Specimens from the FMNH, UF, and UWBM were dissected at the University of Washington under a Wild M5 dissecting microscope and imaged using Leica Acquire V1.0 (©

Leica Microsystems, Buffalo Grove, IL, U.S.A.) on a Leica M125 microscope. Photographs of these specimens were taken with a Canon macro lens EF 100 mm. I dissected the lateral side of the head on the left side of each specimen (photos were mirrored to conform to intuitive anatomical directions). The skin was cut along the medial edge of the mandible and the posterolateral edge of the quadrate (Appendix 2). Connective tissue was cut between the depressor mandibulae and the hyoid apparatus to access the middle ear cavity. Gently prying the side of the head away from the rest of the body allowed observation of the columella. This bone, along with the associated extracolumella, was contained within a membrane, which was carefully removed for the clarity of the photographs.

Ancestral state reconstruction was implemented to explore the evolutionary history of the pterygoid ear in chameleons. Presence or absence of a pterygoid ear was revealed by dissections in this study or noted in the pre-existing literature (Appendix 3). Species known to have a heavily reduced columella were assumed to lack a pterygoid ear, as vibration transfer to the inner ear would be nearly impossible without a functioning columella. This analysis used the phylogeny of Tolley et al. (2013). I used the stochastic character mapping method of Huelsenbeck et al. (2003), which uses a Markov chain Monte Carlo approach to generate posterior probabilities for trait distribution. This procedure was replicated 100 times, and the combined posterior probability was used to assess the likelihood of evolutionary scenarios. The analysis was completed using the programming language R (v. 3.5.3, R Core Team, 2019) and the package phytools (Revell, 2012).

Three species were μ-CT scanned to visualize the middle ear cavity and surrounding tissues: *Ch. chamaeleon*, *Ch. senegalensis*, and *T. jacksonii* (see Appendix 4 for details of each specimen). These specimens were initially fixed in formalin and then stored in a 70% ethanol solution. The *T. jacksonii* specimen (UWBM 8333) has been stored since 1976, so it exhibits more tissue degradation than the other specimens. It should be noted that the *Ch. chamaeleon* specimen (UCMVZ 2364801) was somewhat smaller than the typical adult size for this species

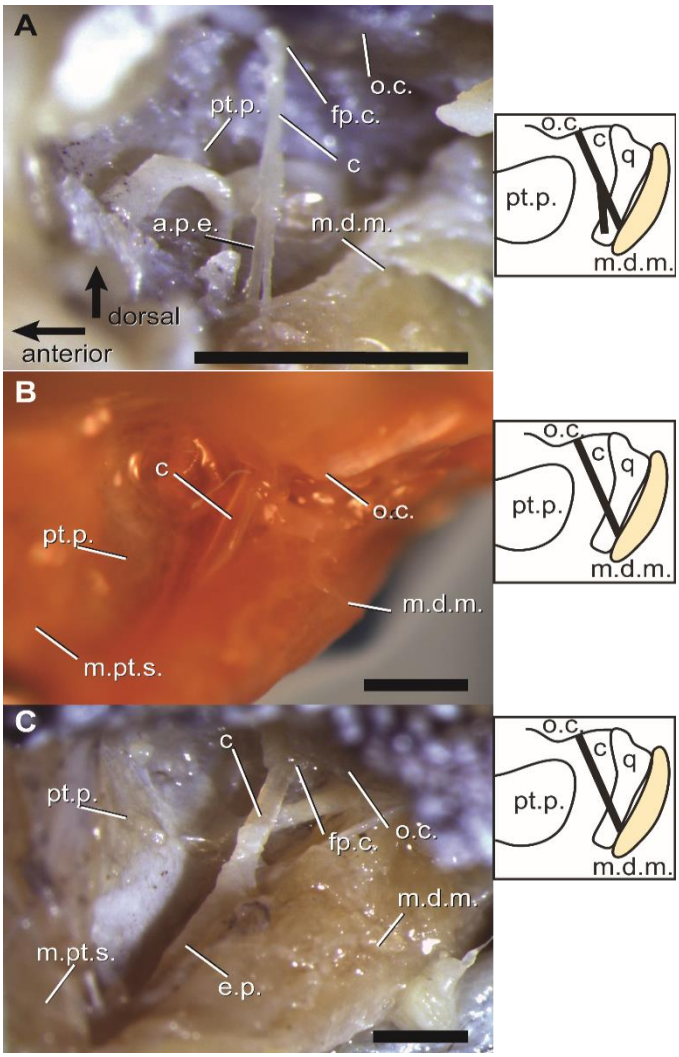

FIGURE 3.1. Middle ear dissections of chameleons with no pterygoid ear in the genus *Trioceros* in medial view, showing the extracolumella morphology. **A)** *Trioceros ellioti*; **B)** *Trioceros jacksonii*; **C)** *Trioceros johnstoni*. Schematics summarize the relevant morphology in each species. The columella and extracolumella are represented by a thick, black bar in the schematics. Scale bars 1 mm.

Abbreviations: a.p.e. = anterior process of the extracolumella; **c** = columella; **e.p.** = extracolumellar plate; **fp.c.** = footplate of the columella; **m.d.m.** = depressor mandibulae muscle; **m.pt.s.** = pterygoideus muscle superficial head; **o.c.** = otic capsule; **pt.p.** = pterygoid plate; **q** = quadrate.

and may not have reached full maturity. Scans were performed using the diceCT method of Gignac et al. (Gignac and Kley, 2014; Gignac et al., 2016). Each specimen was scanned once without staining to get an isolated model of the skull and mandible. These initial scans were conducted at Friday Harbor Laboratories using a Skyscan 1173 scanner and the following parameters: voltage 65 kV, current 123 µA, voxel size 44 (*Ch. chamaeleon* and *Ch. jacksonii*) and 47 (*Ch. senegalensis*) µm. I used Avizo V9.2.0 (© FEI VSG, Hillsboro, OR, U.S.A.) to isolate the skulls and mandibles in the scan via grayscale thresholding and create surface renderings. The specimens were then soaked in a 3% w/v Lugol's iodine (I_2KI) solution for six weeks, and this solution was replaced every two weeks. Scans were taken at two and four weeks into the soaking process at the University of Washington Computed Tomography Facility using an NSI X5000 scanner. When the muscles had reached a

sufficient level of contrast, the specimens were scanned a final time with the Skyscan 1173 scanner with the following parameters: voltage 65 kV, current 122 μA, voxel size 35 μm. Avizo was again used to manually segment all muscles surrounding the middle ear cavity and generate surface renderings. The mandible, quadrate, and pterygoid were also segmented in the final scan to aid in aligning the muscular and skeletal models, which was executed manually in Meshmixer V3.5.474 (©Autodesk, San Rafael, CA, U.S.A.).

3.4 RESULTS

3.4.1 Dissections

The middle ear cavity is well-developed in all the species studied. As has been previously described in chameleons, the middle ear cavity is mostly separate from the pharynx, which is atypical in lizards (Wever, 1978; Christensen-Dalsgaard, 2011). The cavity is bounded laterally by the superficial head of the pterygoideus muscle, the pterygoid plate, and its associated membrane (Figs. 2.1–2.4). Spanning this cavity is the columella, a simple rod with a footplate situated in the fenestra ovalis of the otic capsule. None of the specimens dissected here displayed reduction of the columella. The distal end of the columella is flush with the cartilaginous extracolumella, which extends to the quadrate. Both the columella and extracolumella reside within a thin membrane, as in other lizards (Peterson, 1966). The extracolumella nestles between the quadrate and depressor mandibulae, and here it has a ligamentous connection to the quadrate. The extracolumella is expanded into a plate at its distal end.

As noted by previous work, *T. jacksonii* has no connection between the extracolumella and the pterygoid plate or membrane, and there is no distinct separation between the anterior and posterior processes of the extracolumella (Fig. 3.1B; Wever, 1969). This morphology is also seen in *Ca. brevicorne, T. johnstoni*, *F. lateralis*, *F. oustaleti*, *F. verrucosus, K. multituberculata*

(Figs. 3.1C, 3.2). *T. ellioti* does have an extracolumella divided into an anterior process and a posterior process, as in *Chamaeleo*, but its anterior process does not contact the pterygoid plate or membrane (Fig. 1A). Instead, the anterior process connects to the quadrate, while the

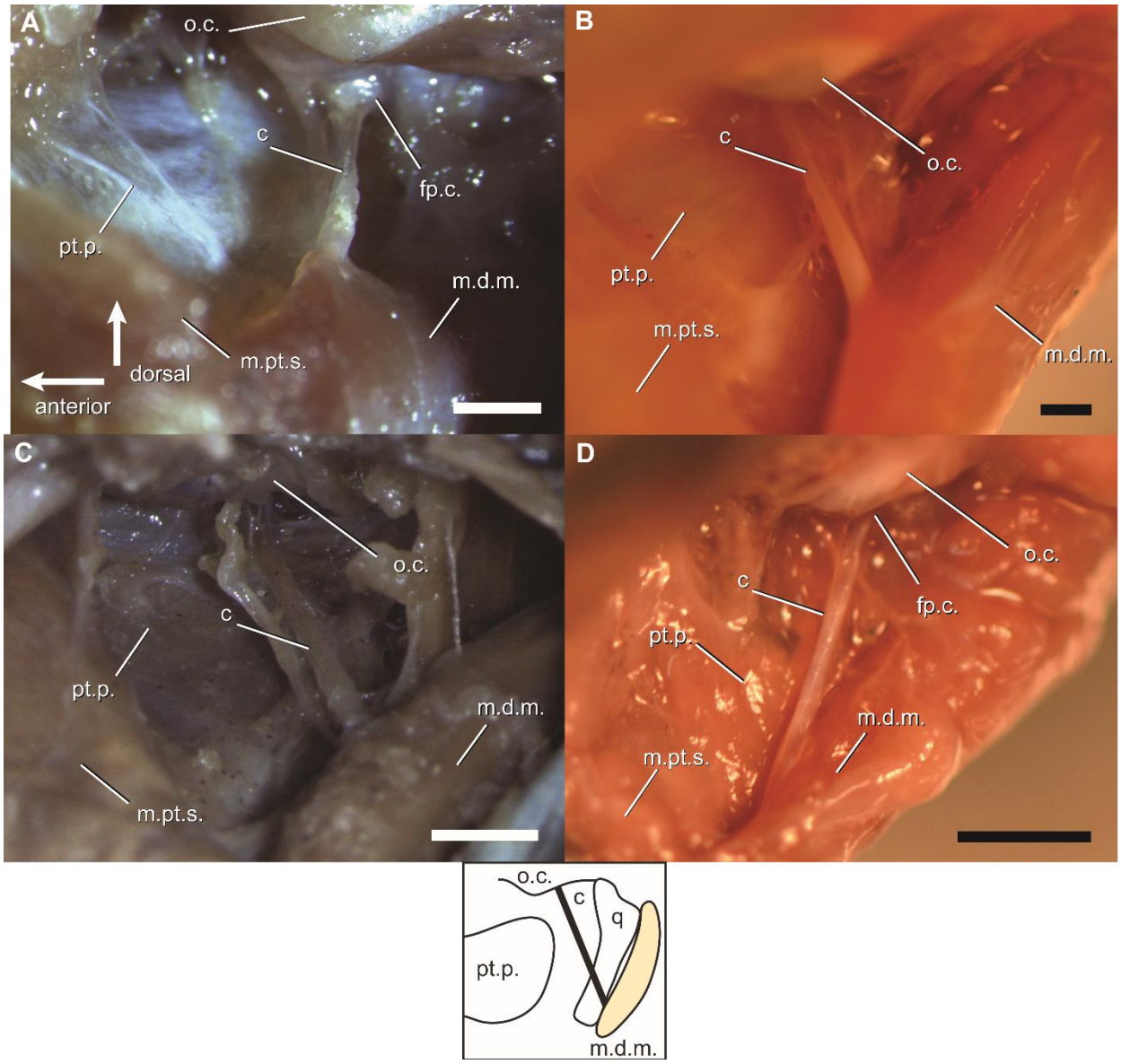

FIGURE 3.2. Middle ear dissections of chameleons with no pterygoid ear in several genera in medial view, showing the extracolumella morphology. **A)** *Calumma brevicorne* (mirrored); **B)** *Furcifer oustaleti* (mirrored); **B)** *F. verrucosus*; **D)** *Kinyongia multituberculata* (mirrored). Schematic summarizes the relevant morphology in all species. The columella and extracolumella are represented by a thick, black bar in the schematic. Scale bars 1 mm. **Abbreviations: c** = columella; **fp. c.** = footplate of the columella; **m.d.m.** = depressor mandibulae muscle; **m.pt.s.** = pterygoideus muscle superficial head; **o.c.** = otic capsule; **pt.p.** = pterygoid plate; **q** = quadrate.

posterior process connects to the depressor mandibulae. These two processes are more defined than they appear to be in Wever's (1978) drawings. The extracolumellar plate of *Ca. brevicorne* is embedded into the depressor mandibulae (Fig. 3.2A). In specimens lacking the pterygoid hearing mechanism, physically pressing against the auditory area at the side of the head did not result in the displacement of the columella.

Previous work has documented a connection between the anterior process of the extracolumella and the pterygoid plate in *Ch. calyptratus* (Wever, 1978), which is confirmed here (Fig. 3.3A). An anterior process contacting the membrane extending from the pterygoid plate was also seen in *Ch. chamaeleon* (Fig. 3.3B), confirming the findings of Wever (1978) and contradicting those of Versluys (1898). This specialized ear arrangement was found in two additional members of the genus *Chamaeleo*: *Ch. gracilis* and *Ch. zeylanicus* (Fig. 3.3C, D). A connection between the extracolumella and the pterygoid plate or membrane was also seen in several species outside this genus: *F. pardalis*, *T. cristatus*, *T. melleri*, and *T. montium* (Fig. 3.4). In species with an anterior process, the extracolumella still forms a plate attached to the quadrate. The extracolumella also forks anteriorly to contact the pterygoid plate or membrane just posterior to the edge of the superficial head of the pterygoideus. This part of the pterygoid is free from muscle attachments. In addition to this anterior process, some of these species also have elaborations of their extracolumellar plate that provides greater contact with the quadrate and/or depressor mandibulae. In *F. pardalis*, the extracolumellar plate is widened into a cup that fits snugly around the depressor mandibulae, reaching the dorsal end of the quadrate (Fig. 3.4A). In *T. melleri*, the extracolumellar plate is greatly expanded dorsoventrally along the full height of the quadrate and depressor mandibulae (Fig. 3.4C). The morphology in *T. cristatus* is especially unique, as the columella and extracolumella articulate at a distinct joint rather than grading into one another as seen in the other studied taxa (Fig. 3.4B). In all species in which the anterior process of the columella contacts the pterygoid plate or membrane, pressing against the auditory area at the side of the head caused displacement of the columella.

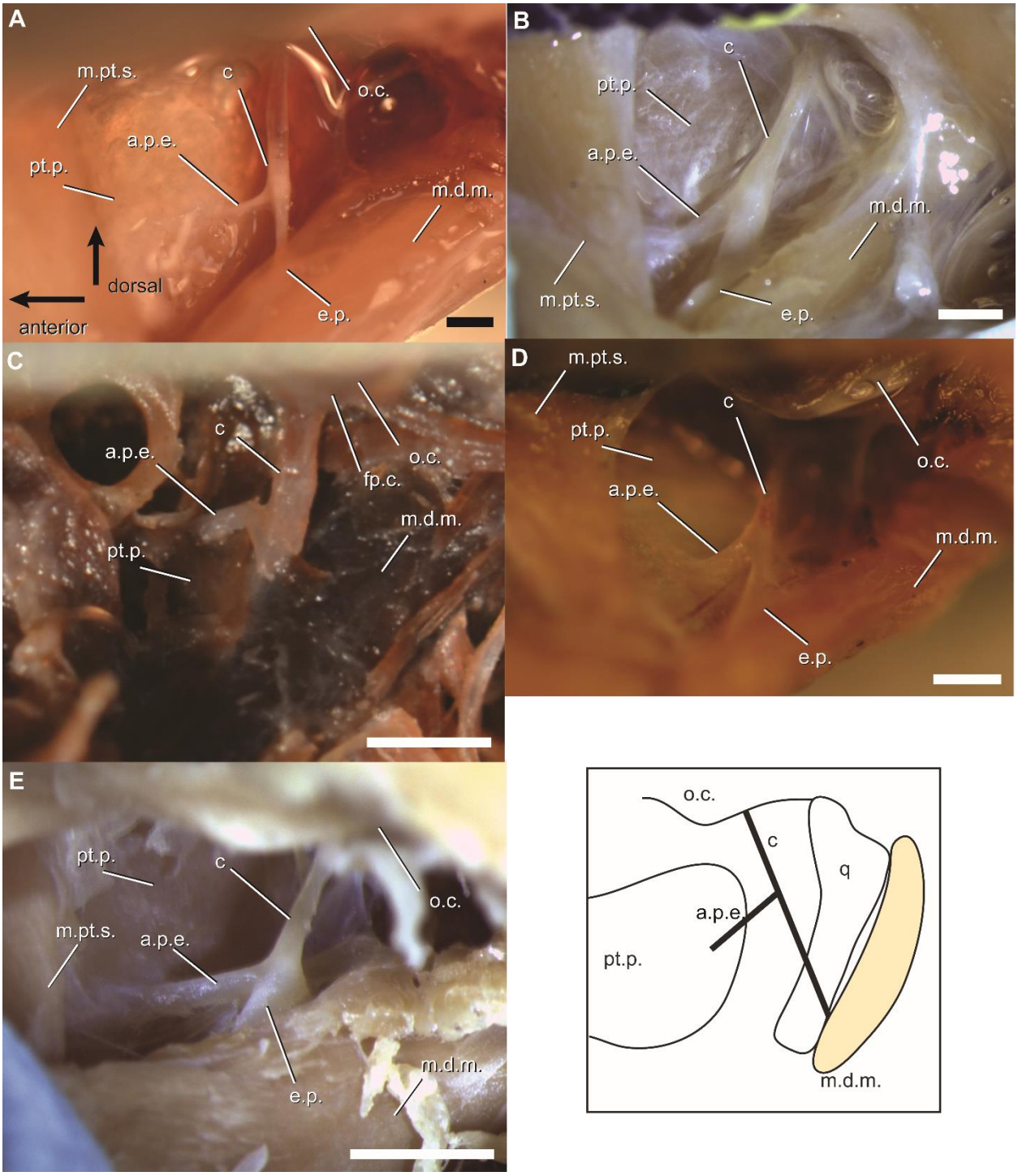

FIGURE 3.3. Middle ear dissections of chameleons with a pterygoid ear in the genus *Chamaeleo* in medial view, showing the extracolumella morphology. **A)** *Ch. calyptratus* (mirrored); **B)** *Ch. chamaeleon*; **C)** *Ch. gracilis*; **D)** *Ch. gracilis* or *senegalensis* (mirrored); **E)** *Ch. zeylanicus*. Schematic summarizes the relevant morphology in all species. The columella and extracolumella are represented by a thick, black bar in the schematic. Scale bars 1 mm. **Abbreviations: a.p.e.** = anterior process of the extracolumella; **c** = columella; **e.p.** = extracolumellar plate;

fp.c. = footplate of the columella; **m.d. m.** = depressor mandibulae muscle; **m.pt.s.** = pterygoideus muscle superficial head; **o.c.** = otic capsule; **pt.p.** = pterygoid plate; **q** = quadrate.

3.4.2 Ancestral state reconstruction

Posterior probabilities from ancestral state reconstruction strongly favor multiple independent acquisitions of a pterygoid-based hearing system (Fig. 3.5). This system was likely present in the common ancestor of all modern *Chamaeleo* species. It also probably arose at least twice in the genus *Trioceros* and once in *Furcifer*.

3.4.3 DiceCT scans

Only the muscles near the middle ear cavity were segmented. The different slips of the adductor mandibulae externus are not readily distinguishable in the scans, but the size and position of the muscles in these groups is similar between species (Fig. 3.6). Deep to these muscles are the adductor posterior and the two slips of the pseudotemporalis. In *T. jacksonii*, the adductor posterior inserts on the dorsomedial surface of the surangular, just anterior to the jaw joint, but in *Ch. senegalensis* this insertion is farther anterior near the coronoid process (Fig. 3.6). The insertion areas for the pseudotemporalis superficialis and pseudotemporalis profundus are also restricted to a more anterior position in *Ch. senegalensis*, whereas they have a broad insertion in *T. jacksonii*. The result of these two differences is that in *Ch. senegalensis*, there are fewer layers of muscle lateral to the pterygoid plate towards its posterior end, providing a more open cavity surrounding the pterygoid plate. *Ch. chamaeleon* has a broad insertion of the adductor posterior, but the insertions for the pseudotemporalis superficialis and pseudotemporalis profundus are anteriorly restricted as in *Ch. senegalensis*. The superficial head of the pterygoideus is virtually identical between the species examined here (Fig. 3.7). The deep head of this muscle is also similar between species. The scan of *Ch. senegalensis* indicates

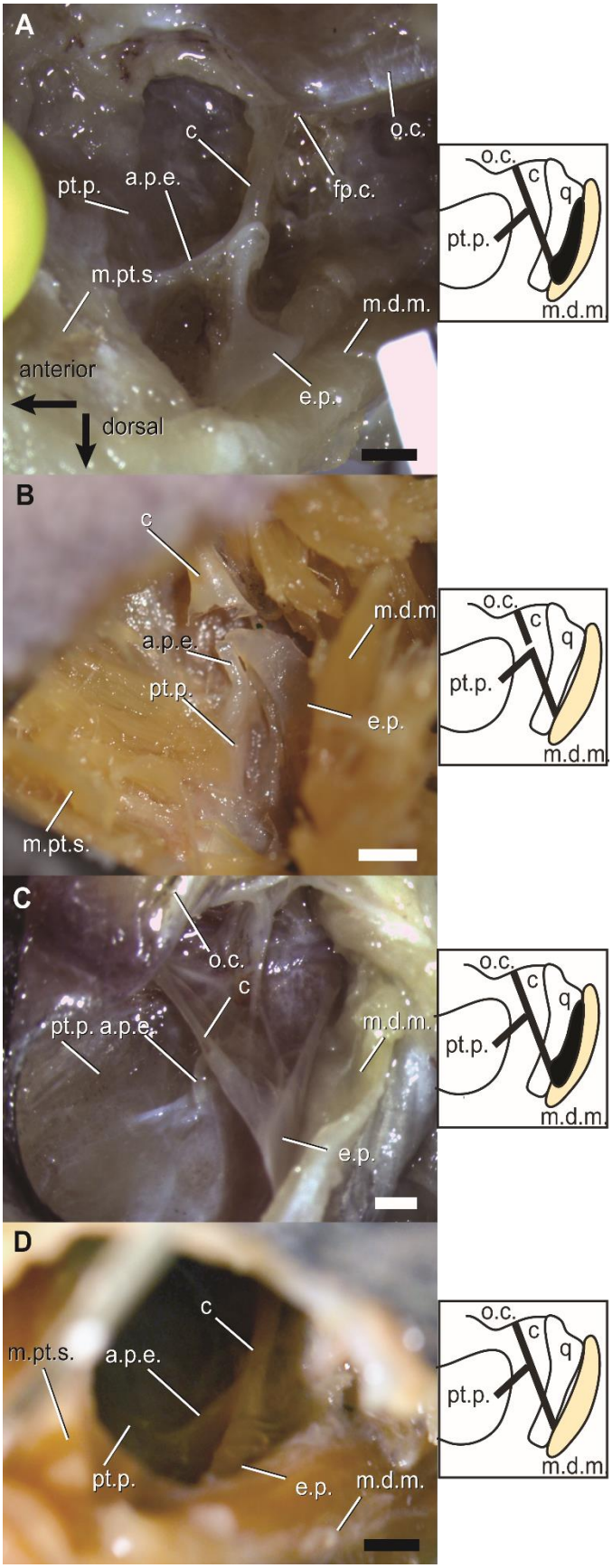

four separate slips of this muscle (Figs. 3.6, 3.7), but it is unclear whether this reflects wear and tear on the specimen or an actual subdivision of the muscle. The contralateral muscle also appears to be subdivided in this specimen. Muscles directly attached to the pterygoid plate are the adductor posterior and both heads of the pterygoideus. The wall of the pharynx also lies against the dorsomedial portion of the pterygoid plate (Fig. 3.7).

FIGURE 3.4. Middle ear dissections of chameleons with a pterygoid ear in several genera in medial view, showing the extracolumella morphology. **A)** *Furcifer pardalis*; **B)** *Trioceros cristatus*; **C)** *T. melleri*; **D)** *T. montium*. Schematics summarize the relevant morphology in each species. The columella and extracolumella are represented by a thick, black bar in the schematics. Scale bars 1 mm. **Abbreviations: a.p.e.** = anterior process of the extracolumella; **c** = columella; **e.p.** = extracolumellar plate; **fp.c.** = footplate of the columella; **m.d.m.** = depressor mandibulae muscle; **m.pt.s.** = pterygoideus muscle superficial head; **o.c.** = otic capsule; **pt.p.** = pterygoid plate; **q** = quadrate.

3.5 DISCUSSION AND CONCLUSIONS

3.5.1 The evolutionary history of the chameleon ear

To my knowledge, the chameleon ear has not been formally described in the literature since Wever's (1978) work. Since that time, chameleon phylogeny has undergone substantial changes. The genus *Chamaeleo* once comprised the majority of chameleon diversity, but detailed morphological research and application of molecular phylogenetics led to its subdivision into the genera *Bradypodion, Calumma, Chamaeleo*, *Furcifer, Kinyongia, Nadzikambia,* and *Trioceros* (Klaver and Böhme, 1986; Tilbury et al., 2006; Tilbury and Tolley, 2009). These genera form a monophyletic clade, in which *Bradypodion* is the earliest-diverging genus (Tolley et al., 2013; Fig. 3.5). There are only a few genera outside this clade, including the 'pygmy chameleons' *Brookesia* and *Rhampholeon* (Tilbury, 2013).

The presence of a well-developed middle ear cavity and columella in all the specimens dissected here is interesting because these structures are commonly reduced or absent in chameleons (Siebenrock, 1893; Brock, 1940; Frank, 1951; Toerien, 1963). However, these studies only documented the reduction of middle ear structures in the genera *Bradypodion*, *Brookesia*, and *Rhampholeon*, all of which lie outside the clade encompassing the sample in this study (Fig. 3.5). It is thus likely that the common ancestor of this clade retained the middle ear cavity and columella. It is possible that these middle ear structures were retained because this ancestor used the depressor mandibulae hearing system, as this hearing system is known to occur in at least some members of *Chamaeleo*, *Trioceros*, and *Kinyongia* (Wever, 1978). The expanded extracolumellar plate overlapping or embedded in the depressor mandibulae in *Ca. brevicorne*, *F. pardalis*, and *T. melleri* suggests the use of this structure as an additional sound receptor by these species. The depressor mandibulae has no major role in hearing in *Ch. dilepis* and *T. jacksonii* (Wever, 1978), but that may represent a secondary loss of this feature. This study focused on the pterygoid hearing system, so the depressor mandibulae was not thoroughly

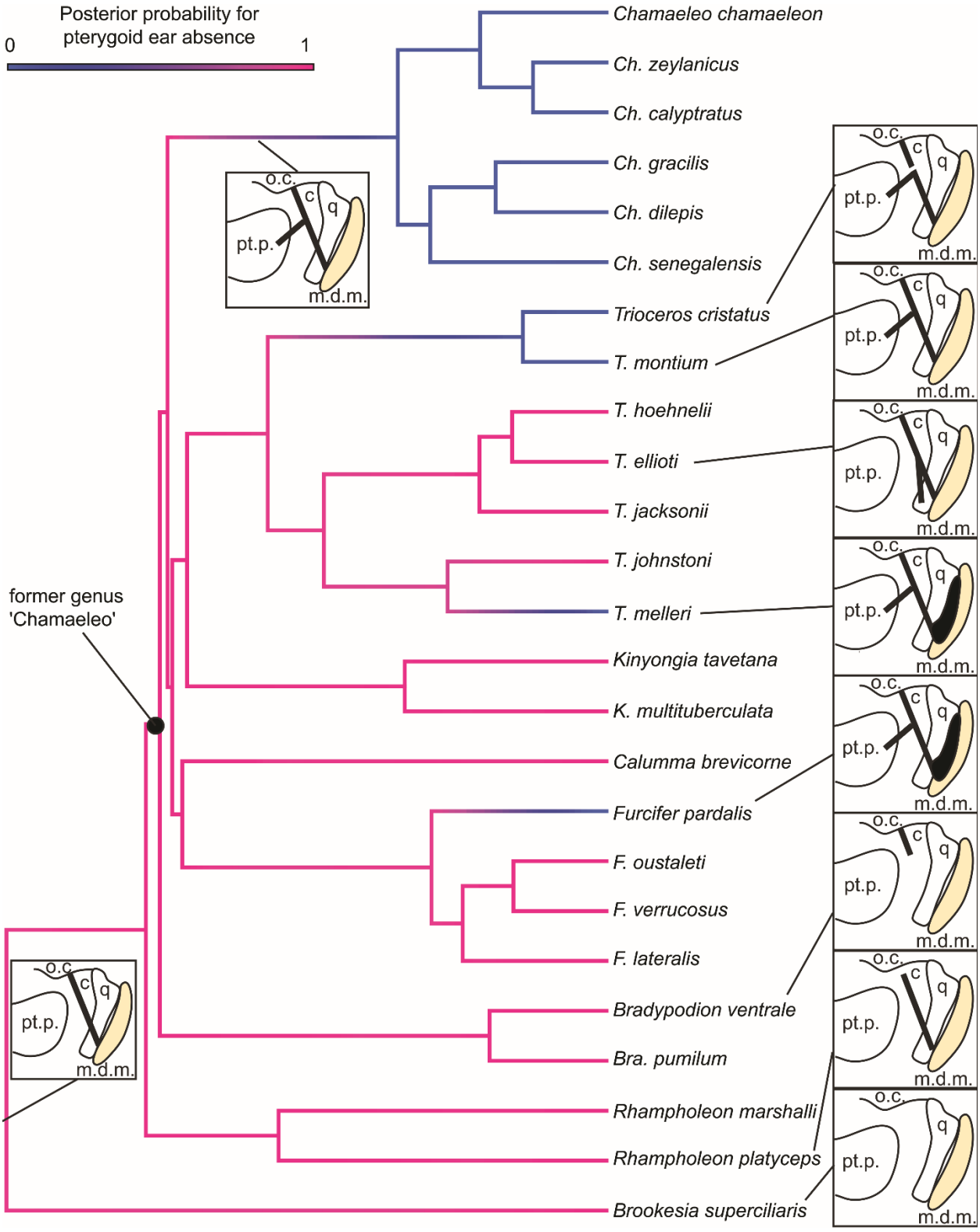
Posterior probability for pterygoid ear absence
0
1
Chamaeleo chamaeleon
Ch. zeylanicus
Ch. calyptratus
Ch. gracilis
Ch. dilepis
Ch. senegalensis
Trioceros cristatus
T. montium
T. hoehnelii
T. ellioti
T. jacksonii
T. johnstoni
T. melleri
Kinyongia tavetana
K. multituberculata
Calumma brevicorne
Furcifer pardalis
F. oustaleti
F. verrucosus
F. lateralis
Bradypodion ventrale
Bra. pumilum
Rhampholeon marshalli
Rhampholeon platyceps
Brookesia superciliaris
former genus 'Chamaeleo'
o.c.
c
q
pt.p.
m.d.m.

FIGURE 3.5. Phylogenetic tree of Chamaeleonidae with posterior probabilities for the presence or absence of a pterygoid ear. Schematics summarize differences in middle ear morphology. Tree based on Tolley et al., 2013. **Abbreviations: c** = columella; **m. d.m.** = depressor mandibulae muscle; **o.c.** = otic capsule; **pt.p.** = pterygoid plate; **q** = quadrate.

investigated. Further research into the distribution of the depressor mandibulae hearing system would help clarify the evolutionary history of the chameleon middle ear.

A connection between the extracolumella and the pterygoid does not necessarily mean that the latter was used for sound reception. However, physiological experiments have demonstrated that this connection transmits sound to the inner ear, where cochlear potentials are generated in response (Wever, 1978), and there is no reason to expect this to differ in the species examined here. Mechanical stimulation of the auditory area during dissection was observed to cause displacement of the columella in all specimens with a connection to the pterygoid, an observation that has been made for other chameleons with a pterygoid ear (Wever, 1968, 1978), so vibrations in the pterygoid would certainly have been transmitted to the inner ear. It is reasonable to assume that these vibrations could stimulate a response from the inner ear, as has been seen in Wever's work.

Ancestral state reconstruction indicates that the pterygoid plate hearing system almost certainly evolved independently at least four times within Chamaeleonidae (Fig. 3.5). The variation in morphology of the extracolumella and its interactions with the pterygoid and depressor mandibulae may reflect different anatomical or developmental constraints governing the evolution of this feature in each lineage. The forked extracolumella of *T. ellioti* bears a striking similarity to those of chameleons with a pterygoid hearing system. This could indicate that the ancestor of *T. ellioti* had a pterygoid ear, but the connection between the anterior process and the pterygoid was lost. However, this scenario is unlikely because none of the close relatives of *T. ellioti* use their pterygoid for hearing (Wever, 1969), and ancestral state reconstruction does not support the presence of the pterygoid ear in its ancestor (Fig. 3.5). It is

more likely that the well-defined anterior process in this species arose to allow stabilization of the columella against the quadrate while the posterior process transfers vibrations from the depressor mandibulae. The presence of an anterior process of the extracolumella in this species

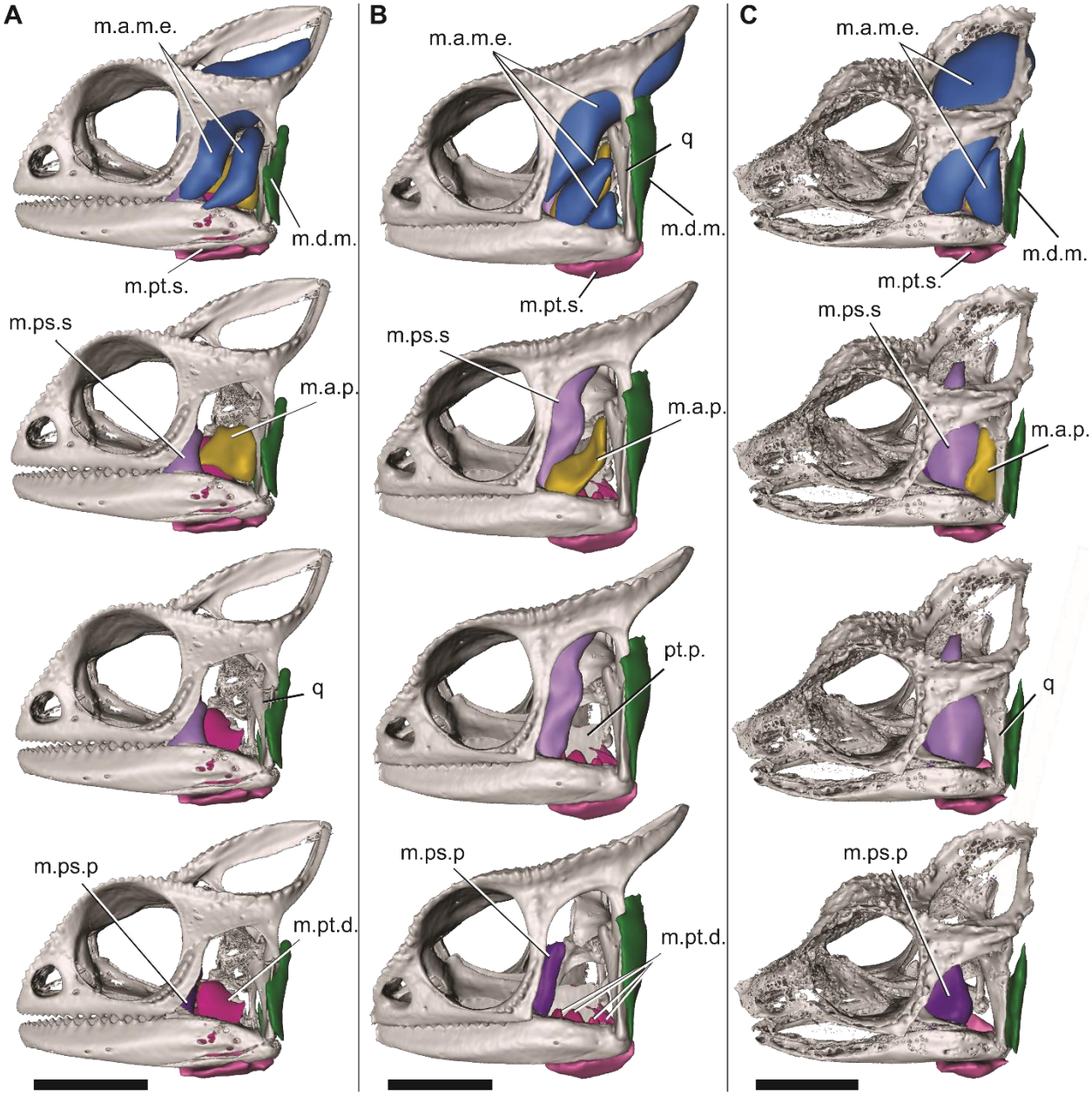

FIGURE 3.6. Segmented diceCT scans in left lateral view showing muscles in close proximity to the middle ear cavity in chameleons. **A)** *Chamaeleo chamaeleon*; **B)** *Ch. senegalensis*; **C)** *Trioceros jacksonii*. Superficial muscles are successively removed down the page to reveal deeper muscles. Scale bars 1 cm. **Abbreviations: m.a.m.e.** = adductor mandibulae externus muscle; **m.a.p.** = adductor posterior muscle; **m.d.m.** = depressor mandibulae muscle; **m.ps.p.** = pseudotemporalis profundus muscle; **m.ps.s.** = pseudotemporalis superficialis muscle; **m.pt.d.** = pterygoideus muscle deep head; **m.pt.s.** = pterygoideus muscle superficial head.

may indicate that this morphology results from simple changes in the development of the extracolumella, which could explain why this morphology was able to evolve independently in *Chamaeleo*, *Trioceros*, and *Furcifer*.

Though the acquisition of a novel hearing system seems complex, the structure of the skull might make such sound conduction pathways relatively easy to establish. The contact between the columella/stapes and the otic capsule is deeply entrenched in vertebrate ancestry

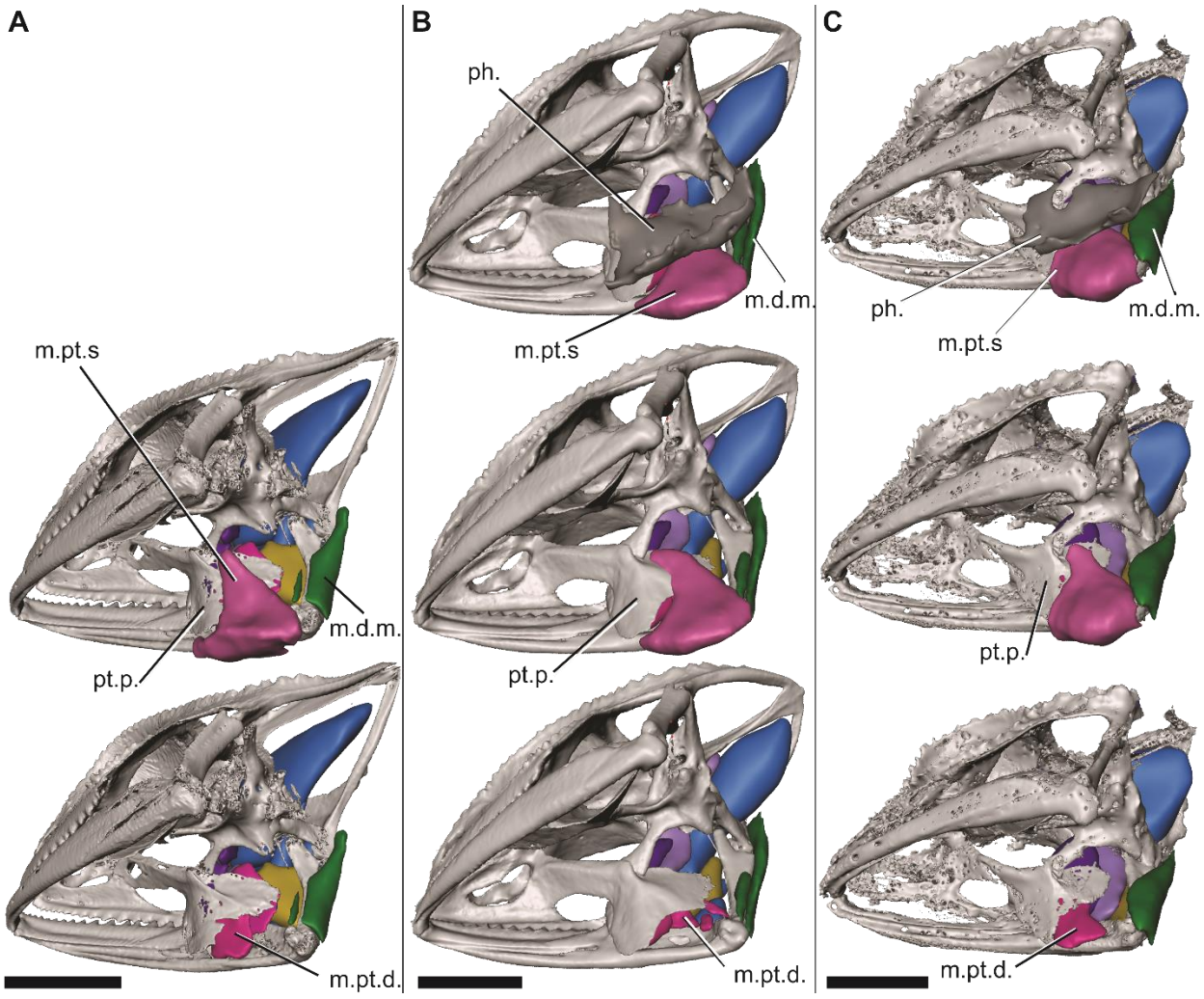

FIGURE 3.7. Segmented diceCT scans in oblique ventromedial view showing pharyngeal wall and muscles in close proximity to the middle ear cavity in chameleons. **A)** *Chamaeleo chamaeleon*; **B)** *Ch. senegalensis*; **C)** *Trioceros jacksonii*. Superficial structures are successively removed down the page to reveal deeper muscles. Scale bars 1 cm. Anterior is to the left. **Abbreviations: m.d.m.** = depressor mandibulae muscle; **m.pt.d.** = pterygoideus muscle deep head; **m.pt.s.** = pterygoideus muscle superficial head; **ph.** = pharyngeal wall.

(Reichert, 1837; Gaupp, 1911), and it provides a conveniently direct pathway by which sound can reach the inner ear. Any link between the columella/stapes and a nearby structure with suitable acoustic properties (e.g., wide surface area, minimal mechanical loading) will result in amplified sound vibrations reaching the inner ear. After such a connection is established, the middle ear may gain basic functionality and become "visible" to selection, allowing further refinement. An example of this can be seen in the evolution of the mammalian middle ear. The sound conduction pathway seen in extant mammals was likely present in their ancestors, but the connection between the middle ear ossicles and the dentary likely hindered its ability to transmit vibrations (Allin and Hopson, 1992). A complete separation between these ossicles and the dentary was accomplished independently at least three times within crown Mammalia, probably requiring only a single genetic change (Martin and Luo, 2005; Urban et al., 2017). Chameleons now provide an additional example of simple evolutionary changes resulting in parallel acquisition of a novel hearing apparatus, as any connection between the extracolumella and the nearby pterygoid will unlock a potential pathway for sound conduction. If the association between the stapes/columella and the otic capsule indeed facilitates the assembly of a functional ear, we may expect to find parallelism in the evolution of other vertebrate hearing systems.

3.5.2 Potential interactions between ear and jaw adductor anatomy

The arrangement of the jaw adductor musculature was overall similar among the scanned specimens, but the following differences may be related to specializations in the sound conduction pathway. The insertions for both slips of the pseudotemporalis are farther posterior in *T. jacksonii* than in *Ch. chamaeleon* and *Ch. senegalensis*. The latter also has an anteriorly-restricted insertion for the adductor posterior. While this pattern could reflect variation in diet and/or jaw adductor function, it may be related to the ear anatomy in these species. A notable consequence of these differences is that there are fewer muscle layers overlying the posterior

end of the pterygoid plate and its associated membrane in *Chamaeleo* than in *T. jacksonii*. The space immediately lateral to the sound receiver in *Chamaeleo* is more open, which may minimize the dampening of vibrations on the pterygoid by surrounding tissues. These muscle insertions may have shifted anteriorly in *Chamaeleo* to accommodate the unique hearing system in this genus. Muscle insertions in *T. jacksonii* would be under no such selective pressure because they lack a pterygoid ear. However, the sample examined here is insufficient to fully assess whether this was the case. Descriptions of chameleon adductor musculature in the literature do not provide details on the posterior extent of the pseudotemporalis insertions (Rieppel, 1981, 1987), so it is unclear which arrangement represents the ancestral condition in chameleons. The position of the adductor posterior in Rieppel's illustrations of *Bradypodion pumilum, Brookesia superciliaris*, and *Rhampholeon kerstenii* is similar to that seen here for *T. jacksonii* and *Ch. chamaeleon*, suggesting that this muscle was indeed shifted anteriorly in *Ch. senegalensis*. *Bra. pumilum* and *Bro. superciliaris* have non-functional middle ears (Siebenrock, 1893; Toerien, 1963), as do the only examined members of *Rhampholeon* (Toerien, 1963). Further investigation into the jaw adductor musculature of chameleons with and without a pterygoid ear would clarify the interaction between these two systems. If the arrangement of the jaw muscles did change in response to the adoption of the pterygoid ear, it would illustrate the impact that the ear can have on surrounding structures.

3.5.3 Function of the pterygoid ear

Given that many chameleons have non-functional middle ears, what selective pressures led the chameleons in this study to independently evolve a novel hearing system multiple times? A sense of hearing can greatly facilitate the localization of resources, depending on the resources required by the taxon in question. The detection of sounds produced by insects, especially buzzing during flight, has been proposed as the main driver in the origin of the middle ear in many tetrapod clades (Clack, 1997; Müller and Tsuji, 2007). Chameleons are extremely

specialized for visual hunting of invertebrates and occasional small vertebrates (Anderson and Higham, 2013; Measey et al., 2013), but a non-visual means for prey detection would likely prove useful in the complex arboreal habitats where many chameleons reside. Insects produce a wide variety of sounds at a vast range of frequencies. The buzzing of insect wings has been recorded with median frequencies of 130–320 Hz for bees (Burkart et al., 2011; Gradišek et al., 2017), 200–400 Hz for large flies (Sueur et al., 2005), and 400–800 Hz for mosquitoes (Arthur et al., 2014). The mating stridulations of crickets, cicadas, and cockroaches range from 2–15 kHz (Pringle, 1954; Walker, 1962; Hartman and Roth, 1967). While high-pitched mating chirps would be undetectable to a chameleon, buzzing sounds of insect flight are well within the frequency range of the pterygoid ear, which is most effective at 200-600 Hz in most species and 600-900 Hz in *Ch. chamaeleon.* (Wever, 1978). The pterygoid ear arrangement would be effective at detecting some insects, so it may have evolved for localizing prey. However, it should be noted that there are no consistent differences in prey or habitat type known to exist between chameleons with and without the pterygoid ear (Akani et al., 2001; Measey et al., 2013; Tolley et al., 2013).

Another potential function for the pterygoid ear is in intraspecific communication, which is hypothesized to be one of the major drivers of hearing evolution (Gans, 1992; Fay and Popper, 2000). Chameleons are quite social, employing complex visual displays to attract mates and ward off competitors (Stuart-Fox, 2013; Ballen et al., 2014). They also seem to communicate via substrate-borne vibrations (Tilbury, 1992; Barnett et al., 1999). It has been hypothesized that these vibrations are produced by muscle contractions amplified by the gular pouch, a diverticulum of the trachea (Tornier, 1905; Huskey et al., 2020; Tegge et al., 2020). Though airborne sound can be produced by these vibrations, only barely-audible sounds have been documented thus far (Tilbury, 1992; Barnett et al., 1999). Still, it is worth noting that six species known to possess a pterygoid ear also have a gular pouch, while only *T. cristatus* has a pterygoid ear and no gular pouch (Huskey et al., 2020). Similarly, five species known to lack a pterygoid

ear also lack the gular pouch, while only *F. lateralis*, *F. oustaleti*, and *F. verrucosus* lack a pterygoid ear and have a gular pouch (Huskey et al., 2020). This general pattern could indicate that the pterygoid ear plays some role in detecting vibrations produced by the gular pouch. It seems unlikely that the pterygoid is particularly useful in receiving substrate-borne vibrations, as all the studied chameleons have a direct connection between their extracolumella and quadrate that would provide a pathway for vibrations to travel from the substrate through the jaw and quadrate to the inner ear. The pterygoid plate has a membranous attachment to the quadrate, so an additional connection between the extracolumella and pterygoid would be redundant with the existing quadrate-based pathway. Another possibility is that the gular pouch is also involved in the production or amplification of airborne sounds such as the hissing that occurs during chameleon confrontations (Bustard, 1967). Such calls could aid in communication between animals on different trees rather than relying solely on substrate-borne vibrations.

Finally, the pterygoid ear could be used to detect predators. Chameleons are primarily preyed on by birds and snakes, although mammals, frogs, and large invertebrates are also known to prey on them (Measey et al., 2013). These predators produce a wide variety of sounds that may be informative for a chameleon with a suitable ear, which makes this hypothesis difficult to test.

The role of the ear in chameleon biology has received little attention because their ears are typically considered to be vestigial and barely functional. However, the widespread occurrence of a well-developed tympanic cavity, repeated evolution of a novel sound conduction pathway, and possible shifting of muscle insertions to accommodate the ear highlight the potential significance of the ear for many chameleons. Further research is needed to understand exactly how these ears are used. Such inquiries will likely reveal a complex and interesting evolutionary history that may inform the origin of the ear in other clades, as well.

4. Allometry of Sound Reception Structures and Evidence for a Mandibular Middle Ear in Non-Mammalian Synapsids

4.1 ABSTRACT

The origin of sensory structures provides an excellent framework for studying how constraints and selective pressures affect the evolution of complex features. The evolution of the mammalian middle ear from the jaw and jaw hinge of non-mammalian synapsids offers valuable information about the early stages of sensory evolution, but it is limited by a poor understanding of hearing in non-mammalian synapsids. This work tests hypotheses of mandibular sound reception in non-mammalian synapsids by exploring the relationship between allometry and hearing use in a structure, as the size of a structure profoundly impacts its vibration. Allometry is investigated in the pterygoid of chameleons, which is used for hearing in some species. Results indicate that chameleons with a pterygoid ear converge on a similar allometric coefficient, while other species have variable coefficients, suggesting stabilizing selection for allometry in sound receivers. I also find substantially reduced variance around the allometric curve in therocephalians and non-bidentalian anomodonts, suggesting a similarly restricted allometric coefficient. This represents the first empirical evidence for hearing use in the postdentary bones of non-mammalian synapsids and suggests that selective pressures for hearing ability were felt by this lineage long before the evolution of the mammalian middle ear.

4.2 INTRODUCTION

Animal sensory systems are a hallmark example of the incredible complexity of form that can evolve. They often rely on a series of interactions between structures, tissues, and cells, so researchers have used sensory evolution to understand how complex changes in the morphology and behavior of an organism occur. While such systems are theoretically capable of assembling rapidly (Nilsson and Pelger, 1994), empirical evidence suggests that sensory systems evolve over long periods of time by successively shifting to stages of more specialized function (Nilsson, 2013; Abitua et al., 2015). While it is easy to assume that improved sensory perception should be highly favored by natural selection, leading to the rapid development of a novel sensory structure, such systems may involve co-option of structures with other functional demands (Crompton and Parker, 1978; Nilsson and Pelger, 1994; Niven and Laughlin, 2008; Capshaw and Soares, 2016). The evolution of sensory systems therefore depends on the balance between the selective pressures and functional constraints placed on them. An active area of research is in characterizing the unique selective pressures placed on sensory structures (Niven and Laughlin, 2008; Nilsson, 2013; Ladich and Schulz-Mirbach, 2016; Borghezan et al., 2021). However, sensory systems rely heavily on soft tissue for the reception, transduction, and processing of signals, making it difficult to gather detailed information about their evolutionary history from the fossil record. Most research on sensory evolution is restricted to extant taxa, which limits our understanding of the timing of the appearance of sensory traits and the nuances of the selective pressures that guided their evolution (Fay and Popper, 1997; Nilsson, 2013).

Arguably the best-documented case of sensory evolution in the fossil record is the origin of the mammalian ear. Not only is the inner ear encased in bone, which can be visualized in fossils through computed tomographic scanning (Luo et al., 2011; Castanhinha et al., 2013; Laaß, 2016; Benoit et al., 2017; Pusch et al., 2019), but the mammalian middle ear relies on a

series of ossicles, making this a sensory system with major components that can potentially fossilize. Studies on embryonic development and a rich synapsid fossil record have documented the reduction of the jaw hinge bones of non-mammalian synapsids and their incorporation into the middle ear of mammals (Allin and Hopson, 1992; Rowe, 1996; Ji et al., 2009; Urban et al., 2017; Meng et al., 2018).

4.2.1 Hypotheses about mammalian middle ear origins

Despite our in-depth knowledge of the anatomical changes that occurred during this transition, the selective pressures that drove the evolution of the mammalian hearing system are still poorly understood. Two scenarios explaining the evolution of the mammalian jaw and ear have been widely discussed in the literature. One is that the adoption of the dentary-squamosal jaw joint in advanced cynodonts rendered the postdentary bones obsolete, making them available to take on a new function in sound conduction (Parrington, 1979). Another possibility is that the postdentary bones were involved in sound transmission earlier in synapsid history, and the shifting of the jaw joint to the dentary was partially a response to a prolonged period of selection for improved hearing ability (Allin, 1975; Crompton and Parker, 1978). Distinguishing between these two hypotheses is important in understanding the pace at which new sensory systems arise and the selective pressures that influence their early stages of evolution.

The relative likelihood of these two scenarios hinges on whether the postdentary bones had a secondary hearing function before the appearance of the dentary-squamosal jaw joint. It is commonly hypothesized that early synapsids detected substrate-borne vibrations by resting their jaw against the ground (Tumarkin, 1968; Laaß, 2016). Vibrations would be transmitted from the postdentary bones to the quadrate, stapes and finally the inner ear. Some authors have even proposed that these bones were involved in airborne sound reception and transmission in the earliest therapsids (Allin, 1975; Allin and Hopson, 1992). They hypothesized that the reflected lamina of the angular, a thin plate of bone homologous with the mammalian

ectotympanic, functioned as a rudimentary sound receiver before the evolution of a tympanum (Figure 4.1B, D). Both ideas are alluring because they would place a rather mammal-like sound transmission pathway deep in synapsid evolution, explaining why these bones were later incorporated into the mammalian middle ear. The latter hypothesis would also explain the reflected lamina's eventual role in supporting the tympanum, as the two would have had a functional association early on.

Unfortunately, the exact function of the reflected lamina in non-mammalian therapsids is notoriously unclear, and a limited range of approaches has been used to evaluate its hypothesized role in sound reception. Several studies have focused on determining how sound transfer might occur in an early therapsid middle ear, and various authors have voiced conflicting opinions about the most likely pathways for sound transfer (Romer and Price, 1940; Hotton, 1959; Allin, 1975; Parrington, 1979; King, 1981; Allin and Hopson, 1992; Laurin, 1998; Kemp, 2007). Kermack (1982) demonstrated the feasibility of the reflected lamina to accomplish impedance matching, the primary function of the tympanum involving the amplification of vibrations sent to the inner ear. Kemp (2007) used the mass of the postdentary bones to calculate the frequency range at which they would be most effective at transmitting airborne sound in the cynodont *Chiniquodon*, concluding that these bones could have served as a poor, but functional middle ear in this taxon. Laaβ (2016) also used basic calculations to estimate the resonant frequency of the reflected lamina, though his results give no indication of the actual displacement of the reflected lamina that would result from receiving airborne sound. Together, these studies provide somewhat conflicting ideas about whether the reflected lamina had the potential to function as a sound receptor.

4.2.2 The allometry of sound receptors

Rather than focusing on functional capability, the present study approaches this problem by looking for evidence of stabilizing selection in the relative size of the reflected lamina that

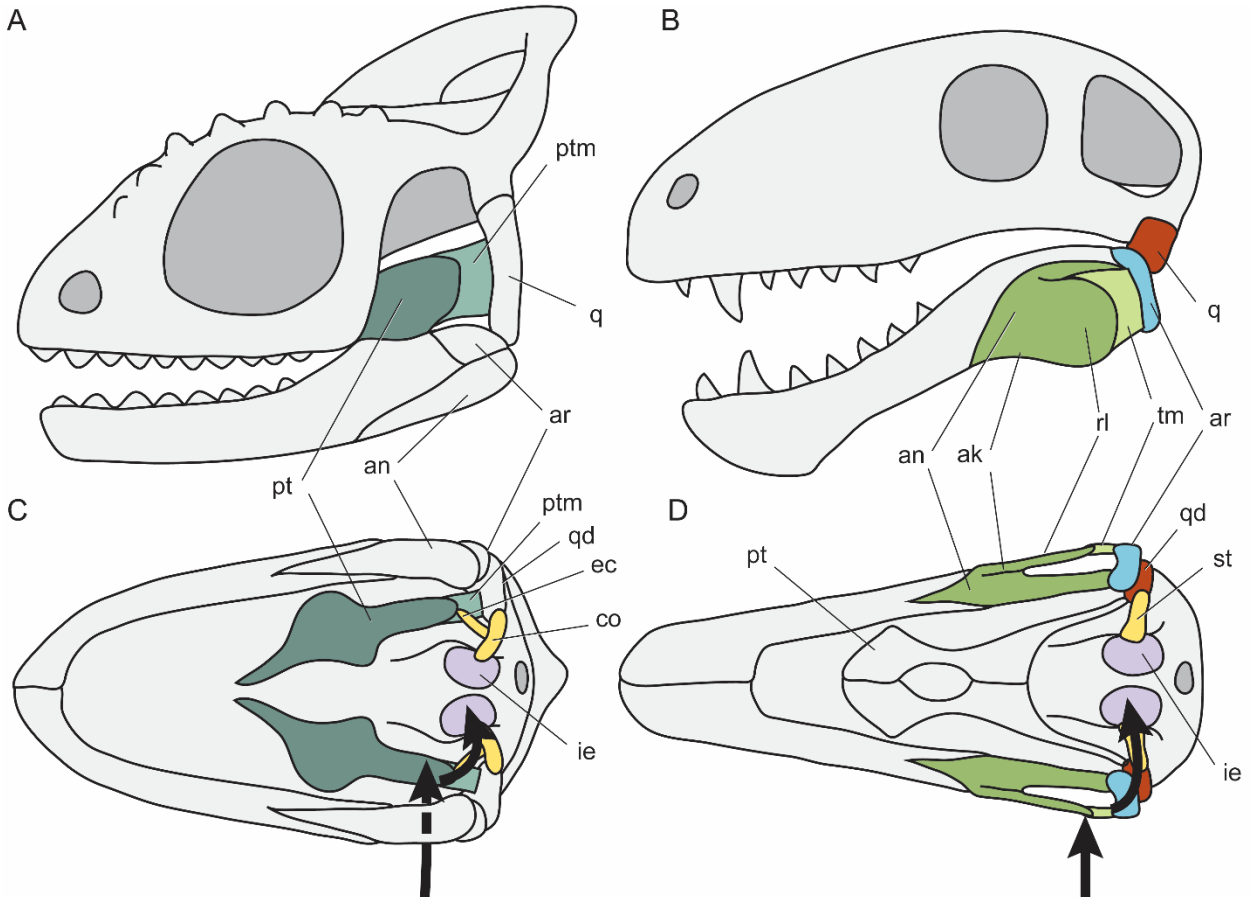

FIGURE 4.1. Schematics illustrating the anatomy of the middle ear in chameleons and the hypothesized middle ear in non-mammalian therapsids. **A)** Generalized chameleon skull and mandible in lateral view; **B)** generalized non-mammalian therapsid skull and mandible in lateral view with hypothesized tympanum location; **C)** generalized chameleon skull and mandible in ventral view; **D)** generalized non-mammalian therapsid skull and mandible in ventral view with hypothesized tympanum location. Black arrows indicate hypothesized routes for the reception of sound vibrations from outside the body and the transmission of those vibrations to the inner ear. Anterior to the left. **Abbreviations: ak** = angular keel; **an** = angular; **ar** = articular; **co** = columella; **ec** = extracolumella; **ie** = inner ear; **pt** = pterygoid; **ptm** = pterygoid membrane; **q** = quadrate; **rl** = reflected lamina of the angular; **st** = stapes; **tm** = hypothesized tympanic membrane.

would be consistent with a hearing function. Sensory structures are likely under strong selection for their size relative to body size. They generally have optimal sizes for their function, which may be independent of body size (Pihlström et al., 2005). Structures involved in the reception and transmission of vibrations should be under especially strong selection to remain at an

optimal size, as the frequency and amplitude at which at object vibrates is largely governed by various aspects of its size. The impedance matching function of a tetrapod sound receiver will depend on the ratio between the receiver area and that of the stapedial footplate (Wever and Lawrence, 1954). Indeed, negative allometry with body size is commonly seen in sensory structures, including several components of the tetrapod middle ear (Ritland, 1982; Rosowski and Graybeal, 1991; Nummela, 1995; Peacock et al., 2020). Thus, a sound reception structure may be expected to follow a strict, negative allometric growth curve with body size.

Assignment of function to extinct morphologies is strengthened by comparisons with analogous extant forms in which the function is better understood (Lauder, 1995). Ideally, the extant taxa would be close relatives of the extinct ones, but the only living synapsids are mammals, which all have a highly specialized middle ear that is no longer functionally similar to the hypothesized non-mammalian therapsid ear. Fortunately, other tetrapods have explored a wide variety of middle ear arrangements and sound reception structures. Chameleons are an excellent study system for characterizing the selective pressures associated with hearing function (Fig. 4.1A, C). In all extant chameleons, the pterygoid is expanded into a thin, wide plate onto which jaw adductor muscles attach. A membrane spans between the pterygoid plate and the quadrate and may represent an unossified portion of the pterygoid itself. Chameleons lack a tympanum, but some species have co-opted the pterygoid plate and its associated membrane for sound reception while others have not (Wever, 1968, 1969, 1978). Recent work has shown that this novel hearing system evolved independently in multiple lineages of chameleons (Olroyd, 2022). This provides an elegant system for studying the selective pressures that impact hearing systems, as the same structure can be compared between species that use it for hearing and those that do not. The chameleon system has the added advantage of being functionally comparable to the hypothesized middle ear of non-mammalian therapsids, as they have co-opted a bony muscle attachment site for receiving airborne sound vibrations.

In order to explore the effects of selection on the allometry of sound reception structures, I measured the allometric coefficients of the pterygoid plate in chameleon species that have a pterygoid ear and those that do not. These results were compared to the allometric growth curves for the orbit and the coronoid process in these species to assess how allometry differs between sensory and non-sensory structures. I then examined the allometry of the reflected lamina and the associated angular keel (AKRL) in therapsids and closely-related "pelycosaurs" to explore how the allometry of these features changed through synapsid evolution and identify shifts that could indicate a selective regime associated with sound reception.

4.3 MATERIALS AND METHODS

4.3.1 Materials

The sample included 426 chameleon specimens from 16 species (nine with a pterygoid ear and seven without). The chameleon specimens were a mix of both sexes, and they were obtained by their institutions through wild capture and donations from zoos and the pet trade. The synapsid sample included 72 genera spanning all major clades of non-mammalian therapsids and several "pelycosaur"-grade synapsids (six "pelycosaurs", seven biarmosuchians, seven dinocephalians, 22 anomodonts, nine gorgonopsians, 13 therocephalians, six non-mammalian cynodonts). The synapsid specimens chosen were the largest of each genus that were available for study, which was done to minimize error introduced by ontogeny. The angular keel and reflected lamina (AKRL) are often broken in synapsid fossils, so specimens were only used if they either had a complete AKRL, had both left and right AKRL that together preserved all parts of these two structures, or had other conspecific specimens that preserved the missing areas. In the latter two cases, information from all sides and/or specimens was used to estimate the total area of the AKRL (see Appendix 5 for details). In general, I avoided including multiple congeneric synapsid species to minimize the underestimation of allometric variation that may

occur when analyzing closely-related species. However, the analysis was run with and without two congeneric *Dimetrodon* species in order to boost sample size for "pelycosaurs", which are important for comparisons with the more derived therapsids. Both analyses produced nearly identical results.

4.3.2 Data collection

I photographed museum specimens of chameleons in lateral, ventral, and ventromedial views and synapsids in lateral view with a Nikon D3100 camera. A Nikon DX AF-S Nikkor 18-55mm lens was used for large synapsid specimens, a Canon MP-E 65mm lens was used for smaller synapsids, and a Canon EF 100mm macro lens was used for chameleons. Photos were taken in ventral view for measuring chameleon basal skull length, lateral view for the orbit and synapsid reflected lamina, posterior view for the chameleon coronoid process, and ventromedial view for the chameleon pterygoid plate. Synapsid specimens were also 3D surface scanned using an Artec Space Spider blue light scanner with a voxel size of 0.3 mm.

The angular keel is an extension of the angular ventral to the body of the angular and continuous with the reflected lamina posteriorly. The angular keel is distinguished from the reflected lamina based on the presence of a space called the angular cleft medial to the reflected lamina. This thin space is rarely prepared out in fossils and varies in size. While its extent generally coincides with specific ornamentation features on the surface of the reflected lamina (Olroyd and Sidor, in prep), these features cannot be used to estimate the extent of the cleft in taxa that lack such ornamentation, such as "pelycosaurs" and dinocephalians. Without a reliable way to delineate the reflected lamina from the angular keel in all studied taxa, the angular keel was included in the measurements of reflected lamina area (AKRL).

For chameleons, ImageJ V1.51j (Rasband, 1997) was used to measure basal skull length, pterygoid plate area, orbit diameter, and coronoid process height from photographs. In synapsids, I measured AKRL area in ImageJ and mandible length and orbit diameter using a

Neiko digital caliper. When photographs and/or caliper measurements were unavailable, the reflected lamina area was measured on the 3D mesh using the 2D footprint area reported by the R package molaR (Pampush et al., 2016), and the mandible length was measured on the mesh directly using the "Units" feature in Meshmixer V3.5.474 (©Autodesk, San Rafael, CA, U.S.A). This feature in Meshmixer was also used to measure the height of the coronoid eminence or coronoid process in scanned specimens. Exact locations for the measurements taken, along with example images and details of how different measurement methods were standardized, can be found in Appendix 5. All measurements were replicated twice for 30% of the specimens. The average of each set of replicates was calculated, and the deviance of measurements from each replicate average was used to estimate measurement error.

As mentioned above, the AKRL is a fragile feature that is rarely preserved, so there were few specimens that preserved these features along with the orbit and the coronoid eminence/process. As a result, measurements of the orbit and coronoid eminence/process were only analyzed in anomodonts, therocephalians, and cynodonts, as sample sizes for these measurements in the other groups were too low for meaningful interpretation.

4.3.3 Data analysis

All analyses were done in the programming language R (v. 3.5.3, R Core Team, 2019). All measurements were log-transformed to fit the linear form of the allometric growth equation for regression analysis. For each chameleon species and therapsid group, a linear regression was performed for each structure against basal skull length in chameleons and jaw length in synapsids. These different measurements of head size were chosen to maximize the number of specimens for which structure size and head size could both be measured, as the pterygoid plate is part of the cranium and the angular is part of the mandible. Note that this dataset represents intraspecific allometry in chameleons, which was not possible to adequately study in the therapsid sample, in which interspecific (sometimes called 'evolutionary') allometry was

characterized instead. Intraspecific and interspecific allometry do not always follow the same pattern (Pélabon et al., 2014), but this should be a reasonable comparison for this study system, as similar selective pressures are expected to act on the ear and its relationship to body size at each life stage. In order to test this assumption, I also ran the analysis with interspecific allometry for the chameleon data using the largest member of each species and grouping them based on pterygoid plate function. Ordinary Least Squares (OLS) regression was used for the chameleon dataset, as it is generally better at representing allometric signals than Reduced Major Axis (RMA) regression (Pélabon et al., 2014; Kilmer and Rodríguez, 2017). Phylogenetic Generalized Least Squares (PGLS) regression was performed with the R package ape (Paradis and Schliep, 2019) for therapsids to account for phylogenetic non-independence between datapoints in each regression. The residuals from all regressions were examined to assess the adequacy of the regression lines in fitting the shape of the data.

In addition to the regressions for each individual species, a linear mixed effects model in the R package lme4 (Bates et al., 2015) summarized differences in allometry between the two groups of chameleons (i.e., those with and without a pterygoid ear). An F-test was conducted to assess the significance of differences in the variance between coefficients in the two chameleon functional groups, and the assumption of a normally distributed dataset was confirmed using Q-Q plots for each set of coefficients. Separate regressions were also run for two subgroups within Anomodontia: the derived clade Bidentalia and a paraphyletic group of non-bidentalian anomodonts. These results were compared with those in the total group Anomodontia because the morphology of the reflected lamina shifts early in bidentalian evolution, which may indicate a change in function. Variance, coefficient, and intercept were used to assess differences in allometric curves between groups. An ANCOVA was also used to assess the statistical significance of differences between coefficients for each therapsid group.

Several methods were also employed to characterize the evolution of the allometric coefficient in each dataset. Felsenstein's (2012) thresholding method for discrete and

continuous characters was implemented in the R package phytools (Revell, 2012) to assess phylogenetic correlation between chameleon ear morphology and the allometric coefficient of the pterygoid plate. This was done using the time-calibrated phylogeny from Tolley et al. (2013), which was downloaded from the Dryad data repository and trimmed to species included in this dataset. Ancestral state reconstruction was performed to show the probable evolution of the pterygoid plate, which is hypothesized to have evolved multiple times independently from an ancestor lacking this feature (Olroyd, 2022). I plotted a phylogram of the allometric coefficients for each structure with the time-calibrated phylogeny and ancestral character states to visualize the evolutionary history of each structure and any correspondence with the evolution of the ear. This ancestral state reconstruction was used to assign selective regimes across the chameleon trees, which were then subjected to Ornstein-Uhlenbeck (OU) Hansen modeling of allometric coefficient evolution in the R package OUwie (Beaulieu et al., 2012). I tested for stabilizing selection for a specific allometric coefficient by comparing these models when the α and σ^2 parameters were allowed to vary between selection regimes or not. The corrected Akaike Information Criterion (AICc) was used to compare these models. For the synapsids, cladograms were constructed in Mesquite V3.11 (Maddison and Maddison, 2021) for each group based on topologies from multiple studies of synapsid relationships, which are summarized in the Supplementary Info. These cladograms were given arbitrary branch lengths and used to construct phylomorphospaces of AKRL area and mandible length to visualize phylogenetic structure in the data.

4.4 RESULTS

4.4.1 **The pterygoid plate of extant chameleons**

Average measurement error was 2–5% for measurements of both chameleons and synapsids. There was no consistent internal structure of the residuals around the regression lines, suggesting that these lines adequately fit the shape of the data.

The linear mixed-effects models returned similar allometric coefficients for the orbit (b = 0.76974) and the coronoid process (b = 0.7602) for the combined chameleon dataset, indicating negative allometry for both structures. The analysis indicated a slight difference between the total allometric coefficients of chameleons with a pterygoid ear (b = 2.29409) and those lacking a pterygoid ear (b = 2.02908), but this difference was not consistent when looking at the regression lines for individual species within those groups (Fig. 4.2E, F), and there was no evidence for unidirectional phylogenetic correlation between hearing ability and pterygoid plate allometry (note that the pterygoid plate area is a squared measurement, so the isometric coefficient of the log-transformed data is 2). The chameleons without a pterygoid ear exhibit a wide range of allometric coefficients and intercepts between species, with both higher and lower values than those seen in chameleons with a pterygoid ear (Table 4.1). On the other hand, chameleon species with a pterygoid ear are highly consistent in both the coefficient and intercept of their pterygoid plate growth curve. This pattern can also be seen when comparing orbit allometry with that of the coronoid process: variance around the growth curve is notably higher in the latter, and there is greater difference in coefficients between species (Fig. 4.2A–D). The F-tests confirm that the variance in the allometric coefficient for the pterygoid plate is significantly lower in species that use this bone for hearing than in species that do not (p = 0.002441361). In chameleon species lacking a pterygoid ear, the variance in the allometric coefficient was also significantly higher in the coronoid process and pterygoid plate than in the orbit (p = 0.043561211 and 0.023434311, respectively), although this difference was not statistically significant in the species with a pterygoid ear.

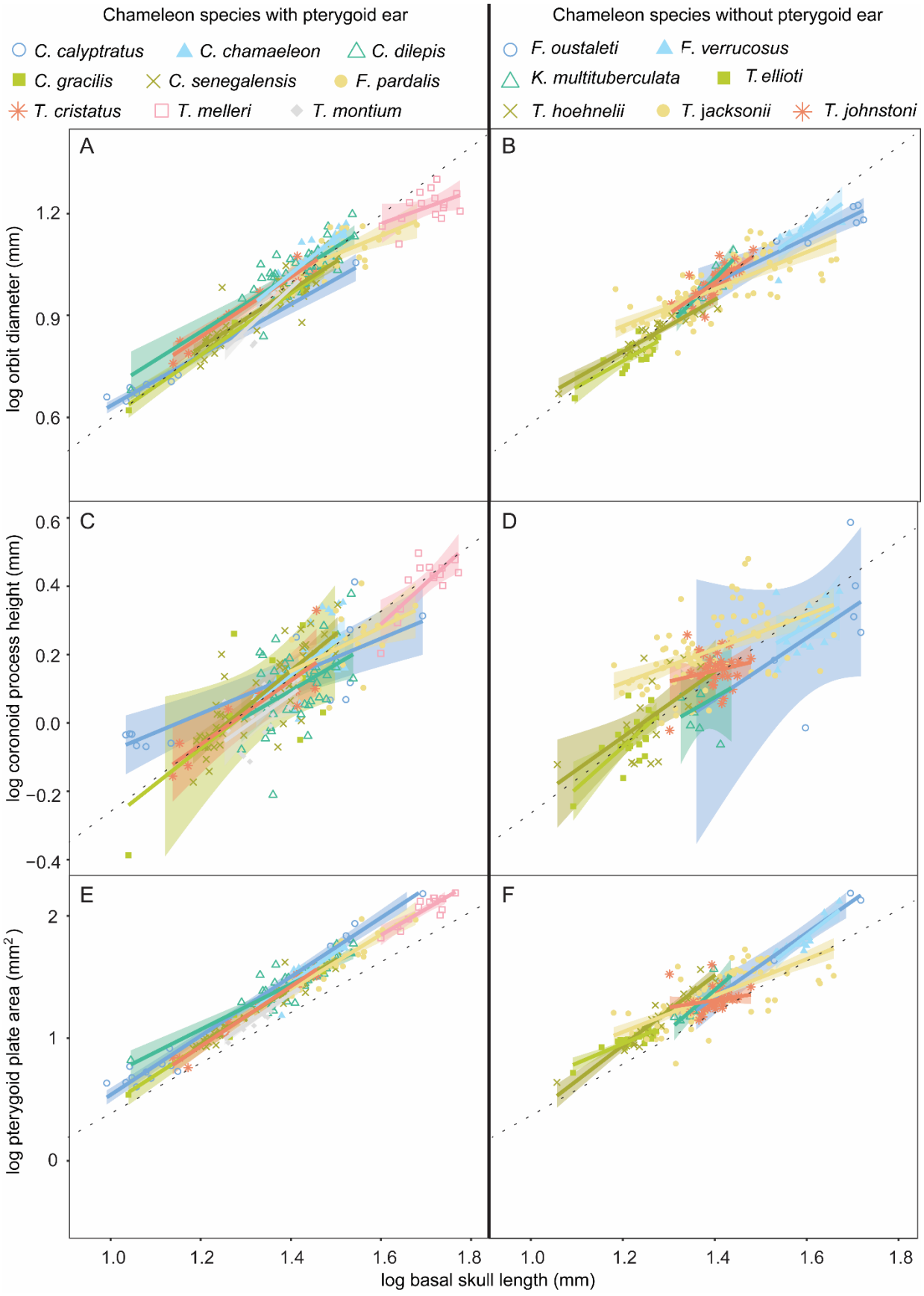
Chameleon species with pterygoid ear
C. calyptratus
C. chamaeleon
C. dilepis
C. gracilis
C. senegalensis
F. pardalis
T. cristatus
T. melleri
T. montium
Chameleon species without pterygoid ear
F. oustaleti
F. verrucosus
K. multituberculata
T. ellioti
T. hoehnelii
T. jacksonii
T. johnstoni
A
B
C
D
E
F
log orbit diameter (mm)
log coronoid process height (mm)
log pterygoid plate area (mm²)
log basal skull length (mm)
1.2
0.9
0.6
0.4
0.2
0.0
−0.2
−0.4
2
1
0
1.0
1.2
1.4
1.6
1.8

FIGURE 4.2. Intraspecific allometric curves from OLS regression against basal skull length in chameleons with and without a pterygoid ear. **A)** Orbit diameter in species with a pterygoid ear; **B)** orbit diameter in species without a pterygoid ear; **C)** coronoid process height in species with a pterygoid ear; **D)** coronoid process height in species without a pterygoid ear; **E)** pterygoid plate area in species with a pterygoid ear; **F)** pterygoid plate area in species without a pterygoid ear. Shaded areas represent 95% confidence interval. Dotted line indicates isometry.

Interspecific allometry in chameleons mirrored the patterns seen for intraspecific allometry. The largest members of each species with a pterygoid ear had a similar allometric coefficient (b = 2.3511) to that seen among different sized individuals within each of these species. The allometric growth curve for the largest individuals of species with a pterygoid ear had a much smaller variance and better overall fit of the trendline (σ^2 = 0.2444, R-squared = 0.962) than that for species lacking the pterygoid ear (σ^2 = 2.0420, R-squared = 0.7091).

Ancestral state reconstruction of hearing ability and allometric coefficients adds nuance to this observed pattern (Fig. 4.3). The evolution of orbital diameter is characterized by small changes to the ancestral allometric coefficient over long time periods. The coronoid process, on the other hand, experienced wild jumps in allometry over the course of chameleon evolution. The evolutionary history of the pterygoid plate appears to be a mix of these two patterns. Chameleon species that do not use this structure for hearing display a saltatory pattern of evolution similar to that seen for the coronoid process, whereas species that use this structure for hearing converged on a similar coefficient, regardless of their ancestral condition. Members of the genus *Chamaeleo*, for which the pterygoid ear is likely plesiomorphic (Olroyd, 2022), only exhibit small allometric changes in the pterygoid plate over the course of their evolution. These results are complemented by the OU Hansen models of coefficient evolution, as the best-supported models featured different parameters for drift (σ^2) or adaptive rate (α) between chameleon species with and without a pterygoid ear (Table 4.2). The model in which both parameters differed between selective regimes was less strongly supported, though this may be a result of overfitting with the added variable.

4.4.2 The reflected lamina and angular keel in non-mammalian synapsids

The orbit showed similar allometric coefficients and intercepts in anomodonts and therocephalians, but cynodonts had a slightly higher coefficient with a lower intercept (Fig. 4.4A). All three clades had similar allometric coefficients for the coronoid eminence/process, but the intercept was notably higher in therocephalians and cynodonts than in anomodonts, reflecting the enlarged, freestanding coronoid process that is characteristic of theriodonts (Fig.

Species	Pterygoid ear present?	Sample size	Allometric coefficient for log pterygoid plate area vs. log basal skull length	Allometric coefficient for log coronoid process height vs. log basal skull length	Allometric coefficient for log orbit diameter vs. log basal skull length
C. calyptratus	Yes	19	2.446215	0.5487181	0.7499224
C. chamaeleon	Yes	28	2.681772	0.9909764	1.0621700
C. dilepis	Yes	42	2.000826	0.7652541	0.8344326
C. gracilis	Yes	10	2.422720	1.0366550	0.9114390
C. senegalensis	Yes	50	2.299637	1.0771140	0.8409610
F. pardalis	Yes	23	2.273800	0.6441444	0.5496517
T. cristatus	Yes	10	2.445461	0.9332126	0.8830840
T. melleri	Yes	15	2.260507	1.3146810	0.4800713
T. montium	Yes	16	2.574977	0.9252990	1.2292000
F. oustaleti	No	7	2.807464	0.8977960	0.6575808
F. verrucosus	No	13	3.056195	0.7557319	0.9681135
K. multituberculata	No	9	2.798658	0.7654224	1.392778
T. ellioti	No	21	1.465018	1.2000810	0.7649167
T. hoehnelii	No	24	2.608260	0.8898845	0.8593343
T. jacksonii	No	91	1.502356	0.4985831	0.5465321
T. johnstoni	No	39	1.430534	0.3134138	0.9259978

TABLE 4.1. Results from OLS regressions against log basal skull length in each chameleon species. Note that isometry has a coefficient of 2 for pterygoid plate area, as this is a log-transformed, squared measurement.

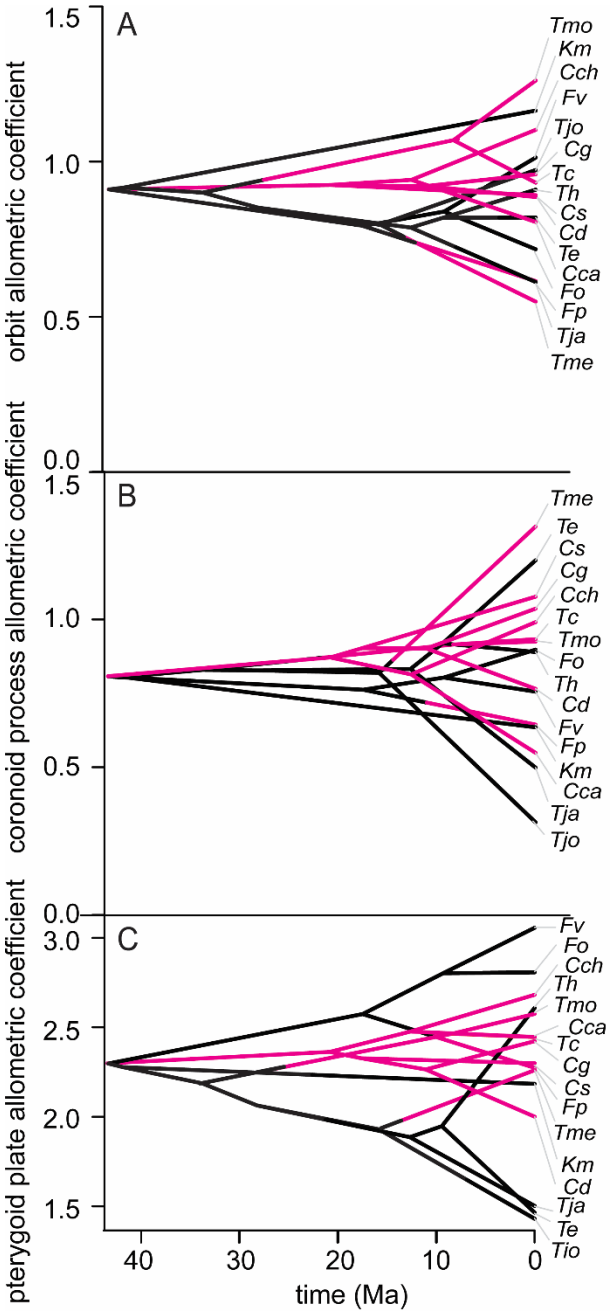

4.4B; Hopson and Barghusen, 1986). The coronoid process had a slightly higher variance around the trendline than the orbit except in non-bidentalian anomodonts, in which the two features had a similar variance.

The angular keel and reflected lamina (AKRL) in "pelycosaurs" exhibited slightly positive allometry with high variance around the trendline (Fig. 4.4B; Table 4.3). The intercept of the allometric curve increased in therapsids compared to "pelycosaurs", signifying a proportionally larger reflected lamina in the former. Most therapsid clades also exhibit negative allometry in their AKRL and have a lower allometric coefficient than that seen in "pelycosaurs", although this difference is only statistically significant for non-bidentalian anomodonts ($p = 0.00119$). However, therocephalians and bidentalian

FIGURE 4.3. Phylogram showing the evolution of allometric coefficients for chameleons with and without a pterygoid ear. **A)** Orbit diameter; **B)** coronoid process height; **C)** pterygoid plate area. Pink represents the acquisition of a pterygoid ear based on ancestral state reconstruction. **Tip labels:** ***Cca*** = *Chamaeleo calyptratus*; ***Cch*** = *C. chamaeleon*; ***Cd*** = *C. dilepis*; **Cg** = *C. gracilis*; ***Cs*** = *C. senegalensis*; **Fo** = *Furcifer oustaleti*; ***Fp*** = *F. pardalis*; ***Fv*** = *F. verrucosus*; ***Km*** = *Kinyongia multituberculata*; ***Tc*** = *Trioceros cristatus*; ***Te*** = *T. ellioti*; ***Th*** = *T. hoehnelii*; ***Tja*** = *T. jacksonii*; ***Tjo*** = *T. johnstoni*; ***Tme*** = *T. melleri*; ***Tmo*,** = *T. montium*. Note that the allometric coefficient for an area value will be twice that of a length value, so the Y-axis in C has been scaled to match that of A and B for easier comparison.

dicynodonts have very nearly isometric reflected laminae (Table 4.3).

The AKRL data exhibits wide variance around the trendline in “pelycosaurs”, biarmosuchians, dinocephalians, and gorgonopsians, but the variance is substantially lower in anomodonts and therocephalians. Splitting the anomodonts into bidentalian and non-bidentalian subgroups reveals that the derived bidentalians exhibit a high variance comparable to that of “pelycosaurs”, while the more basal anomodonts adhere tightly to their allometric trajectory (Fig. 4.5B; Table 4.3). The low variance in therocephalians and non-bidentalian anomodonts is unlikely to be the sole result of slightly better sampling in these groups, as bidentalians have a similar sample size and a much higher variance.

Cynodonts exhibit a lower intercept of the AKRL allometric curve, indicating an overall reduction in the size of the reflected lamina, a shift that has long been recognized in the literature (Kemp, 1972; Hopson and Barghusen, 1986). When analyzed together, they exhibit high variance around the allometric growth curve, but this may be a phylogenetic artefact, as basal cynodonts had a relatively much larger reflected lamina than the derived eucynodonts (Fig. 4.5D). The cynodont dataset also shows slight positive allometry for the AKRL, although this may be another product of phylogenetic averaging and would need to be confirmed with better sampling within Cynodontia.

Model	AICc	BIC
All parameters identical	30.53	29.98
Different α and σ^2	33.12	28.43
Different α, same σ^2	27.10	24.97
Same α, different σ^2	26.73	24.60

TABLE 4.2. Corrected Akaike Information Criteria (AICc) and Bayesian Information Criteria (BIC) for OU Hansen models of chameleon pterygoid plate allometric coefficient evolution in which parameters of drift (σ^2) and adaptive rate (α) were allowed to vary or not between chameleons with and without a pterygoid ear.

4.5 DISCUSSION

4.5.1 Allometry of sensory structures

The chameleon data show no evidence for a shift towards negative allometry in chameleons that use their pterygoid for hearing, which indicates that sound

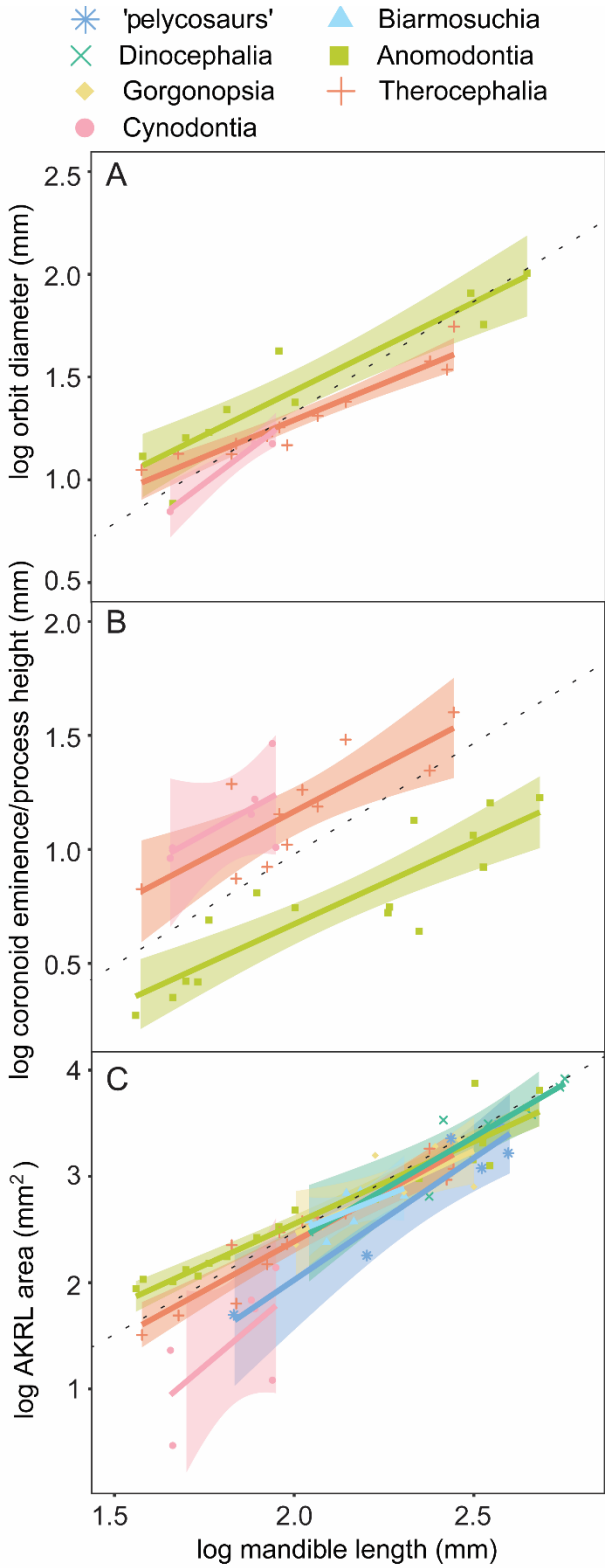

reception structures are not necessarily under directional selection for negative allometry. Rather, sensory structures seem to have more conserved allometric coefficients between species than structures used only for muscle attachment (Fig. 4.2; Tables 4.1, 4.2), suggesting that sensory structures are under strict stabilizing selection to maintain an optimum relative size for their function. The pterygoid ear exhibits especially conservative allometric coefficients, which may indicate that allometry with body size is of particular importance for the function of a sound reception structure. The vibration of such a structure is likely heavily influenced by surrounding tissues, so maintaining a specific size ratio with nearby structures may be important to ensure similar hearing performance throughout ontogenetic and phylogenetic changes in body size. Further research on the scaling factors for the dampening effect of surrounding tissues on a vibrating structure is needed to confirm this

FIGURE 4.4. Interspecific allometric curves from OLS regression against mandible length in "pelycosaurs" and the major therapsid clades. **A)** Orbit diameter; **B)** coronoid eminence/process height; **C)** area of angular keel and reflected lamina (AKRL). Shaded areas represent 95% confidence interval. Dotted line indicates isometry.

hypothesis. The physics of sound localization might also explain the tight relationship between pterygoid plate size and skull size, as the pressure-gradient system used by non-mammalian tetrapods relies on a particular balance between the frequencies heard by the organism and the distance between the two ears (Christensen-Dalsgaard, 2011). It is also possible that the restricted allometry found here is only a feature of the chameleon ear, so similar research in other taxa with novel sound reception structures such as the opercularis system in some amphibians (Capshaw and Soares, 2016; Pereyra et al., 2016) or the swim bladder in many teleosts (Braun and Grande, 2008) would clarify how generalizable these patterns are.

Reconstructed evolutionary patterns also differed between sensory and non-sensory structures. The sensory structures examined showed conserved, slow evolution in their allometric coefficient, rarely straying from phylogenetically historic values, whereas the structures with a sole function in muscular attachment made large evolutionary jumps, possibly related to exploration of different jaw function (Fig. 4.3, Table 4.2). The pterygoid plate seems to illustrate a shift between these two patterns upon acquisition of a novel hearing function.

Group	Allometric coefficient for log AKRL vs. log mandible length	Variance for log AKRL vs. log mandible length	Variance for log coronoid height vs. log mandible length	Variance for log orbit diameter vs. log mandible length
'pelycosaurs'	2.2446	1.0687	NA	NA
Biarmosuchia	1.3628	3.7101	NA	NA
Dinocephalia	1.2666	0.8534	NA	NA
Anomodontia	1.5485	0.2051	0.3132	0.1655
non-bidentalians	1.4336	0.0751	0.1226	0.2348
Bidentalia	1.7441	1.0475	NA	NA
Gorgonopsia	1.6009	2.8207	NA	NA
Therocephalia	1.9908	0.1890	0.2501	0.0495
Cynodontia	3.0439	1.4173	0.5331	0.1331

TABLE 4.3. Results from OLS regressions against log mandible length in each synapsid group. Note that isometry has a coefficient of 2 for AKRL area, as this is a log-transformed, squared measurement.

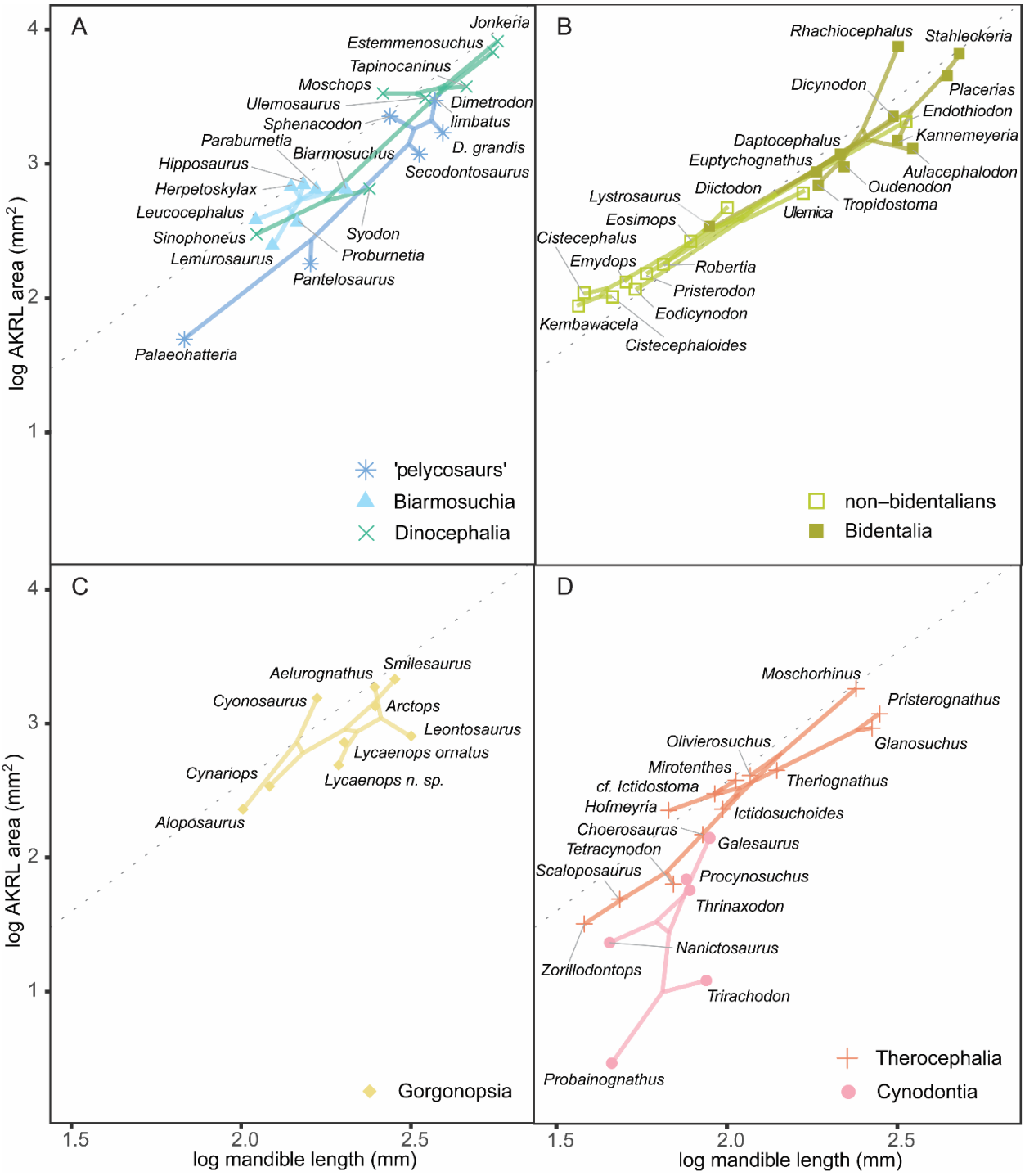

FIGURE 4.5. Phylomorphospace showing phylogenetic structure in the scaling of the angular keel and reflected lamina (AKRL) in each synapsid group studied. **A)** "Pelycosaurs", biarmosuchians, and dinocephalians; **B)** anomodonts; **C)** gorgonopsians; **D)** therocephalians and cynodonts. See Supplementary Info for sources for phylogenetic topologies used here. Dotted line indicates isometry.

Results of the analysis suggest that lineages that acquired a hearing function for this structure quickly evolved towards the presumed optimal coefficient. This functional shift happened early in the genus *Chamaeleo* (Olroyd, 2022), after which point the clade exhibited gradual evolution akin to that seen in the orbit, suggesting strong stabilizing selection favoring a specific allometric pattern. Though morphological diversity certainly exists in sensory systems, they also tend to exhibit general conservatism, as organisms with different ecologies use their senses for the same basic tasks (e.g., sound source localization) governed by the same laws of physics (Popper and Fay, 1997).

4.5.2 Allometry of purported middle ear structures in Therapsida

There were several shifts in the allometry of the angular keel and reflected lamina (AKRL) throughout synapsid evolution that suggest the adoption of a hearing function in these structures. The decreased allometric coefficient in biarmosuchians, dinocephalians, gorgonopsians, and non-bidentalian anomodonts compared to the condition in “pelycosaurs” could indicate that these groups were converging on a lower coefficient that was beneficial for hearing use (Fig. 4.4C, Table 4.3). However, non-bidentalians were the only group with a statistically significant decrease in the allometric coefficient compared to “pelycosaurs”, so this signal is uncertain for the other therapsid groups. Therocephalians and non-bidentalian anomodonts also had a substantially lower variance around their AKRL allometric growth curve than in “pelycosaurs” and other therapsids, which could indicate that their AKRL allometry was under strong stabilizing selection comparable to that inferred for the chameleon pterygoid. This could indicate that the reflected lamina was used as a sound reception structure in therocephalians and non-bidentalian anomodonts. These two groups also have particularly thin reflected laminae, often reaching sub-millimeter thickness, and complex ornamentation on the lateral surface of their angular compared to other therapsids. Multiple lines of evidence offer

strong support for the presence of a mandibular ear in non-bidentalian anomodonts and weaker support for this feature in most other therapsid clades.

The wide variation around the allometric trajectory in cynodonts is likely an artefact of sampling, as there are relatively few cynodonts covering a vast array of evolutionary change in this sample. As such, allometric shifts that occurred during cynodont evolution are averaged together in this dataset. It is well-known that eucynodonts substantially reduced the relative size of the reflected lamina compared with other therapsids (Kemp, 1972; Hopson and Barghusen, 1986), resulting in a lower intercept for their allometric trajectory than that seen in the more basal cynodonts (Fig. 4.5D). The one thing that can be gleaned from the current dataset is that there were two negative shifts in the intercept of the allometric curve that occurred in this clade relative to other therapsids: one at the base of Cynodontia and one at the base of Eucynodontia. These two stages in cynodont evolution are characterized by substantial changes in the size and shape of the entire postdentary series, including the reflected lamina, so a corresponding change in the allometry of the hearing apparatus would be expected in order to accommodate new relationships with surrounding tissues (Hopson and Barghusen, 1986; Sidor, 2003). More detailed sampling of each stage of cynodont evolution is needed to tease apart the changes in reflected lamina allometry that occurred within this group.

It is notable that the coronoid eminence/process exhibits an increase in overall size in theriodonts compared to anomodonts without a corresponding change in size in the AKRL. The coronoid eminence/process likely concentrated the insertions of jaw adductors, so one might expect allometric shifts in other adductor insertion sites in theriodonts to accommodate the new organization of the jaw closing apparatus in this clade. The absence of such a shift in the size of the AKRL suggest that these structures were either not sites for adductor insertion as proposed by several authors (Barghusen, 1968; Kemp, 1969, 1982; King, 1981) or that they were multifunctional structures under strong stabilizing selection for a size-reliant second function. As demonstrated here, sound-reception structures likely experience strong stabilizing selection

in their relative size, so the decoupling between the evolution of the coronoid eminence/process and that of the AKRL could further indicate that the latter was at least partially involved in sound reception. Another possibility is that the AKRL was not a site of attachment for jaw adductors, but it was for other muscles, such as those involved in throat constriction or tongue movement (Janensch, 1952; Barghusen, 1968; King, 1981; Kemp, 1982).

These results provide the first empirical evidence that the reflected lamina was not only capable of being used for hearing, but was indeed used for hearing in at least some non-mammalian therapsids. It should be noted that there could be other causes for restricted allometry of the AKRL, such as developmental constraints or a different function for which allometry with mandible size was important. However, the constricted allometry in anomodonts and therocephalians coincides with other morphological changes in the angular (thinner reflected lamina, deepening of the angular cleft, more complex angular ornamentation) which are consistent with shifts towards improved hearing ability. Numerous aspects of this potential mandibular middle ear remain uncertain: 1) whether it was used for the detection of substrate-borne or airborne sound, 2) how effective it was at its hearing function, 3) which frequencies it was capable of detecting, 4) whether the reflected lamina supported a membrane homologous with the mammalian tympanum, 5) in what way the structure vibrated and passed those vibrations to the inner ear, 6) whether the ornamentation on the angular was involved in sound reception, and 7) for how long the proposed function in muscular attachment in “pelycosaurs” persisted for the therapsid reflected lamina. Further research may illuminate some of these questions, but many of them are unanswerable in the absence of detailed knowledge of the soft tissues that surrounded the postdentary bones in non-mammalian therapsids.

The exact timing of the adoption of the mandibular middle ear in Therapsida is unclear from the data. The best evidence for a mandibular middle ear is in non-bidentalian anomodonts, with a possible loss of hearing function in derived bidentalian dicynodonts (see below). The low variance seen in the AKRL of therocephalians suggests that they also had a mandibular middle

ear, although their allometric coefficient was notably higher than that of early-diverging anomodonts. Biarmosuchians, dinocephalians, and gorgonopsians share a similar allometric coefficient with anomodonts, and all non-cynodont therapsids have a similar intercept, but none of these other clades exhibited the low variance seen in therocephalians and non-bidentalian anomodonts. Thus, this data lends some level of support to two possibilities: acquisition of a functional mandibular middle ear at the base of Therapsida or independently in Anomodontia and Therocephalia. The limited cynodont data offered no direct support for the presence of a mandibular middle ear in non-mammalian cynodonts, but the likely presence of this feature in therocephalians could indicate that this feature was present in the common ancestor of therocephalians and cynodonts, especially given that the distinct hook shape of the reflected lamina in higher cynodonts is generally inferred to indicate the presence of a tympanic membrane.

4.5.3 Possible losses of mandibular middle ear function

The therapsid clade that shows the least evidence for a difference in allometric scaling from the "pelycosaur" condition is the bidentalian dicynodonts, which attained large body sizes and a relatively thick AKRL. This is one clade in which a mandibular middle ear was least likely to be functional due to the massive size of the potential middle ear bones, so its exception to the patterns noted above for other therapsids is consistent with the idea that these patterns reflect the adoption of the reflected lamina as a hearing structure.

It is unknown whether the surface ornamentation that characterizes the angular of most therapsids has any relationship to a hearing function in this bone, but it should be noted that bidentalians also lack such complex angular ornamentation. This ornamentation was greatly simplified in bidentalians, especially in dicynodontoids and large cryptodonts, compared to more basal anomodonts, and this change coincided with multiple independent increases in body size. The smaller, more basal bidentalians, on the other hand, retained some complexity in their

angular ornamentation, and they also adhered closely to the allometric curve followed by the non-bidentalians, possibly indicating that they, too, used their reflected lamina for sound reception (Fig. 4.5B). It is possible that the ornamentation played some role in sound reception in a therapsid mandibular middle ear, and the reduced ornamentation in dinocephalians and large bidentalians may represent a loss of hearing. These results complement previous work showing a trend towards the reduction of postdentary bones in theriodonts and an opposite trend in anomodonts, which was interpreted as a lack of selection for hearing ability in the latter (Sidor, 2003).

Loss of hearing ability is common among tetrapods (Manning, 1923; Toerien, 1963; Wever, 1978; Capshaw and Soares, 2016), and extreme body size can pose an often insurmountable challenge to the mechanical functioning of the middle ear (Hetherington, 1992). It would not be surprising if some therapsids lost their hearing ability with dramatic increases in body size. However, it should be noted that dinocephalians also attained large body sizes and a particularly thick, simplified reflected lamina while also having a low AKRL allometric coefficient, though this was not found to be significantly lower than in “pelycosaurs” and thus may not conflict with the interpretation that large therapsids lost their sense of hearing.

Another potential factor to consider is that the anomodonts included in this study span a wide stratigraphic range in the fossil record. All non-bidentalian anomodonts examined were from the Permian, while most bidentalians were from the Triassic. The allometric differences between these two subgroups may reflect changes that happened over time or in relation to the end-Permian mass extinction. The loss of large predators such as gorgonopsians and large therocephalians during this extinction may have left Triassic dicynodonts with little need for an acute sense of hearing. The vast majority of the anomodonts in this dataset are from the Karoo Basin of South Africa, which experienced acute aridification and loss of surface vegetation across the Permo-Triassic boundary (Smith and Botha-Brink, 2014), which may have altered the environmental soundscape in which anomodonts lived. Regardless, the potential loss of hearing

ability in bidentalian dicynodonts reflects the complexity of non-mammalian synapsid evolution, which cannot be distilled into a linear march towards “mammalness” (Sidor, 2003; LeBlanc et al., 2018; Whitney and Sidor, 2019; Lungmus and Angielczyk, 2021).

4.5.4 Evolutionary novelty and the origin of sensory structures

Darwin (1859) famously posed the vertebrate eye as an evolutionary conundrum, but he grappled with its apparent perfection by proposing a series of small changes that could lead to its gradual evolution. Sensory systems in general are complicated and often finely tuned for their function, and a body of research has focused on understanding the small steps and selective pressures that produced them. While they seem intimidatingly complex at first glance, sensory systems evolve the same way any novel feature evolves, through adoption of a novel function by existing features and subsequent refinement by selection. Sensory structures in the earliest phases of co-option are probably barely capable of their new sensory function, but they elicit enough of a behavioral response to benefit the organism and become “visible” to selection (Nilsson, 2013).

The postdentary bones of synapsids seem to provide an excellent example of the sequence of events that has been proposed to characterize the appearance of novel sensory structures. Researchers have long noted that the bulky postdentary bones, quadrate, and stapes would have made poor sound conductors (Parrington, 1979; King, 1981; Kemp, 1982, 2007), leading some to argue that these bones could not have been used as a middle ear before they were released from their role in the jaw hinge. However, these results suggest that at some point fairly early in therapsid history, these bones gained some basic functionality in sensing vibrations in a way that provided useful information to the organism. The mandibular ear of non-mammalian therapsids may have been limited to low frequencies or substrate-borne vibration, but the important thing is that they were visible to selection, apparently experiencing stabilizing selection consistent with a function in sound reception. This hearing system probably

remained poorly functional in early therapsids, as it was made up of bones that were constrained by their ancestral function as components of the jaw. Once the dentary-squamosal jaw hinge relieved them of that function, the postdentary bones, quadrate, and stapes underwent further refinement for their hearing function. This case indicates that the evolution of novel structures via co-option can be a drawn-out process, as a structure may retain its previous function—and its associated constraints—for millions of years. Extant chameleons likely represent an example of a clade experiencing functional constraints that limit the elaboration of a sensory system, as the pterygoid plate is still a crucial component of the jaw-closing apparatus and may be unable to further specialize for its role in the ear. Complex, multifunctional features are often highly constrained by functional integration, so we should expect cases of evolutionary novelty to be characterized by periods of stasis until pre-existing functional obligations are released (Lauder, 1981).

The first steps in the acquisition of a new sensory apparatus require a bit of luck, as there must be an association between neurons with the ability to react to a particular stimulus, structures that can expose those cells to the stimulus, and a selectively advantageous behavioral response (Nilsson, 2013). Vertebrate ears invariably utilize the pressure-sensitive cells of the fluid-filled inner ear, whose original function was likely related to orientation (Clack, 2016). The plesiomorphic association between the stapes/columella and the inner ear provides a convenient pathway for sound to reach the inner ear from outside the body. Accordingly, parallel evolution is commonly seen in tetrapod hearing systems, as any structure that gains the ability to transfer sound vibrations from outside the body to the stapes/columella can relatively easily produce a middle ear with basic functionality (Clack, 1993; Martin and Luo, 2005; Müller and Tsuji, 2007; Capshaw and Soares, 2016; Olroyd, 2022). If the mandibular middle ear indeed originated independently in multiple groups of therapsids, it would provide another example of parallel evolution of a novel hearing apparatus from the same existing structures, supporting the

idea that the first appearance of a novel sensory structure relies heavily on fortuitous interactions between structures.

4.6 CONCLUSIONS

Data from extant chameleons indicate that negative allometry does not characterize all sensory structures, but interspecific variation in the allometric coefficient is generally lower for sensory structures than for non-sensory ones. This decreased variation is likely caused by strong stabilizing selection for a specific allometric trajectory. This pattern is especially clear for sound receivers, in which the size of the receiver relative to surrounding structures and the head in general likely impact its effectiveness in receiving and transmitting vibrations.

Corresponding data from the reflected lamina and angular keel provide evidence support for allometric shifts in therocephalians and non-bidentalian anomodonts that are consistent with a sound reception function. Bidentalian anomodonts appear to have partially reverted to a more “pelycosaur”-like allometric pattern in their reflected lamina, which could indicate that the function of the mandibular middle ear was lost as members of this clade attained a larger body size. The existence of a bulky mandibular middle ear long before the appearance of the dentary-squamosal jaw joint demonstrates that novel sensory structures can arise through co-option of existing structures for basic sensory functions. These structures may retain poor functionality for millions of years if constraints prevent further refinement of their novel sensory function.

5. Conclusions

The ancestral condition for the angular of therapsids seems to be a quadripartite pattern of surface topography, and most clades exhibit a characteristic variation on this ancestral pattern. Thus, the function of these surface features is expected to be similar for most therapsids, and clade-specific muscle attachments to these features are not a viable explanation for their existence. The angular cleft does not underlie the entire surface of the angular that bears ridges and fossae on its surface. This space is also not accessible to insertion by the posterior pterygoideus in all therapsids, so the angular cleft was unlikely to function solely as a site for the insertion of this muscle. The morphology of the angular complex could possibly relate to hearing, but further investigation would be required to determine exactly what role the angular topography would have played in this function.

This work also reveals complexity in the evolution of the ear in chameleons. The unique pterygoid ear of chameleons is widely present and evolved at least four times independently. A depressor mandibulae-based sound reception system also appears to be present in several species. The jaw adductor muscles of chameleons with a pterygoid ear insert farther anteriorly on the jaw than in other species, and this may prevent dampening of the vibrating pterygoid. Chameleons with a pterygoid ear also seem to be confined to an optimum allometric coefficient for their pterygoid plate with head size, which suggests that sound receptors in general follow strict allometric scaling to maintain vibration properties relevant to impedance matching, amplification, and/or sound localization.

This work presents the first evidence for selection for improved hearing function in the mandible of non-mammalian therapsids. Based on the presence of constricted allometry, it is highly likely that therocephalians and basal anomodonts used their reflected lamina for sound reception. A shift towards negative allometry in other non-cynodont therapsids may also relate to a hearing function, but this is less certain. If the mandibular ear was limited to basal

anomodonts and therocephalians, then the quadripartite surface pattern of the therapsid angular was not related to a hearing function. Anomodont evolution captures a change in both angular surface complexity and reflected lamina allometry variability in bidentalian dicynodonts, suggesting some role in hearing for the angular surface features and possibly indicating a loss of hearing in bidentalians.

Both the chameleon and synapsid study systems provide insights about the evolution of the ear. Although a new sensory system can theoretically evolve in a short period of time, the appearance and refinement of a novel sensory structure can be a complicated, drawn-out process because such structures are not necessarily highly advantageous for every organism. Sensory structures are initially co-opted from structures with existing functions, and the constraints associated with the original functions may outweigh the benefits of improved sensory ability. The usefulness of a given sense depends on the organism, so sensory evolution does not follow a steady accumulation of improvements. Sensory evolution stagnates at suboptimal levels, small improvements happen where possible and necessary, sensory ability is lost when other biological changes are more beneficial, and lineages independently arrive at similar evolutionary solutions to their sensory problems.

Acknowledgments

This project was funded by the AAUW American Fellowship, the University of Washington WRF-Hall Fellowship and Snyder Award, the Society of Vertebrate Paleontology Cohen Prize, the Paleontological Society Feldmann Grant (all to Savannah Olroyd), and the NSF ANT-1341304 and EAR 1337569 (to Christian Sidor). Lianna Marilao segmented many of the muscles in the diceCT scans, Alexandria Brannick performed one of the CT scans, and Chet Merklin collected CT measurements. Museum collections access and assistance was generously provided by Kenneth Angielczyk, Eva-Maria Bendel, Julien Benoit, Elize Butler, Christina Byrd, Neftali Camacho, Aliénor Duhamel, Heidi Fourie, Mark Goodwin, Patricia Holroyd, Sifelani Jirah, Stevie Kennedy-Gold, Adam Leache, Peter Miller, Jessica Maisano, Nonhlanhla Mchunu, Sterling Nesbitt, Alan Resetar, José Rosado, Coleman Sheehy, Jennifer Sheridan, William Simpson, Zaituna Skosan, Carol Spencer, Michelle Stocker, Adrienne Stroup, Lauren Vonnahme, Gregory Watkins-Colwell, and Bernhard Zipfel. I thank Ricardo Araújo, Eva-Maria Bendel, Julien Benoit, Aliénor Duhamel, Jessica Maisano, Luisa Pusch, DigiMorph.org, the Evolutionary Studies Institute in Johannesburg, and the Museum für Naturkunde in Berlin for providing access to CT data. I would like to thank my supervisory committee for guidance and resource access: Christian Sidor, Sharlene Santana, Gregory Wilson-Mantilla, and Patricia Kramer. Christopher Anderson, Chuck Beightol, Dave Grossnickle, Jim Hopson, Steve Huskey, Zoe Kulik, Chris Law, Brandon Peecook, Katie Stanchak, and Megan Whitney provided feedback that greatly improved the project. I thank Abigail Curtis, Ron Eng, Meredith Rivin, Adam Summers, and the staff at Friday Harbor Laboratories for training and access to equipment. Several specimen photographs were provided by Brandon Peecook and Christian Sidor. Christian Kammerer and Adam Huttenlocker aided with taxonomic identification for some specimens. I would like to extend a special thank you to Steve Huskey for sending me chameleon

specimens for dissections. I thank Arun Doogar for his aid in translating German literature. I would also like to thank Catherine Early, Devin Hoffman, Kelsey Jenkins, Luke Musher, Viktor Radermacher, Rosemary Romero, and Roger Smith for their hospitality during my museum visits.

References

Abdala, N. F. 2021. Permo-Jurassic cynodonts: the early road to mammalness; in Alderton, D. and Elias, S.A., eds., Encyclopedia of Geology. Springer, Amsterdam.

Abdala, F., B. S. Rubidge, and J. van den Heever. 2008. The oldest therocephalians (Therapsida, Eutheriodontia) and the early diversification of Therapsida. Palaeontology 51:1011–1024.

Abitua, P. B., T. B. Gainous, A. N. Kaczmarczyk, C. J. Winchell, C. Hudson, K. Kamata, M. Nakagawa, M. Tsuda, T. G. Kusakabe, and M. Levine. 2015. The pre-vertebrate origins of neurogenic placodes. Nature 524:462–465.

Adams, L. A. 1919. A memoir on the phylogeny of the jaw muscles in recent and fossil vertebrates. Annals of the New York Academy of Sciences 28:51–166.

Akani, G. C., O. K. Ogbalu, and L. Luiselli. 2001. Life–history and ecological distribution of chameleons (Reptilia, Chamaeleonidae) from the rain forests of Nigeria: conservation implications. Animal Biodiversity and Conservation 24:1–15.

Allin, E. F. 1975. Evolution of the mammalian middle ear. Journal of Morphology 147:403–437.

Allin, E. F., and J. A. Hopson. 1992. Evolution of the auditory system in Synapsida ("mammal-like reptiles" and primitive mammals) as seen in the fossil record; pp. 587–614 in The evolutionary biology of hearing. Springer, New York, NY.

Anderson, C. V., and T. E. Higham. 2013. Chameleon anatomy; pp. 7–56 in The Biology of Chameleons. University of California Press, Berkeley.

Angielczyk, K. D., and B. S. Rubidge. 2010. A new pylaecephalid dicynodont (Therapsida, Anomodontia) from the *Tapinocephalus* Assemblage Zone, Karoo Basin, Middle Permian of South Africa. Journal of Vertebrate Paleontology 30:1396–1409.

Angielczyk, K. D., and B. S. Rubidge. 2013. Skeletal morphology, phylogenetic relationships and stratigraphic range of *Eosimops newtoni* Broom, 1921, a pylaecephalid dicynodont

(Therapsida, Anomodontia) from the middle Permian of South Africa. Journal of Systematic Palaeontology 11:191–231.

Angielczyk, K. D., and C. F. Kammerer. 2018. Non-mammalian synapsids: the deep roots of the mammalian family tree; pp. 117–198 in F. E. Zachos and R. J. Asher (eds.), Handbook of Zoology: Mammalia: Mammalian Evolution, Diversity and Systematics. De Grutyer, Berlin.

Angielczyk, K. D., and J. Benoit. 2021. A new tusked cistecephalid dicynodont (Therapsida, Anomodontia) from the upper Permian upper Madumabisa Mudstone formation, Luangwa Basin, Zambia. Papers in Palaeontology 7:405–446.

Angielczyk, K. D., J. Liu, and W. Yang. 2021. A redescription of *Kunpania scopulusa*, a bidentalian dicynodont (Therapsida, Anomodontia) from the ?Guadalupian of northwestern China. Journal of Vertebrate Paleontology 41: e1922428.

Angielczyk, K. D., B. S. Rubidge, M. O. Day, and F. Lin. 2016. A reevaluation of *Brachyprosopus broomi* and *Chelydontops altidentalis*, dicynodonts (Therapsida, Anomodontia) from the middle Permian *Tapinocephalus* Assemblage Zone of the Karoo Basin, South Africa. Journal of Vertebrate Paleontology e1078342.

Arthur, B. J., K. S. Emr, R. A. Wyttenbach, and R. R. Hoy. 2014. Mosquito (*Aedes aegypti*) flight tones: Frequency, harmonicity, spherical spreading, and phase relationships. Journal of the Acoustical Society of America 135:933–941.

Atayman-Güven, S., B. S. Rubidge, and F. Abdala. 2009. Taxonomic re-evaluation of tapinocephalid dinocephalians. Palaeontologia Africana 44:83–87.

Ballen, C., R. Shine, and M. Olsson. 2014. Effects of early social isolation on the behaviour and performance of juvenile lizards, *Chamaeleo calyptratus*. Animal Behaviour 88:1–6.

Barghusen, H. 1968. The lower jaw of cynodonts (Reptilia, Therapsida) and the evolutionary origin of mammal-like adductor jaw musculature. Postilla 116:1–49.

Barghusen, H. 1973. The adductor jaw musculature of *Dimetrodon* (Reptilia, Pelycosauria).

Journal of Paleontology, 1:823–834.

Barghusen, H. 1975. A review of fighting adaptations in dinocephalians (Reptilia, Therapsida). Paleobiology, 1:295–311.

Barghusen, H. 1976. Notes on the adductor jaw musculature of *Venjukovia*, a primitive anomodont therapsid from the Permian of the USSR. Annals of the South African Museum 69:249–260.

Barnett, K., R. B. Cocroft, and L. J. Fleishman. 1999. Possible communication by substrate vibration in a chameleon. Copeia 1:225–228.

Bates, D., Mächler, B. Bolker, and S. Walker. 2015. Fitting linear mixed-effects models using lme4. Journal of Statistical Software 67:1–48.

Beaulieu, J. M., D.-C. Jhwueng, C. Boettiger, and B. C. O'Meara. 2012. Modeling stabilizing selection: Expanding the Ornstein-Uhlenbeck model of adaptive evolution. Evolution 66:2369–2383.

Bendel, E.-M., C. F. Kammerer, N. Kardjilov, V. Fernandez, and J. Fröbisch. 2018a. Cranial anatomy of the gorgonopsian *Cynariops robustus* based on CT-reconstruction. PLOS One 13:e0207367.

Bendel, E.-M., C. F. Kammerer, N. Kardjilov, V. Fernandez, and J. Fröbisch. 2018b. Cranial Anatomy of the Gorgonopsian *Cynariops robustus* Based on CT-Reconstruction. Data Publisher: Museum für Naturkunde Berlin (MfN) - Leibniz Institute for Evolution and Biodiversity Science.

Benoit, J., P. Manger, V. Fernandez, and B. S. Rubidge. 2016. Cranial bosses of *Choerosaurus dejageri* (Therapsida, Therocephalia): Earliest evidence of cranial display structures in eutheriodonts. PLoS One 11(8): e0161457.

Benoit, J., P. Manger, V. Fernandez, and B. S. Rubidge. 2017. The bony labyrinth of late Permian Biarmosuchia: palaeobiology and diversity in non-mammalian Therapsida. Palaeontologia Africana 52:58–77.

Boistel, R., T. Aubin, P. Cloetens, F. Peyrin, T. Scotti, P. Herzog, J. Gerlach, N. Pollet, and J.-F. Aubry. 2013. How minute sooglossid frogs hear without a middle ear. PNAS 10:15360–15364.

Borghezan, E. d. A., T. H. d. S. Pires, T. Ikeda, J. Zuanon, and S. Kohshima. 2021. A review on fish sensory systems and Amazon water types with implications to biodiversity. Frontiers in Ecology and Evolution 8:589760.

Botha, J., F. Abdala, and R. M. H. Smith. 2007. The oldest cynodont: new clues on the origin and early diversification of the Cynodontia. Zoological Journal of the Linnean Society 149:77–492.

Bramble, D. M. 1978. Origin of the mammalian feeding complex: models and mechanisms. Paleobiology 4:271–301.

Braun, C. B., and T. Grande. 2008. Evolution of peripheral mechanisms for the enhancement of sound peception; pp. 99–144 in Fish Bioacoustics. Springer, New York, NY.

Brock, G. T. 1940. The skull of the chameleon, *Lophosaura ventralis* (Gray); some Developmental Stages. Journal of Zoology 110:219–241.

Broom, R. 1932. The Mammal-like Reptiles of South Africa and the Origin of Mammals. Witherby, London, 376 pp.

Burkart, A., K. Lunau, and C. Schlindwein. 2011. Comparative bioacoustical studies on flight and buzzing of neotropical bees. Journal of Pollination Ecology 6:118–124.

Bustard, R. 1967. The comparative behavior of chameleons: Fight behavior in *Chameleo gracilis* Hallowell. Herpetologica 23:44–50.

Camp, C. L. 1948. The dicynodont ear. Special Publications of the Royal Society of South Africa, Rober Broom Commemmorative Volume 109–111.

Capshaw, G., and D. Soares. 2016. Hearing in plethodontid salamanders: A review. Copeia 104:157–164.

Castanhinha, R., R. Araújo, L. C. Junior, K. D. Angielczyk, G. Martins, R. M. S. Martins, C. Chaouiya, F. Beckman, and F. Wilde. 2013. Bringing dicynodonts back to life: Paleobiology and anatomy of a new emydopoid genus from the upper Permian of Mozambique. PLOS One 8:e80974.

Christensen-Dalsgaard, J. 2011. Vertebrate pressure-gradient receivers. Hearing Research 273:37–45.

Clack, J. A. 1993. Homologies in the fossil record: The middle ear as a test case. Acta Biotheoretica 41:391–409.

Clack, J. A. 1997. The evolution of tetrapod ears and the fossil record. Brain, Behavior and Evolution 50:198–212.

Clack, J. A. 2016. Vertebrate diversity in a sensory system: The fossil record of otic evolution; pp. 1–16 in Evolution of the Vertebrate Ear. Springer, Cham.

Cox, C. B., and K. D. Angielczyk. 2015. A new endothiodont dicynodont (Therapsida, Anomodontia) from the Permian Ruhuhu Formation (Songea Group) of Tanzania and its feeding system. Journal of Vertebrate Paleontology 35:e935388.

Cranford, T. W., P. Krysl, and J. A. Hildebrand. 2008. Acoustic pathways revealed: simulated sound transmission and reception in Cuvier's beaked whale (*Ziphius cavirostris*). Bioinspiration & Biomimetics 3:016001.

Crompton, A. W. 1963. The evolution of the mammalian jaw. Evolution 17:431–439.

Crompton, A. W. 1972. The evolution of the jaw articulation of cynodonts; pp. 231–251 in K. A. Joysey and T. S. Kemp (eds.), Studies in Vertebrate Evolution. Oliver and Boyd, Edinburgh.

Crompton, A. W., and N. Hotton. 1967. Functional morphology of the masticatory apparatus of two dicynodonts (Reptilia, Therapsida). Postilla 108:1–51.

Crompton, A. W., and P. Parker. 1978. Evolution of the mammalian masticatory apparatus. American Scientist 66:192–201.

Darwin, C. R. 1859. On the Origin of Species by Means of Natural Selection. John Murray, London.

DeMar, R. E., and H. Barghusen. 1972. Mechanics and the evolution of the synapsid jaw. Evolution 26:622–637.

Engelbrecht, D. van Z. 1951. Contributions to the cranial morphology of the chameleon *Microsaura pumila* Daudin. Annals of the University of Stellensbosch 27:3–31.

Farmer, C. G. 2000. Parental care: the key to understanding endothermy and other convergent features in birds and mammals. The American Naturalist 155:326–334.

Fay, R. R. 2009. Soundscapes and the sense of hearing of fishes. Integrative Zoology 4:26–32.

Fay, R. R., and A. N. Popper. 1974. Acoustic stimulation of the ear of the goldfish (*Carassius auratus*). Journal of Experimental Biology 61:243–260.

Fay, R. R. and Popper, A. N. 1997. Preface. Brain, Behavior and Evolution 50:187–188.

Fay, R. R., and A. N. Popper. 2000. Evolution of hearing in vertebrates: the inner ears and processing. Hearing Research 149:1–10.

Felsenstein, J. 2012. A comparative method for both discrete and continuous characters using the threshold model. The American Naturalist 179:145–156.

Frank, G. H. 1951. Contributions to the cranial morphology of *Rhampholeon platyceps* Gunther. Annals of the University of Stellensbosch 27:33–67.

Gans, C. 1992. An overview of the evolutionary biology of hearing; pp. 3–13 in The Evolutionary Biology of Hearing. Springer New York, New York, NY.

Gaupp, E. 1911. Beiträge zur Kenntnis des Unterkiefers der Wirbeltiere. I. Der Processus anterior (Folli) des Hammers der Säuger und das Goniale der Nichtsäuger. Anatomischer Anzeiger 39:97–135.

Gignac, P. M., and N. J. Kley. 2014. Iodine-enhanced micro-CT imaging: Methodological refinements for the study of the soft-tissue anatomy of post-embryonic vertebrates.

Journal of Experimental Zoology Part B: Molecular and Developmental Evolution 322:166–176.

Gignac, P. M., N. J. Kley, J. A. Clarke, M. W. Colbert, A. C. Morhardt, D. Cerio, I. N. Cost, P. G. Cox, J. D. Daza, C. M. Early, M. S. Echols, R. M. Henkelman, A. N. Herdina, C. M. Holliday, Z. Li, K. Mahlow, S. MErchant, J. Müller, C. P. Orbson, D. J. Paluh, M. L. Thies, H. P. Tsai, and L. M. Witmer. 2016. Diffusible iodine-based contrast-enhanced computed tomography (diceCT): an emerging tool for rapid, high-resolution, 3-D imaging of metazoan soft tissues. Journal of Anatomy 228:889–909.

Gradišek, A., G. Slapničar, J. Šorn, M. Luštrek, M. Gams, and J. Grad. 2017. Predicting species identity of bumblebees through analysis of flight buzzing sounds. Bioacoustics 26:63–76.

Hartman, H. B., and L. M. Roth. 1967. Stridulation by the cockroach *Nauphoeta cinera* during courtship behaviour. Journal of Insect Physiology 13:579–586.

Hetherington, T. E. 1992. The effects of body size on the evolution of the amphibian middle ear; pp. 421–437 in The Evolutionary Biology of Hearing. Springer New York, New York, NY.

Hopson, J. A. 2012. The role of foraging mode in the origin of therapsids: Implications for the origin of mammalian endothermy. Fieldiana Life and Earth Sciences 5:126–148.

Hopson, J. A., and H. Barghusen. 1986. An analysis of therapsid relationships; pp. 83–106 in The ecology and biology of mammal-like reptiles.

Hotton, N. 1959. The pelycosaur tympanum and the early evolution of the middle ear. Evolution 13:99–121.

Huelsenbeck, J. P., R. Nielsen, and J. P. Bollback. 2003. Stochastic mapping of morphological characters. Systematic Biology 52:131–158.

Huskey, S., S. M. Tegge, C. V. Anderson, M. E. Smith, and K. Barnett. 2020. Gular pouch diversity in the Chamaeleonidae. The Anatomical Record 303:2248–2261.

Huttenlocker, A. K. 2009. An investigation into the cladistic relationships and monophyly of therocephalian therapsids (Amniota: Synapsida). Zoological Journal of the Linnean

Society 157:865–891.

Huttenlocker, A. K., and C. A. Sidor. 2016. The first karenitid (Therapsida, Therocephalia) from the upper Permian of Gondwana and the biogeography of Permo-Triassic therocephalians. Journal of Vertebrate Paleontology e1111897.

Huttenlocker, A. K., and C. A. Sidor. 2020. A basal nonmammaliaform cynodont from the Permian of Zambia and the origins of mammalian endocranial and postcranial anatomy. Journal of Vertebrate Paleontology 40:e1827413.

Huttenlocker, A. K., S. A. Singh, A. C. Henrici, and S. S. Sumida. 2021. A Carboniferous synapsid with caniniform teeth and a reappraisal of mandibular size-shape heterodonty in the origin of mammals. Royal Society Open Science 8:211237.

Janensch, V. W. 1952. Über den Unterkiefer der Therapsiden. Paläontologische Zeitschrift 26:229–247.

Ji, Q., Z. X. Luo, X. Zhang, C. X. Yuan, and L. Xu. 2009. Evolutionary development of the middle ear in Mesozoic therian mammals. Science 326:278–281.

Jones, K. E., K. D. Angielczyk, D. Polly, J. J. Head, V. Fernandez, J. K. Lungmus, S. Tulga, and S. E. Pierce. 2018. Fossils reveal the complex evolutionary history of the mammalian regionalized spine. Science 361:1249–1252.

Kahana, Y., and P. A. Nelson. 2006. Numerical modelling of the spatial acoustic response of the human pinna. Journal of Sound and Vibration 292:148–172.

Kammerer, C. F. 2011. Systematics of the Anteosauria (Therapsida: Dinocephalia). Journal of Systematic Palaeontology 9:261–304.

Kammerer, C. F., and V. Masyutin. 2018. Gorgonopsian therapsids (*Nochnitsa* gen. nov. and *Viatkogorgon*) from the Permian Kotelnich locality of Russia. PeerJ 6:e4954.

Kammerer, C. F., and M. D. Ordoñez. 2021. Dicynodonts (Therapsida: Anomodontia) of South America. Journal of South American Earth Sciences 108:10317.

Kemp, T. S. 1969. On the functional morphology of the gorgonopsid skull. Philosophical Transactions of the Royal Society of London B 256:1–83.

Kemp, T. S. 1972. Whaitsiid Therocephalia and the origin of cynodonts. Philosophical Transactions of the Royal Society of London B 264:1–54.

Kemp, T. S. 1982. Mammal-like Reptiles and the Origin of Mammals. Academic Press, Inc., London, 363 pp.

Kemp, T. S. 2007. Acoustic transformer function of the postdentary bones and quadrate of a nonmammalian cynodont. Journal of Vertebrate Paleontology 27:431–441.

Kemp, T. S. 2009. Phylogenetic interrelationships and pattern of evolution of the therapsids: testing for polytomy. Palaeontologia Africana 44:1–12.

Kermack, K. A. 1982. The ear in the Theropsida. Geobios 6:151–156.

Kermack, K. A., and F. Mussett. 1983. The ear in mammal-like reptiles and early mammals. Acta Palaeontologica Polonica 28:147–158.

Kermack, K. A., F. Mussett, and H. W. Rigney. 1981. The skull of *Morganucodon*. Zoological Journal of the Linnean Society 71:1–158.

Keyser, A. W. 1974. Evolutionary trends in Triassic Dicynodontia. Palaeontologia Africana 17:57–68.

Keyser, A. W., and A. R. I. Cruickshank. 1979. The origin and classification of Triassic dicynodonts. Transactions of the Geological Society of South Africa 82:81–108.

Kilmer, J. T., and R. L. Rodríguez. 2017. Ordinary least squares regression is indicated for studies of allometry. Journal of Evolutionary Biology 30:4–12.

King, G. M. 1981. The functional anatomy of a Permian dicynodont. Philosophical Transactions of the Royal Society of London B 291:243–322.

King, G. M. 1988. Anomodontia; pp. 1–84 in O. Kuhn (ed.), Handbuch der Paläoherpetologie, 17th ed. Fischer-Verlag, Stuttgart.

King, G. M., B. W. Oelofsen, and B. S. Rubidge. 1989. The evolution of the dicynodont feeding

system. Zoological Journal of the Linnean Society 96:185–211.

Kitazawa, T., M. Takechi, T. Hirasawa, N. Adachi, N. Narboux-Nême, H. Kume, K. Maeda, T. Hirai, S. Miyagawa-Tomita, Y. Kurihara, J. Hitomi, G. Levi, S. Kuratani, and H. Kurihara. 2015. Developmental genetic bases behind the independent origin of the tympanic membrane in mammals and diapsids. Nature Communications 6:1–7.

Klaver, C. J. J., and W. Böhme. 1986. Phylogeny and classification of the Chamaeleonidae (Sauria) with special reference to hemipenis morphology. Bonner Zoologische Monographien 22:1–64.

Laaß, M. 2015. Bone-conduction hearing and seismic sensitivity of the late Permian anomodont *Kawingasaurus fossilis*. Journal of Morphology 276:121–143.

Laaß, M. 2016. Virtual reconstruction and description of the cranial endocast of *Pristerodon mackayi* (Therapsida, Anomodontia). Journal of Morphology 276:1089–1099.

Ladich, F., and T. Schulz-Mirbach. 2016. Diversity in fish auditory systems: One of the riddles of sensory biology. Frontiers in Ecology and Evolution 4:28.

Lauder, G. V. 1981. Form and function: structural analysis in evolutionary morphology. Paleobiology 7:430–442.

Lauder, G. V. 1995. On the inference of function from structure; pp. 1–18 in J. J. Thomason (ed.), Functional morphology in vertebrate paleontology. Cambridge University Press.

Laurin, M. 1998. New data on the cranial anatomy of *Lycaenops* (Synapsida, Gorgonopsidae), and reflections on the possible presence of streptostyly in gorgonopsians. Journal of Vertebrate Paleontology 18:765–776.

Lautenschlager, S., P. Gill, Z. X. Luo, M. J. Fagan, and E. J. Rayfield. 2017. Morphological evolution of the mammalian jaw adductor complex. Biological Reviews of the Cambridge Philosophical Society 92:1910–1940.

LeBlanc, A. R. H., K. S. Brink, M. R. Whitney, F. Abdala, and R. R. Reisz. 2018. Dental ontogeny in extinct synapsids reveals a complex evolutionary history of the mammalian tooth attachment system. Proceedings of the Royal Society B 285:20181792.

Liu, J. 2013. Osteology, ontogeny, and phylogenetic position of *Sinophoneus yumenensis* (Therapsida, Dinocephalia) from the Middle Permian Dashankou Fauna of China. Journal of Vertebrate Paleontology 33:1394–1407.

Liu, J. 2020. *Taoheodon baizhijuni*, gen. et sp. nov. (Anomodontia, Dicynodontoidea), from the Upper Permian Sunjiagou Formation of China and its implications. Journal of Vertebrate Paleontology 40:e1762088.

Liu, J., and F. Abdala. 2017. Therocephalian (Therapsida) and chroniosuchian (Reptiliomorpha) from the Permo-Triassic transitional Guodikeng Formation of the Dalongkou Section, Jimsar, Xinjiang, China. Vertebrata PalAsiatica 55:24–40.

Liu, J., B. S. Rubidge, and J. Li. 2010. A new specimen of *Biseridens qilianicus* indicates its phylogenetic position as the most basal anomodont. Proceedings of the Royal Society B 277:rspb20090883.

Lombard, R. E., and J. R. Bolt. 1979. Evolution of the tetmpod ear: an overview and reinterpretation. Biological Journal of the Linnean Society of London 11:19–76.

Lungmus, J. K., and K. D. Angielczyk. 2021. Phylogeny, function and ecology in the deep evolutionary history of the mammalian forelimb. Proceedings of the Royal Society B 288:20210494.

Luo, Z. X., I. Ruf, J. A. Schultz, and T. Martin. 2011. Fossil evidence on evolution of inner ear cochlea in Jurassic mammals. Proceedings of the Royal Society B 278:28–34.

Maddison, W. P., and D. R. Maddison. 2021. Mesquite: A Modular System for Evolutionary Analysis.

Maier, W., and J. A. van den Heever. 2002. Middle ear structures in the Permian *Glanosuchus* sp. (Therocephalia, Therapsida), based on thin sections. Fossil Record 5:309–318.

Maier, W., and I. Ruf. 2016. Evolution of the mammalian middle ear: a historical review. Journal of Anatomy 228:270–283.

Manning, F. B. 1923. Hearing in rattlesnakes. Comparative Psychology 3:241.

Mariaux, J., N. Lutzmann, and J. Stipala. 2008. The two-horned chamaeleons of East Africa. Zoological Journal of the Linnean Society 152:367–391.

Martin, T., and Z. X. Luo. 2005. Homoplasy in the mammalian ear. Science 307:861–861.

Measey, G. J., A. Raselimanana, and A. Herrel. 2013. Ecology and life history of chameleons; pp. 139–173 in The Biology of Chameleons. University of California Press, Berkeley.

Meng, J., S. Bi, X.-T. Zheng, and X.-L. Wang. 2018. Ear ossicle morphology of the Jurassic euharamiyidan *Arboroharamiya* and evolution of mammalian middle ear. Journal of Morphology 279:441–457.

Müller, J., and L. A. Tsuji. 2007. Impedance-matching hearing in Paleozoic reptiles: evidence of advanced sensory perception at an early stage of amniote evolution. PLOS One 2:e0000889.

Nilsson, D. E. 2013. Eye evolution and its functional basis. Visual Neuroscience 30:5–20.

Nilsson, D. E., and S. Pelger. 1994. A pessimistic estimate of the time required for an eye to evolve. Proceedings of the Royal Society B 256:53–58.

Niven, J. E., and S. B. Laughlin. 2008. Energy limitation as a selective pressure on the evolution of sensory systems. Journal of Experimental Biology 211:1792–1804.

Nummela, S. 1995. Scaling of the mammalian middle ear. Hearing Research 85:18–30.

Olroyd, S. L. 2022. Independent origins of a novel atympanic middle ear system within Chamaeleonidae. The Anatomical Record.

Olroyd, S. L., C. A. Sidor, and K. D. Angielczyk. 2018. New materials of the enigmatic dicynodont *Abajudon kaayai* (Therapsida, Anomodontia) from the lower Madumabisa Mudstone Formation, middle Permian of Zambia. Journal of Vertebrate Paleontology 37:e1403442.

Olroyd, S. L., A. R. H. LeBlanc, R. Araújo, K. D. Angielczyk, A. Duhamel, and J. Benoit. 2021. Histology and μCT reveal the unique evolution and development of multiple tooth rows in the synapsid *Endothiodon*. Scientific Reports 11:16875.

Palmer, R. W. 1913. Note on the lower jaw and ear ossicles of a foetal *Perameles*. Anatomischer Anzeiger 43:510–515.

Pampush, J. D., J. M. Winchester, P. E. Morse, A. Q. Vining, D. M. Boyer, and R. F. Kay. 2016. Introducing molaR: a new R package for quantitative topographic analysis of teeth (and other topographic surfaces). Journal of Mammalian Evolution 23:397–412.

Paradis, E., and K. Schliep. 2019. ape 5.0: an environment for modern phylogenetics and evolutionary analyses in R. Bioinformatics 35:526–528.

Parker, W. K. 1881. On the structure of the skull in the chameleons. Transactions of the Zoological Society of London 11:77–105.

Parrington, F. R. 1955. On the cranial anatomy of some gorgonopsids and the synapsid middle ear. Proceedings of the Zoological Society of London 25:1–40.

Parrington, F. R. 1979. The evolution of the mammalian middle and outer ears: A personal review. Biological Reviews of the Cambridge Philosophical Society 54:369–387.

Peacock, J., G. M. Spellman, N. T. Greene, and D. J. Tollin. 2020. Scaling of the avian middle ear. Hearing Research 395:108017.

Pélabon, C., C. Firmat, G. H. Bolstad, K. L. Voje, D. Houle, J. Cassara, A. Le Rouzic, and T. F. Hansen. 2014. Evolution of morphological allometry. Annals of the New York Academy of Sciences 1320:58–75.

Pereyra, M. O., M. C. Womack, J. S. Barrionuevo, B. L. Blotto, D. Baldo, M. Targino, J. J. Opsina-Sarria, J. M. Guayasamin, L. A. Coloma, K. L. Hoke, T. Grant, and J. Faivovich. 2016. The complex evolutionary history of the tympanic middle ear in frogs and toads (Anura). Scientific Reports 6:34130.

Peterson, E. A. 1966. Hearing in the lizard: Some comments on the auditory capacities of a nonmammalian ear. Herpetologica 22:161–171.

Pihlström, H., M. Fortelius, S. Hemilä, R. Forsman, and T. Reuter. 2005. Scaling of mammalian ethmoid bones can predict olfactory organ size and performance. Proceedings of the Royal Society B 272:957–962.

Popper, A. N., and R. R. Fay. 1997. Evolution of the ear and hearing: Issues and questions. Brain, Behavior and Evolution 50:213–221.

Pringle, J. W. S. 1954. A physiological analysis of cicada song. Journal of Experimental Biology 31:525–560.

Pusch, L., J. Ponstein, C. F. Kammerer, and J. Fröbisch. 2019. Novel endocranial data on the early therocephalian *Lycosuchus vanderrieti* underpin high character variability in early theriodont evolution. Frontiers in Ecology and Evolution 7:464.

Pusch, L., J. Ponstein, C. F. Kammerer, and J. Fröbisch. 2019b. Cranial Anatomy of *Lycosuchus vanderrieti*. Data Publisher: Museum für Naturkunde Berlin (MfN) - Leibniz Institute for Evolution and Biodiversity Science.

R Core Team. 2019. R: A Language and Environment for Statistical Computing. R Foundation for Statistical Computing, Vienna, Austria, pp.

Rasband, W. S. 1997. ImageJ. U. S. National Institute of Health, Bethesda, Maryland, USA.

Reichert, C. 1837. Über die Visceralbögen der Wirbeltiere im Allgemeinen und deren Metamorphosen bei den Vögeln und Säugetieren. Archiv Für Anatomie, Physiologie Und Wissenschaftliche Medizin 120–222.

Reisz, R. R. 1986. Pelycosauria; pp. 1–102 in P. Wellnhofer (ed.), Encyclopedia of Paleoherpetology, Part 17A. Gustav Fischer, Stuttgart.

Reisz, R. R., D. S. Berman, and D. Scott. 1992. The cranial anatomy and relationships of *Secodontosaurus*, an unusual mammal-like reptile (Synapsida: Sphenacodontidae) from the early Permian of Texas. Zoological Journal of the Linnean Society 104:127–184.

Revell, L. J. 2012. phytools: An R package for phylogenetic comparative biology (and other things). Methods in Ecology and Evolution 3:217–223.

Rieppel, O. 1981. The skull and jaw adductor musculature in chamaeleons. Revue Suisse de Zoologie 88:433–445.

Rieppel, O. 1987. The phylogenetic relationships within the Chamaeleonidae, with comments on some aspects of cladistic analysis. Zoological Journal of the Linnean Society 89:41–62.

Ritland, S. 1982. The allometry of the vertebrate eye. Ph.D., University of Chicago, Chicago, IL

Romer, A. S., and L. I. Price. 1940. Review of the Pelycosauria. Special Papers of the Geological Society of America 28.

Rosowski, J. J., and A. Graybeal. 1991. What did *Morganucodon* hear? Zoological Journal of the Linnean Society 101:131–168.

Rowe, T. B. 1980. The morphology, affinities, and age of the dicynodont *Geikia elginensis*; pp. 269–294 in L. L. Jacobs (ed.), Aspects of Vertebrate History: Essays in Honor of Edwin Harris Colbert. Museum of Northern Arizona Press.

Rowe, T. B. 1988. Definition, diagnosis, and the origin of Mammalia. Journal of Vertebrate Paleontology 8:241–164.

Rowe, T. B. 1996. Coevolution of the mammalian middle ear and neocortex. Science 273:651–654.

Rubidge, B. S., and J. A. Hopson. 1996. A primitive anomodont therapsid from the base of the Beaufort Group (upper Permian) of South Africa. Zoological Journal of the Linnean Society 117:115–139.

Rubidge, B. S., and C. A. Sidor. 2001. Evolutionary patterns among Permo-Triassic therapsids. Annual Review of Ecology and Systematics 32:449–480.

Rubidge, B. S., and C. A. Sidor. 2002. On the cranial morphology of the basal therapsids *Burnetia* and *Proburnetia* (Therapsida: Burnetiidae). Journal of Vertebrate Paleontology 22:257–267.

Rybczynski, N. 2000. Cranial anatomy and phylogenetic position of *Suminia getmanovi*, a basal anomodont (Amniota: Therapsida) from the late Permian of Eastern Europe. Zoological Journal of the Linnean Society 130:329–373.

Sidor, C. A. 2000. Evolutionary trends and relationships within the Synapsida. University of Chicago, Chicago, 370 pp.

Sidor, C. A. 2003. Evolutionary trends and the origin of the mammalian lower jaw. Paleobiology 29:605–640.

Sidor, C. A. 2015. The first biarmosuchian from the upper Madumabisa Mudstone Formation (Luangwa Basin) of Zambia. Palaeontologia Africana 49:1–7.

Sidor, C. A., and J. A. Hopson. 1998. Ghost lineages and "mammalness": Assessing the temporal pattern of character acquisition in the Synapsida. Paleobiology 24:254–273.

Sidor, C. A., and B. S. Rubidge. 2006. *Herpetoskylax hopsoni*, a new biarmosuchian (Therapsida: Biarmosuchia) from the Beaufort; pp. 76–113 in Amniote Paleobiology: Perspectives on the Evolution of Mammals, Birds, and Reptiles. The University of Chicago Press, Chicago.

Sidor, C. A., J. A. Hopson, and A. W. Keyser. 2004. A new burnetiamorph therapsid from the Teekloof Formation, Permian, of South Africa. Journal of Vertebrate Paleontology 24:938–950.

Siebenrock, F. 1893. Das Skelet von Brookesia superciliaris Kuhl. Naturwissenschaftlichen Classe Der Kaiserlichen Akademie Der Wissenschaften 102:71–118.

Sigogneau-Russell, D. 1989. Theriodontia I; pp. 1–127 in P. Wellnhofer (ed.), Encyclopedia of Paleoherpetology, Part 17B. vol. 17C. Gustav Fischer, Stuttgart.

Sigogneau-Russell, D., and P. K. Tchudinov. 1972. Reflections on some Russian eotheriodonts (Reptilia, Synapsida, Therapsida). Palaeovertebrata 5:79–109.

Slabbekoorn, H. 2018. Soundscape ecology of the Anthropocene. Acoustics Today 14:42–49.

Smith, R. M. H. and Botha-Brink, J. 2014. Anatomy of a mass extinction: Sedimentological and taphonomic evidence for drought-induced die-offs at the Permo-Triassic boundary in the main Karoo Basin, South Africa. Palaeogeography, Palaeoclimatology, Palaeoecology 396:99–118.

Smith, R. M. H., B. S. Rubidge, and C. A. Sidor. 2006. A new burnetiid (Therapsida: Biarmosuchia) from the upper Permian of South Africa and its biogeographic implications. Journal of Vertebrate Paleontology 26:331–343.

Spindler, F. 2016. Morphological description and taxonomic status of *Palaeohatteria* and *Pantelosaurus* (Synapsida: Sphenacodontia). Freiberger Forschungshefte (C: Paläontologie, Stratigraphie, Fazies) 550:1–57.

Stuart-Fox, D. 2013. Chameleon behavior and color change; pp. 174–194 in The Biology of Chameleons. University of California Press, Berkeley.

Sueur, J., E. J. Tuck, and D. Robert. 2005. Sound radiation around a flying fly. The Journal of the Acoustical Society of America 118:530–538.

Sullivan, C., and R. R. Reisz. 2005. Cranial anatomy of the late Permian dicynodont *Diictodon*. Annals of Carnegie Museum 74:45–75.

Tegge, S. M., C. V. Anderson, M. E. Smith, and S. Huskey. 2020. The role of hyoid muscles in biotremor production in *Chamaeleo calyptratus*. Journal of Experimental Biology 223:jeb227603.

Tilbury, C. R. 1992. A new dwarf forest chameleon (Sauria: *Rhampholeon* Günther 1874) from Malawi, central Africa. Tropical Zoology 5:1–9.

Tilbury, C. R. 2013. Overview of the systematics of the Chamaeleonidae; pp. 221–250 in The Biology of Chameleons. University of California Press, Berkeley.

Tilbury, C. R., and K. A. Tolley. 2009. A re-appraisal of the systematics of the African genus *Chamaeleo* (Reptilia: Chamaeleonidae). Zootaxa 2079:57–68.

Tilbury, C. R., K. A. Tolley, and W. R. Branch. 2006. A review of the systematics of the genus *Bradypodion* (Sauria: Chamaeleonidae), with the description of two new genera. Zootaxa 1363:23–38.

Toerien, M. J. 1963. The sound-conducting systems of lizards without tympanic membranes. Evolution 17:540–547.

Tolley, K. A., T. M. Townsend, and M. Vences. 2013. Large-scale phylogeny of chameleons suggests African origins and Eocene diversification. Proceedings of the Royal Society B 280:20130184.

Tornier, G. 1905. Bau und betätigung der kopflappen und halsluftsäcke bei chamäleon. Zoologisches Jahrbuch Für Anatomie 21:1–40.

Tucker, A. S. 2017. Major evolutionary transitions and innovations: the tympanic middle ear. Philosophical Transactions of the Royal Society of London B 372:20150483.

Tumarkin, A. 1968. The evolution of the auditory conducting apparatus in terrestrial vertebrates; pp. 18–37 in A. S. de Reuck and J. Knight (eds.), Ciba Foundation Symposium on Hearing Mechanisms in Vertebrates. Churchill, London.

Urban, D. J., N. Anthwal, Z. X. Luo, J. A. Maier, A. Sadier, A. S. Tucker, and K. E. Sears. 2017. A new developmental mechanism for the separation of the mammalian middle ear ossicles from the jaw. Proceedings of the Royal Society B 284:20162416.

Versluys, J. 1898. Die mittlere und äussere Ohrsphäre der Lacertilia und Rhynchocephalia. Doctoral, G. Fischer, 247 pp.

Walker, T. J. 1962. Factors responsible for intraspecific variation in the calling songs of crickets. Evolution 16:407–428.

Watson, D. M. S. 1912. On some reptilian lower jaws. Annals and Magazine of Natural History 10:573–587.

Watson, D. M. S. 1953. The evolution of the mammalian ear. Evolution 7:159–177.

Watson, D. M. S., and A. S. Romer. 1956. A classification of therapsid reptiles. Bulletin of the

Museum of Comparative Zoology 114:37–89.

Westoll, T. S. 1943. The hyomandibular of *Eusthenopteron* and the tetrapod middle ear. Proceedings of the Royal Society B 131:393–414.

Wever, E. G. 1968. The ear of the chameleon: *Chamaeleo senegalensis* and *Chamaeleo quilensis*. Journal of Experimental Zoology Part A: Ecological Genetics and Physiology 168:423–436.

Wever, E. G. 1969. The ear of the chameleon*: Chamaeleo höhnelii* and *Chamaeleo jacksoni*. Journal of Experimental Zoology Part A: Ecological Genetics and Physiology 17:305–312.

Wever, E. G. 1978. The Reptile Ear. Princeton University Press, Princeton, New Jersey, 1024 pp.

Wever, E. G., and M. Lawrence. 1954. Physiological Acoustics. Princeton University Press, Princeton, New Jersey, 475 pp.

Whitney, M. R., and C. A. Sidor. 2016. A new therapsid from the Permian Madumabisa Mudstone Formation (Mid-Zambezi Basin) of southern Zambia. Journal of Vertebrate Paleontology: e1150767.

Whitney, M. R., and C. A. Sidor. 2019. Histological and developmental insights into the herbivorous dentition of tapinocephalid therapsids. PLOS One 14.

Appendices

APPENDIX 1

Clade	Identification	Specimen number	Stratigraphic position	Digitization method	Preservation notes
Anomodontia	*"Eodicynodon" oosthuizeni*	BP/1/6230	*Eodicynodon* Assemblage Zone, Karoo Basin, South Africa	Blue light	
	Abajudon kaayai	NHCC LB135	lower Madumabisa Mudstone Formation, Luangwa Basin, Zambia	Blue light	ventral portion of reflected lamina missing
	Aulacephalodon bainii	UCMP42699	*Cistecephalus* Assemblage Zone, Karoo Basin, South Africa	Blue light	
	Aulacephalodon bainii	FMNH UC 1532	lower Cistecephalus Assemblage Zone, Murraysburg, Karoo Basin, South Africa	Blue light	posterodorsal portion of reflected lamina broken
	Cistecephaloides boonstrai	SAM-PK-6243	*Cistecephalus* Assemblage Zone, Karoo Basin, South Africa	Blue light	
	Cistecephalus microrhinus	BP/1/253	lower-middle *Cistecephalus* Assemblage Zone, Karoo Basin, South Africa	Blue light	matrix obscuring posterodorsal reflected lamina
	Daptocephalus leoniceps	AMNH FR5582	*Daptocephalus* Assemblage Zone, Karoo Basin, South Africa	Blue light	
	Daptocephalus sp.	NMT RB329	Usili Formation, Ruhuhu Basin, Tanzania	Blue light	
	Daptocephalus sp.	NHCC LB218	Upper Madumabisa Mudstone Formation, Luangwa Basin, Zambia	Blue light	
	Dicynodon lacerticeps	BP/1/2098	upper *Cistecephalus* Assemblage Zone, Karoo Basin, South Africa	Blue light	
	Diictodon feliceps	BP/1/695	lower-middle *Cistecephalus* Assemblage Zone, Karoo Basin, South Africa	photographed only	surface breakage on posterior portion
	Diictodon feliceps	BP/1/853	lower-middle *Cistecephalus* Assemblage Zone, Karoo Basin, South Africa	photographed only	ventral portion of reflected lamina broken
	Diictodon feliceps	NHCC LB191	Upper Madumabisa Mudstone Formation, Luangwa Basin, Zambia	Blue light	
	Diictodon feliceps	UCMP41767	*Endothiodon* Assemblage Zone, Karoo Basin, South Africa	Blue light	Reflected lamina missing but mold preserves corrugation shape
	Diictodon feliceps	AMNH FR8167	*Endothiodon* Assemblage Zone, Karoo Basin, South Africa	Blue light	dorsal reflected lamina obscured by martrix
	Diictodon feliceps	BP/1/1294	*Endothiodon* Assemblage Zone, Karoo Basin, South Africa	photographed only	posterodorsal reflected lamina broken
	Diictodon feliceps	BP/1/1429	*Endothiodon* Assemblage Zone, Karoo Basin, South Africa	photographed only	angular keel and dorsal edge of reflected lamina missing
	Diictodon feliceps	BP/1/356	*Endothiodon* Assemblage Zone, Karoo Basin, South Africa	photographed only	posterior edge of reflected lamina nearly reaches articular

	Diictodon feliceps	BP/1/8140	*Endothiodon* Assemblage Zone, Karoo Basin, South Africa	photographed only	
	Diictodon feliceps	UCMP41757	*Endothiodon* Assemblage Zone, Beaufort Formation, Karoo Basin, South Africa	Blue light	
	Diictodon feliceps	UCMP42025	*Endothiodon* Assemblage Zone, Beaufort Formation, Karoo Basin, South Africa	Blue light	
	Diictodon feliceps	UCMP42828	*Endothiodon* Assemblage Zone, Beaufort Formation, Karoo Basin, South Africa	Blue light	
	Diictodon feliceps	CGP/1/1234	*Cistecephalus* Assemblage Zone, Karoo Basin, South Africa	photographed only	
	Diictodon feliceps	CGP/1/1981	*Cistecephalus* Assemblage Zone, Karoo Basin, South Africa	photographed only	
	Dolichuranus sp.	NMT RB654	Lifua Member, Manda Beds, Ruhuhu Basin, Tanzania	Blue light	
	Emydops arctatus	BP/1/1307	*Endothiodon* Assemblage Zone, Karoo Basin, South Africa	Blue light	
	Emydops arctatus	BP/1/366	*Endothiodon* Assemblage Zone or *Cistecephalus* Assemblage Zone, Karoo Basin, South Africa	Blue light	fossae filled by matrix. Ventral portion missing
	Endothiodon bathystoma	AMNH FR5534	*Endothiodon* Assemblage Zone, Karoo Basin, South Africa	Blue light	ventral edge missing
	Endothiodon bathystoma	AMNH FR5565	*Endothiodon* Assemblage Zone, Karoo Basin, South Africa	Blue light	
	Endothiodon bathystoma	AMNH FR5615	*Endothiodon* Assemblage Zone, Karoo Basin, South Africa	Blue light	ventral edge missing
	Endothiodon bathystoma	SAM-PK-K11131	*Endothiodon* Assemblage Zone, Karoo Basin, South Africa	Blue light	
	Endothiodon bathystoma	SAM-PK-K11134	*Endothiodon* Assemblage Zone, Karoo Basin, South Africa	Blue light	preserves ventral connection with angular body well. Angular keel and posterodorsal reflected lamina missing
	Eosimops newtoni	BP/1/6674	*Tapinocephalus* Assemblage Zone, Karoo Basin, South Africa	Blue light	only observed cast
	?Euptychognathus sp.	NHCC LB200	Upper Madumabisa Mudstone Formation, Luangwa Basin, Zambia	Blue light	ventral portion poorly preserved
	Kannemeyeria simocephalus	UCMP38372	*Cynognathus* Assemblage Zone, Beaufort Group, Karoo Basin, South Africa	Blue light	preserves ventral connection with angular body well
	Kannemeyeria vanhoepeni	UCMP42916	*Cynognathus* Assemblage Zone, Beaufort Group, Karoo Basin, South Africa	Blue light	ventral portion missing
	Kembawacela kitchingi	NHCC LB18	Upper Madumabisa Mudstone Formation, Luangwa Basin, Zambia	Blue light	
	Lystrosaurus sp.	AMNH FR8250	*Lystrosaurus declivis* Assemblage Zone, Karoo Basin, South Africa	Blue light	
	Lystrosaurus sp.	BP/1/5190	*Lystrosaurus declivis* Assemblage Zone, Karoo Basin, South Africa	photographed only	
	Lystrosaurus curvatus	BP/1/5086	*Lystrosaurus declivis* Assemblage Zone, Karoo Basin, South Africa	Blue light	
	Lystrosaurus declivis	BP/1/1383	*Lystrosaurus declivis* Assemblage Zone, Karoo Basin, South Africa	photographed only	
	Lystrosaurus declivis	BP/1/267	*Lystrosaurus declivis* Assemblage Zone, Karoo Basin, South Africa	photographed only	ventral edge broken
	Lystrosaurus declivis	BP/1/4343	*Lystrosaurus declivis* Assemblage Zone, Karoo Basin, South Africa	photographed only	
	Lystrosaurus declivis	BP/1/4624	*Lystrosaurus declivis* Assemblage Zone, Karoo Basin, South Africa	photographed only	

	Lystrosaurus declivis	NMQR164	*Lystrosaurus declivis* Assemblage Zone, Karoo Basin, South Africa	photographed only	
	Lystrosaurus declivis	NMQR815	*Lystrosaurus declivis* Assemblage Zone, Karoo Basin, South Africa	photographed only	
	Lystrosaurus maccaigi	BP/1/4052	*Lystrosaurus declivis* Assemblage Zone, Karoo Basin, South Africa	photographed only	ventral edge broken
	Lystrosaurus maccaigi	NMQR3635	*Lystrosaurus declivis* Assemblage Zone, Karoo Basin, South Africa	photographed only	posterodorsal reflected lamina broken
	Lystrosaurus murrayi	BP/1/1379	*Lystrosaurus declivis* Assemblage Zone, Karoo Basin, South Africa	photographed only	
	Lystrosaurus murrayi	BP/1/3904	*Lystrosaurus declivis* Assemblage Zone, Karoo Basin, South Africa	photographed only	posteroventral portion of reflected lamina missing, but mold preserves shape
	Lystrosaurus murrayi	BP/1/3975	*Lystrosaurus declivis* Assemblage Zone, Karoo Basin, South Africa	photographed only	three individuals in one block
	Lystrosaurus murrayi	BP/1/4507	*Lystrosaurus declivis* Assemblage Zone, Karoo Basin, South Africa	photographed only	
	Lystrosaurus murrayi	NMQR395	*Lystrosaurus declivis* Assemblage Zone, Karoo Basin, South Africa	photographed only	
	Lystrosaurus murrayi	UCMP31360	*Lystrosaurus declivis* Assemblage Zone, Karoo Basin, South Africa	Blue light	
	Lystrosaurus murrayi	UCMP31361	*Lystrosaurus declivis* Assemblage Zone, Karoo Basin, South Africa	Blue light	
	Niassodon mfumukasi	ML1620	K5 formation, Metangula Graben, Niassa Province, Mozambique	CT	not observed in person. Posterior and ventral edges missing
	Oudenodon bainii	BP/1/4260	*Daptocephalus* Assemblage Zone, Karoo Basin, South Africa	Blue light	
	Oudenodon bainii	AMNH FR5542	*Cistecephalus* Assemblage Zone, Karoo Basin, South Africa	Blue light	
	Oudenodon bainii	FMNH UC 2503	uppermost Hoedemaker to Steenkampsvlakte Member, Teekloof Formation, Karoo Basin, South Africa	Blue light	
	Placerias hesternus	UCMP137369	Placerias Quarry, Chinle Formation, Arizona, USA	Blue light	middle section of reflected lamina is reconstructed
	Pristerodon mackayi	BP/1/6685	*Cistecephalus* Assemblage Zone, Karoo Basin, South Africa	Blue light	
	Pristerodon mackayi	SAM-PK-K10153	*Tropidostoma-Gorgonops* Subzone, Dunedin, Beaufort West, Karoo Basin, South Africa	Blue light	preserves ventral connection with angular body well
	Pristerodon mackayi	SAM-PK-10161	*Tropidostoma-Gorgonops* Subzone, Dunedin, Beaufort West, Karoo Basin, South Africa	Blue light	ventral portion obscured by matrix
	Pristerodon mackayi	SAM-PK-1658		Blue light	
	Rhachiocephalus magnus	TM 4456	*Tropidostoma-Gorgonops* Subzone, Karoo Basin, South Africa	Blue light	posterior and dorsal surfaces of reflected lamina poorly preserved
	Robertia broomiana	BP/1/7934	*Tapinocephalus* Assemblage Zone, Karoo Basin, South Africa	Blue light	matrix in posteroventral fossa
	Stahleckeria potens	AMNH FR3857	Upper Rio do Rasto Formation, Paraná Basin, Brazil	Blue light	only observed cast

	Suminia getmanovi	PIN 2212-62	Kotel'nich locality, Kirov, Russia	photographed only	not observed in person
	Tropidostoma microtrema	CM RS20		Blue light	
	Tropidostoma microtrema	SAM-PK-8633	Teekloof Formation, Karoo Basin, South Africa	Blue light	preserves ventral connection with angular body well
	Ulemica invisa	PIN157/1112	Isheevo Subassemblage, Cis-Urals region, Russia	photographed only	not observed in person
Biarmosuchia	*Biarmosuchus tener*	PIN1758/2	Ocher Subassemblage, Cis-Urals region, Russia	photographed only	not observed in person
	Bullacephalus jacksoni	BP/1/5387	*Tapinocephalus* Assemblage Zone, Karoo Basin, South Africa	Blue light	missing ventral edge
	Hipposaurus sp.	CGP/1/66	*Tapinocephalus* Assemblage Zone, Karoo Basin, South Africa	CT	not observed in person
	Hipposaurus boonstrai	SAM-PK-8950	*Diictodon/Styracocephalus* Subzone, Karoo Basin, South Africa	Blue light	surface badly broken
	Lemurosaurus pricei	NMQR 1702	*Cistecephalus* Assemblage Zone, Karoo Basin, South Africa	Blue light	only examined cast
	Paraburnetia sneeubergensis	SAM-PK-K10037	Lowermost *Cistecephalus* Assemblage Zone, upper Teekloof Formation, Karoo Basin, South Africa	Blue light	
Cynodontia	*Galesaurus planiceps*	BP/1/5064	*Lystrosaurus declivis* Assemblage Zone, Karoo Basin, South Africa	Blue light	
	Galesaurus planiceps	BP/1/4597	*Lystrosaurus declivis* Assemblage Zone, Karoo Basin, South Africa	Blue light	surface poorly preserved
	Galesaurus planiceps	SAM-PK-K9956	10m above P/Tr boundary, Karoo Basin, South Africa	Blue light	posterior edge of reflected lamina missing
	Galesaurus planiceps	SAM-PK-K1119	*Lystrosaurus declivis* Assemblage Zone, Karoo Basin, South Africa	Blue light	ventral edge broken
	Galesaurus planiceps	TM83	*Lystrosaurus declivis* Assemblage Zone, Karoo Basin, South Africa	Blue light	surface on ventral portion poorly preserved
	Nanictosaurus rubidgei	TM279	*Daptocephalus* Assemblage Zone, Karoo Basin, South Africa	Blue light	dorsal reflected lamina poorly preserved
	Nshimbodon muchingaensis	NHCC LB277	Upper Madumabisa Mudstone Formation, Luangwa Basin, Zambia	CT	posterior reflected lamina missing
	Probainognathus jenseni	PVSJ410	Ischigualasto Formation, San Juan Province, Argentina	CT	not observed in person
	Procynosuchus delaharpeae	BP/1/226	*Cistecephalus* Assemblage Zone, Karoo Basin, South Africa	Blue light	posterior edges of reflected lamina broken
	Procynosuchus delaharpeae	BP/1/3748	*Cistecephalus* Assemblage Zone, Karoo Basin, South Africa	Blue light	surface very poorly preserved
	Thrinaxodon liorhinus	BP/1/2820	*Lystrosaurus declivis* Assemblage Zone, Karoo Basin, South Africa	Blue light	posterodorsal portion of reflected lamina broken
	Thrinaxodon liorhinus	BP/1/5372	*Lystrosaurus declivis* Assemblage Zone, Karoo Basin, South Africa	Blue light	posterior edges of reflected lamina broken
	Thrinaxodon liorhinus	BP/1/2513	*Lystrosaurus declivis* Assemblage Zone, Karoo Basin, South Africa	Blue light	
	Thrinaxodon liorhinus	SAM-PK-K11034	*Lystrosaurus declivis* Assemblage Zone, Karoo Basin, South Africa	Blue light	posterior and dorsal edges of reflected lamina broken

	Thrinaxodon liorhinus	TM81	*Lystrosaurus declivis* Assemblage Zone, Karoo Basin, South Africa	Blue light	mostly broken, but medial view of reflected lamina is visible
	Thrinaxodon liorhinus	BP/1/2753	*Lystrosaurus declivis* Assemblage Zone, Karoo Basin, South Africa	Blue light	ventral and posterior edges broken
	Trirachodon berryi	BP/1/4658	*Trirachodon-Kannemeyeria* Subzone, Karoo Basin, South Africa	Blue light	
Dinocephalia	*"Delphinognathus" conocephalus*	SAM-PK-713	*Tapinocephalus* Assemblage Zone, Karoo Basin, South Africa	Blue light	
	Jonkeria truculenta	AMNH FR5633	*Tapinocephalus* Assemblage Zone, Karoo Basin, South Africa	Blue light	
	Jonkeria truculenta	SAM-PK-K12030	*Tapinocephalus* Assemblage Zone, Karoo Basin, South Africa	Blue light	
	Moschops capensis	SAM-PK-K11832	*Tapinocephalus* Assemblage Zone, Karoo Basin, South Africa	Blue light	
	Moschops capensis	AMNH FR5550	*Tapinocephalus* Assemblage Zone, Karoo Basin, South Africa	Blue light	
	Moschops capensis	AMNH FR5602	*Tapinocephalus* Assemblage Zone, Karoo Basin, South Africa	Blue light	
	Sinophoneus yumenensis	IVPP V18120	Dashankou locality, Qingtoushan Formation	Blue light	only observed cast
	Struthiocephalus whaitsi	SAM-PK-3015	*Tapinocephalus* Assemblage Zone, Karoo Basin, South Africa	Blue light	surface poorly preserved
	Syodon biarmicum	PIN157/2	Isheevo Subassemblage, Cis-Urals region, Russia	photographed only	not observed in person
	Tapinocaninus pamelae	NMQR2986	*Eodicynodon* Assemblage Zone, Karoo Basin, South Africa	Blue light	ventral edge missing
Gorgonopsia	*Aelurognathus tigriceps*	BP/1/1566	*Cistecephalus* Assemblage Zone, Karoo Basin, South Africa	Blue light	ventral edge broken
	Aelurognathus tigriceps	NHCC LB350	Upper Madumabisa Mudstone Formation, Luangwa Basin, Zambia	Blue light	ventral edge broken
	Aloposaurus gracilis	AMNH FR5317	*Cistecephalus* Assemblage Zone, Karoo Basin, South Africa	Blue light	
	Arctops willistoni	NHCC LB396	Upper Madumabisa Mudstone Formation, Luangwa Basin, Zambia	Blue light	ventral portion broken and offset from dorsal portion
	Cynariops robustus	MB.R.999	*Tropidostoma/Gorgonops* Subzone, Biesiespoort locality, North Cape Province, Karoo Basin, South Africa	CT	not observed in person
	Cyonosaurus sp.	BP/1/605	lower-middle *Cistecephalus* Assemblage Zone, Karoo Basin, South Africa	Blue light	ventral and posterior edges missing
	Cyonosaurus longiceps	BP/1/2109	upper *Cistecephalus* Assemblage Zone, Karoo Basin, South Africa	Blue light	ventral edge broken
	Cyonosaurus longiceps	BP/1/2598	*Cistecephalus* Assemblage Zone, Karoo Basin, South Africa	Blue light	ventral and posterior edges missing
	Cyonosaurus rubidgei	BP/1/3847	*Daptocephalus* Assemblage Zone, Karoo Basin, South Africa	Blue light	
	Cyonosaurus rubidgei	BP/1/2867	*Cistecephalus* Assemblage Zone, Karoo Basin, South Africa	Blue light	anteroventral surface obscured by matrix
	Leontosaurus vanderhorsti	BP/1/743	middle-upper *Cistecephalus* Assemblage Zone, Karoo Basin, South Africa	Blue light	
	Lycaenops minor	BP/1/209	*Cistecephalus* Assemblage Zone, Karoo Basin, South Africa	Blue light	
	Lycaenops n. sp.	NHCC LB178	Upper Madumabisa Mudstone Formation, Luangwa Basin, Zambia	Blue light	ventral edge missing

	Lycaenops ornatus	BP/1/881	middle-upper *Cistecephalus* Assemblage Zone, Karoo Basin, South Africa	Blue light	
	Lycaenops ornatus	BP/1/2470	lower-middle *Cistecephalus* Assemblage Zone, Karoo Basin, South Africa	Blue light	
	Scylacocephalus sp.	NHCC LB177	Upper Madumabisa Mudstone Formation, Luangwa Basin, Zambia	Blue light	ventral edge missing
	Smilesaurus ferox	BP/1/2465	lower-middle *Cistecephalus* Assemblage Zone, Karoo Basin, South Africa	Blue light	
Sphenacodontidae	*Dimetrodon grandis*	MCZ VPRA2029	Clear Fork Group, Baylor County, Texas, USA	Blue light	middle section of reflected lamina is missing
	Dimetrodon limbatus	FMNH UC1001	Briar Creek Bonebed, Nocona Formation, Archer County, Texas, USA	Blue light	
	Secodontosaurus obtusidens	MCZ VPRA1124	Nocona Formation, Wichita Group, Archer County, Texas, USA	Blue light	
	Secodontosaurus obtusidens	MCZ VPRA2028	Archer City Formation, Bowie Group, Archer County, Texas, USA	Blue light	surface heavily broken
	Secodontosaurus longiramus	AMNH FR4091	Petrolia Formation, Archer County, Texas, USA	Blue light	posterior reflected lamina missing
	Sphenacodon ferox	MCZ VPRA8732	Abo Formation, Rio Arriba County, New Mexico, USA	Blue light	only medial view prepared
Therocephalia	Pristerognathidae indet.	CGP RMS 1185	*Tapinocephalus* Assemblage Zone, Karoo Basin, South Africa	Blue light	
	Choerosaurus dejageri	SAM-PK-8797	*Cistecephalus* Assemblage Zone, Karoo Basin, South Africa	Blue light	surface features flattened
	Glanosuchus macrops	AMNH FR5559	*Tapinocephalus* Assemblage Zone, Karoo Basin, South Africa	Blue light	
	Hofmeyria atavus	TM254		Blue light	
	cf. Ictidostoma sp.	BP/1/3155	*Endothiodon* Assemblage Zone, Karoo Basin, South Africa	Blue light	matrix filling some fossae
	Ictidosuchoides longiceps	BP/1/218	*Cistecephalus* Assemblage Zone, Karoo Basin, South Africa	Blue light	ventral portion missing
	Ictidosuchoides longiceps	BP/1/223	*Cistecephalus* Assemblage Zone, Karoo Basin, South Africa	Blue light	
	Ictidosuchoides longiceps	NHCC LB365	Upper Madumabisa Mudstone Formation, Luangwa Basin, Zambia	Blue light	ventral portion missing
	Ictidosuchoides longiceps	NMQR385	"Katberg Formation", Karoo Basin, South Africa	Blue light	ventral portion missing
	Ictidosuchoides longiceps	NMQR3686	Balfour Formation, Karoo Basin, South Africa	Blue light	
	Ictidosuchoides longiceps	SAM-PK-8659	*Endothiodon* Assemblage Zone, Teekloof Formation, Karoo Basin, South Africa	Blue light	
	Ictidosuchoides longiceps	BP/1/2294	middle *Cistecephalus* Assemblage Zone, Karoo Basin, South Africa	Blue light	matrix in dorsal notch and anteroventral fossa
	Lycosuchus vanderrieti	MB.R.995	*Tapinocephalus* Assemblage Zone, Karoo Basin, South Africa	CT	not observed in person. Ventral edge missing
	Mirotenthes digitipas	UCMP40467	*Cistecephalus* Assemblage Zone, Karoo Basin, South Africa	Blue light	only observed cast
	Moschorhinus kitchingi	BP/1/4227	*Lystrosaurus declivis* Assemblage Zone, Karoo Basin, South Africa	Blue light	
	Moschorhinus kitchingi	NMQR3835	Palingkloof Member, Balfour Formation, Karoo Basin, South Africa	Blue light	
	Olivierosuchus parringtoni	BP/1/3849	*Lystrosaurus declivis* Assemblage Zone, Karoo Basin, South Africa	Blue light	
	Olivierosuchus parringtoni	NMQR3605	lowermost *Lystrosaurus declivis* Assemblage Zone, Balfour Formation, Karoo Basin, South Africa	Blue light	anteroventral edge obscured by other bones

	Olivierosuchus parringtoni	NMQR62	lowermost *Lystrosaurus declivis* Assemblage Zone, Balfour Formation, Karoo Basin, South Africa	Blue light	
	Pristerognathus polyodon	SAM-PK-11942	*Diictodon/Styracocephalus* Subzone, Karoo Basin, South Africa	Blue light	posterior edge broken, medial view of reflected lamina visible
	Scaloposaurus constrictus	BP/1/1341	*Lystrosaurus declivis* Assemblage Zone, Karoo Basin, South Africa	Blue light	posterior and ventral edges broken
	Scaloposaurus constrictus	SAM-PK-K11543	*Lystrosaurus declivis* Assemblage Zone, Karoo Basin, South Africa	Blue light	matrix obscuring angular keel
	Scaloposaurus constrictus	NMQR 1457	*Lystrosaurus declivis* Assemblage Zone, Karoo Basin, South Africa	Blue light	posterior reflected lamina missing, but mold preserves shape
	Tetracynodon darti	BP/1/2710	*Lystrosaurus declivis* Assemblage Zone, Karoo Basin, South Africa	Blue light	
	Tetracynodon darti	BP/1/6026	*Lystrosaurus declivis* Assemblage Zone, Karoo Basin, South Africa	Blue light	
	Tetracynodon darti	SAM-PK-K10800	*Lystrosaurus declivis* Assemblage Zone, Karoo Basin, South Africa	Blue light	
	Theriognathus microps	BP/1/164	*Dicynodon/Theriognathus* Subzone, Karoo Basin, South Africa	Blue light	ventral edge broken
	Theriognathus microps	BP/1/182	*Dicynodon/Theriognathus* Subzone, Karoo Basin, South Africa	Blue light	
	Theriognathus microps	BP/1/844	*Dicynodon/Theriognathus* subzone	Blue light	posterior and ventral edges broken
	Theriognathus microps	BP/1/2243	lower *Cistecephalus* Assemblage Zone, Karoo Basin, South Africa	Blue light	posterodorsal reflected lamina deformed
	Theriognathus microps	BP/1/4093	upper *Cistecephalus* Assemblage Zone	Blue light	matrix obscuring posterodorsal reflected lamina
	Theriognathus microps	NMQR3375	Upper *Cistecephalus* Assemblage Zone, Karoo Basin, South Africa	Blue light	
	Zorillodontops gracilis	SAM-PK-1392	*Lystrosaurus declivis* Assemblage Zone, Edonville, Karoo Basin, South Africa	Blue light	posterior reflected lamina edges broken, but mold preserves shape

APPENDIX 2

Photograph of dissection location on a specimen of *Furcifer verrucosus* (FMNH 76088). White line indicates incision.

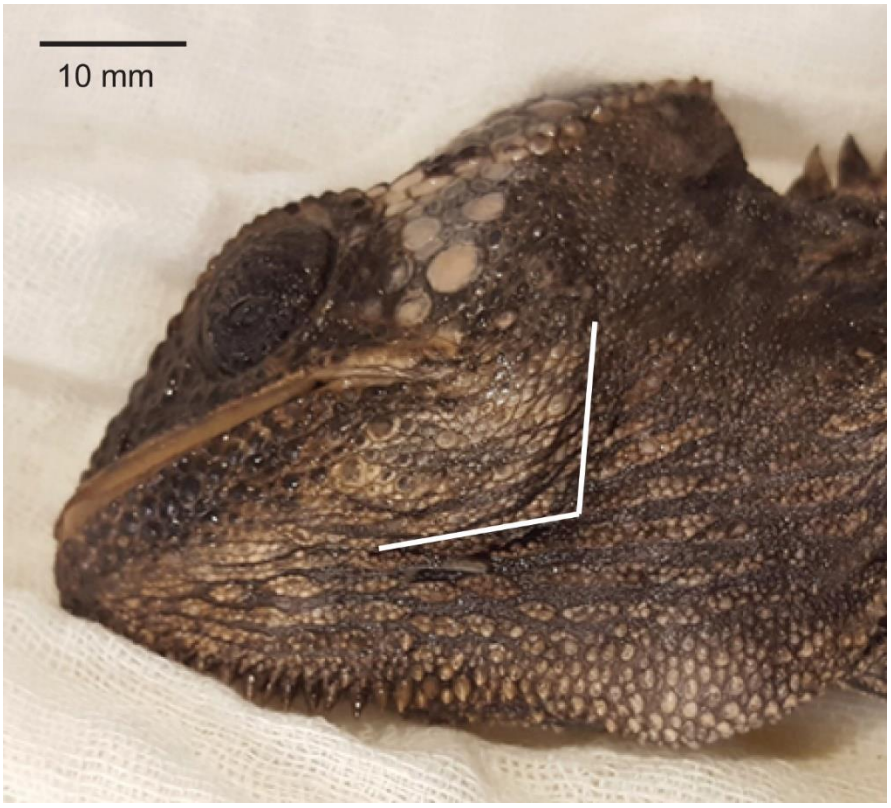

APPENDIX 3

Presence and absence of pterygoid ear among chameleons

Species	Pterygoid ear	Evidence	Source
Bradypodion pumilum	No	Histological sectioning	Toerien, 1963
Bradypodion ventrale	No	Histological sectioning	Brock, 1940
Brookesia superciliaris	No	Examination of skeleton	Siebenrock, 1893
Calumma brevicornis	No	Dissection	This paper
Chamaeleo calyptratus	Yes	Dissection	This paper
Chamaeleo chamaeleon	Yes	Dissection	This paper
Chamaeleo dilepis	Yes	Dissection	Wever, 1968
Chamaeleo gracilis	Yes	Dissection	This paper
Chamaeleo senegalensis	Yes	Dissection	Wever, 1968
Chamaeleo zeylanicus	Yes	Dissection	This paper
Furcifer lateralis	No	Dissection	This paper
Furcifer oustaleti	No	Dissection	This paper
Furcifer pardalis	Yes	Dissection	This paper
Furcifer verrucosus	No	Dissection	This paper
Kinyongia tavetana	No	Dissection	Wever, 1978
Kinyongia multituberculata	No	Dissection	This paper
Rhampholeon marshallii	No	Histological sectioning	Toerien, 1963
Rhampholeon platyceps	No	Histological sectioning	Toerien, 1963
Trioceros cristatus	Yes	Dissection	This paper
Trioceros ellioti	No	Dissection	This paper
Trioceros hoehnelii	No	Dissection	Wever, 1969
Trioceros jacksonii	No	Dissection	This paper
Trioceros johnstoni	No	Dissection	This paper
Trioceros melleri	Yes	Dissection	This paper
Trioceros montium	No	Dissection	This paper

APPENDIX 4: Distribution of the pterygoid ear among chameleons

Table with details of all dissected and CT scanned chameleon specimens

Method	Species	Specimen number	Sex	Means of acquisition
Dissection	*Chamaeleo calyptratus*	VTPE.LA.0560	Male	Pet trade
Dissection	*Ch. chamaeleon*	UF 87596	Unknown	Wild caught
Dissection	*Ch. gracilis*	YPM HERR 008366	Unknown	Wild caught
Dissection	*Ch. gracilis* or *Ch. senegalensis*	VTPE.LA.0551	Female	Pet trade
Dissection	*Ch. zeylanicus*	FMNH 283990	Unknown	Wild caught
Dissection	*Calumma brevicorne*	UWBM 10411	Male	Unknown
Dissection	*Furcifer lateralis*	VTPE.LA.0511	Unknown	Pet trade
Dissection	*F. oustaleti*	VTPE.LA.0564	Unknown	Pet trade
Dissection	*F. pardalis*	UWBM 10412	Female	Unknown
Dissection	*F. pardalis*	UWBM 10413	Female	Unknown
Dissection	*F. verrucosus*	FMNH 76088	Unknown	Wild caught
Dissection	*Kinyongia multituberculata*	VTPE.LA.0508	Female	Pet trade
Dissection	*Trioceros cristatus*	CM 130348	Female	Wild caught
Dissection	*T. ellioti*	UF 50439	Unknown	Wild caught
Dissection	*T. jacksonii*	VTPE.LA.0552	Female	Pet trade
Dissection	*T. johnstoni*	UF 72850	Female	Wild caught
Dissection	*T. melleri*	UWBM 10414	Female	Unknown
Dissection	*T. montium*	YPM HERR 008818	Male	Wild caught
DiceCT	*Ch. chamaeleon*	UCMVZ 2364801	Unknown	Wild caught
DiceCT	*Ch. senegalensis*	UWBM 5966	Female	Wild caught
DiceCT	*T. jacksonii*	UWBM 8333	Female	Zoo

Note: The VT specimens were subsequently skeletonized for osteological study by the institution.

APPENDIX 5

Specifications of measurements taken for allometry analysis

Chameleons—Measurements were taken on the most complete side of each specimen, as the pterygoid plate was often broken or chipped at the edges. When necessary, the extent of these broken edges was approximated based on the extent and angle of surrounding unbroken edges. Basal skull length (BSL) was measured in ventral view along the midline of the skull from the anteriormost tip of the premaxilla to the posteriormost end of the occipital condyle. In many specimens, the lower jaw was immovably attached to the cranium, so the anterior endpoint for BSL measurement was instead the anteriormost tip of the dentary. This was only done if the tip of the dentary was lined up with the premaxilla underneath, and measurements were not conducted on specimens in which the dentary was shifted too far to allow accurate approximation of this measurement. The height of the coronoid process was measured as the height from the posteriormost part of its base to its apex. The pterygoid plate was photographed in ventral view for almost all specimens, as this provided the clearest view of its total area. However, this view was obstructed by dried soft tissue in a few specimens, so the lateral view of the pterygoid plate was also photographed and measured in a subset of the sample, and a linear regression between the lateral and ventral measurements was used to estimate the ventral measurement for the obstructed specimens.

In some specimens, the skull and jaw were completely disarticulated. For these specimens, the isolated coronoid and pterygoid bones were photographed in a position similar to that seen in the intact specimens to minimize warping of the measurements based on different perspectives of the photos. The postorbital and jugal bones were carefully rearticulated and photographed, allowing the exact same orbit diameter measurement to be taken on these specimens as in the intact specimens. BSL was impossible to measure in these specimens, so instead the mandible was rearticulated and photographed. Jaw length was measured for a

subset of the intact specimens, and a linear regression between jaw length and BSL was used to estimate BSL in the disarticulated specimens.

Synapsids—Specimens were photographed in lateral view at an angle at which the angular keel and reflected lamina (AKRL) were oriented horizontally. The extent of the reflected lamina was estimated using anatomical landmarks that coincide with the extent of the angular cleft (Olroyd and Sidor, in prep). In cases where the different parts of the AKRL were preserved on opposite mandibles or multiple conspecific specimens, scaled surface scans were used to generate a composite mesh of the AKRL. A screenshot of this mesh in lateral view was overlayed onto the specimen photograph to serve as a guide while measuring AKRL area. Coronoid eminence/process height was measured as the dorsoventral height from the highest point on the coronoid eminence/process to the level of the lowest point on the dentary anterior to the coronoid eminence/process.

For specimens on which the use of calipers was prohibited, the mandible was photographed in lateral view, and the length was measured in ImageJ. Some specimens were surface scanned and not photographed, so the mandible length was measured using the 'Units' function in Meshmixer V3.5.474 (©Autodesk, San Rafael, CA, U.S.A). All measurements were taken on every specimen possible, and regressions between measurements taken with calipers, photographs, and 3D meshes were used to standardize measurements between methods.

APPENDIX 6

Chameleon skull and jaw measurements

Pterygoid ear	Species	Specimen #	log basal skull length (mm)	log pterygoid plate area (mm^2)	log orbit diameter (mm)	log coronoid process height (mm)
Absent	*Furcifer oustaleti*	VTPE.LA.0252	1.59719	1.800318	1.112471	-0.01412
Absent	*Furcifer oustaleti*	VTPE.LA.0251	1.529289	1.60168	1.117868	0.183839
Absent	*Furcifer oustaleti*	VTPE.LA.0250	1.359551	1.231724	0.95928	0.10551
Absent	*Furcifer oustaleti*	VTPE.LA.0245	1.705958	2.203645	1.223963	0.401573
Absent	*Furcifer oustaleti*	UF166109	1.702474	2.166001	1.172399	0.311118
Absent	*Furcifer oustaleti*	YPM HERR14377	1.695473	2.183164	1.21982	0.587149
Absent	*Furcifer oustaleti*	YPM HERR19181	1.71792	2.14897	1.180814	0.26529
Absent	*Furcifer verrucosus*	AMNH R-71189	1.641682	1.961355	1.204337	0.37328
Absent	*Furcifer verrucosus*	AMNH R-71190	1.607487	1.792041	1.19187	0.221936
Absent	*Furcifer verrucosus*	AMNH R-71820	1.582393	1.803846	1.152808	0.273696
Absent	*Furcifer verrucosus*	AMNH R-71821	1.53676	1.691877	1.128948	0.15412
Absent	*Furcifer verrucosus*	AMNH R-71822	1.599829	1.746089	1.174815	0.306425
Absent	*Furcifer verrucosus*	AMNH R-71823	1.59395	1.707672	1.1557	0.301898
Absent	*Furcifer verrucosus*	AMNH R-71824	1.578685	1.756697	1.137101	0.204663
Absent	*Furcifer verrucosus*	AMNH R-71825	1.638359	2.014071	1.20793	0.235276
Absent	*Furcifer verrucosus*	AMNH R-71826	1.594536	1.737185	1.166104	0.22763
Absent	*Furcifer verrucosus*	AMNH R-71827	1.605219	1.772937	1.180069	0.343409
Absent	*Furcifer verrucosus*	AMNH R-71828	1.556652	1.756096	1.139911	0.236537
Absent	*Furcifer verrucosus*	CM119085	1.533518	1.620303	1.000998	0.381296
Absent	*Furcifer verrucosus*	YPM HERR11101	1.671256	2.098827	1.17234	0.384712
Absent	*Kinyongia multituberculata*	VTPE.LA.0230	1.435494	1.492243	1.090857	0.168497
Absent	*Kinyongia multituberculata*	VTPE.LA.0253	1.397923	1.498917	1.044932	0.184407
Absent	*Kinyongia multituberculata*	MCZ R24316	1.366684	1.273441	0.985112	-0.01592
Absent	*Kinyongia multituberculata*	MCZ R24324	1.354397	1.189041	0.94601	0.030195
Absent	*Kinyongia multituberculata*	MCZ R24333	1.412108	1.261976	0.983446	-0.06349
Absent	*Kinyongia multituberculata*	MCZ R131522	1.324982	1.13149	0.912435	0.073718
Absent	*Kinyongia multituberculata*	MCZ R131524	1.368807	1.253992	0.949585	0.084576
Absent	*Kinyongia multituberculata*	MCZ R147428	1.346529	1.241297	0.916296	-0.00789
Absent	*Kinyongia multituberculata*	MCZ R147429	1.312368	1.140099	0.912806	

Absent	*Trioceros ellioti*	MCZ R41718	1.211067	0.920228	0.777282	0.080626
Absent	*Trioceros ellioti*	MCZ R47216	1.261334	0.965249	0.797821	0.067443
Absent	*Trioceros ellioti*	UF51247	1.153562	0.949097	0.767601	-0.07263
Absent	*Trioceros ellioti*	UF51248	1.215627	0.939869	0.813448	-0.06753
Absent	*Trioceros ellioti*	UF51378	1.266185	1.009323		0.025715
Absent	*Trioceros ellioti*	UF51380	1.235463	0.975248	0.769746	-0.1107
Absent	*Trioceros ellioti*	UF51381	1.234823	0.989049		-0.06198
Absent	*Trioceros ellioti*	UF51382	1.211742	0.887111	0.789722	-0.07366
Absent	*Trioceros ellioti*	UF51384	1.247409	0.909556	0.771734	-0.09745
Absent	*Trioceros ellioti*	UF51385	1.272582	0.987219	0.8355	0.017033
Absent	*Trioceros ellioti*	UF51386	1.249538	0.962369	0.800236	-0.04721
Absent	*Trioceros ellioti*	UF51387	1.200298	0.922985	0.74186	-0.16115
Absent	*Trioceros ellioti*	UF51389	1.208119	0.944729	0.800923	-0.02136
Absent	*Trioceros ellioti*	UF51390	1.194475	0.956984	0.729003	-0.06956
Absent	*Trioceros ellioti*	UF53367	1.247003	1.031812	0.776483	-0.00524
Absent	*Trioceros ellioti*	UF53368	1.255627	1.041787	0.787035	0.037825
Absent	*Trioceros ellioti*	UF53369	1.204315	0.872797	0.749968	-0.06098
Absent	*Trioceros ellioti*	UF53370	1.091308	0.679791	0.655619	-0.24413
Absent	*Trioceros ellioti*	UF53371	1.189254	0.928549	0.791901	-0.03386
Absent	*Trioceros ellioti*	UF53372	1.229759	0.976075	0.853029	0.003029
Absent	*Trioceros ellioti*	UF51249	1.248731	1.026043	0.836071	-0.04383
Absent	*Trioceros hoehnelii*	CM144863	1.352235	1.382557	0.903307	0.040602
Absent	*Trioceros hoehnelii*	CM144864	1.401399	1.460552	0.918869	0.172311
Absent	*Trioceros hoehnelii*	CM144866	1.27677	1.172282	0.873844	-0.11351
Absent	*Trioceros hoehnelii*	CM144867	1.283735	1.07813	0.872681	
Absent	*Trioceros hoehnelii*	MCZ R29471	1.22417	0.910998	0.81697	-0.11919
Absent	*Trioceros hoehnelii*	MCZ R41754	1.332438	1.365338	0.883377	0.189771
Absent	*Trioceros hoehnelii*	MCZ R131525	1.223833	0.933892	0.790426	-0.03386
Absent	*Trioceros hoehnelii*	MCZ R131526	1.236008	0.892262	0.79872	-0.01592
Absent	*Trioceros hoehnelii*	MCZ R131527	1.203386	0.907411	0.783689	-0.0575
Absent	*Trioceros hoehnelii*	MCZ R131529	1.341889	1.15791	0.929368	0.048442
Absent	*Trioceros hoehnelii*	MCZ R131530	1.056638	0.53084	0.669038	-0.12148
Absent	*Trioceros hoehnelii*	MCZ R131531	1.301984	1.2398	0.898122	0.176959
Absent	*Trioceros hoehnelii*	MCZ R131532	1.237242	1.072397	0.857332	0.044148
Absent	*Trioceros hoehnelii*	UF55065	1.260269	1.013217	0.834039	-0.11919
Absent	*Trioceros hoehnelii*	UF55898	1.245323	1.049761	0.855337	0.189771
Absent	*Trioceros hoehnelii*	UF55899	1.207704	0.891649	0.814447	-0.00568
Absent	*Trioceros hoehnelii*	UF62564	1.272225	1.11401	0.861654	-0.03386
Absent	*Trioceros hoehnelii*	UF63843	1.263016	1.12785	0.840294	0.122544
Absent	*Trioceros hoehnelii*	UF63945	1.270793	1.250956	0.87668	0.017868
Absent	*Trioceros hoehnelii*	YPM HERR11340	0.905526	0.294687	0.552181	-0.23882

Absent	*Trioceros hoehnelii*	YPM HERR11341	0.918764	0.319106	0.539076	-0.32514
Absent	*Trioceros hoehnelii*	YPM HERR11342	0.869349	-0.05601	0.472025	
Absent	*Trioceros hoehnelii*	YPM HERR17900	1.369123	1.532754	0.904986	0.164947
Absent	*Trioceros hoehnelii*	YPM HERR18561	1.218536	0.982814	0.786041	-0.1152
Absent	*Trioceros jacksonii*	VTPE.LA.	1.647862	1.528621	1.061679	0.324077
Absent	*Trioceros jacksonii*	VT14	1.530891	1.284904	0.95347	0.138618
Absent	*Trioceros jacksonii*	VT15	1.516099	1.292012	1.009876	0.144263
Absent	*Trioceros jacksonii*	VT16	1.516297	0.968996	0.961516	0.149527
Absent	*Trioceros jacksonii*	VT17	1.386945	0.953131	0.874714	0.03623
Absent	*Trioceros jacksonii*	VT18	1.629165	1.444544	1.003029	0.151982
Absent	*Trioceros jacksonii*	VT19	1.315151	0.79796	0.789369	0.022016
Absent	*Trioceros jacksonii*	VT20	1.626125	1.470822	1.021437	0.307924
Absent	*Trioceros jacksonii*	VT21	1.658974	1.492425	1.064757	0.257679
Absent	*Trioceros jacksonii*	LACM 163866	1.366031	1.330515	1.017659	0.183555
Absent	*Trioceros jacksonii*	LACM 164164	1.346764	1.291968	1.012795	0.18949
Absent	*Trioceros jacksonii*	LACM 164165	1.332135	1.184123	0.963504	0.2398
Absent	*Trioceros jacksonii*	LACM 164608	1.515622	1.59719	1.086893	0.322633
Absent	*Trioceros jacksonii*	LACM 164658	1.484883	1.57725	1.067926	0.264346
Absent	*Trioceros jacksonii*	LACM 164683	1.518303	1.620219	1.10968	0.402089
Absent	*Trioceros jacksonii*	LACM 164687	1.4275	1.50496	1.059601	0.170262
Absent	*Trioceros jacksonii*	LACM 168686	1.410946	1.555034	1.037187	0.233757
Absent	*Trioceros jacksonii*	VTPE.LA.0198	1.350616	1.353993	0.979457	0.231979
Absent	*Trioceros jacksonii*	VTPE.LA.0199	1.248782	1.039652	0.873611	0.135451
Absent	*Trioceros jacksonii*	VTPE.LA.0200	1.332176	1.283866	0.951192	0.239299
Absent	*Trioceros jacksonii*	VTPE.LA.0201	1.396809	1.387336	0.963835	0.160469
Absent	*Trioceros jacksonii*	VTPE.LA.0202	1.359551	1.282894	0.966939	0.211654
Absent	*Trioceros jacksonii*	VTPE.LA.0203	1.43252	1.490534	1.041787	0.245019
Absent	*Trioceros jacksonii*	VTPE.LA.0206	1.447577	1.539628	1.064121	0.391288
Absent	*Trioceros jacksonii*	VTPE.LA.0205	1.37696	1.33696	0.970904	0.172019
Absent	*Trioceros jacksonii*	VTPE.LA.0204	1.439048	1.497289	1.074926	0.367356

Absent	*Trioceros jacksonii*	VTPE.LA.0189	1.37236	1.323932	0.980231	0.173186
Absent	*Trioceros jacksonii*	VTPE.LA.0190	1.237368	1.053078	0.879898	0.106871
Absent	*Trioceros jacksonii*	VTPE.LA.0211	1.357306	1.28845	0.997605	0.172019
Absent	*Trioceros jacksonii*	VTPE.LA.0197	1.358259	1.244302	0.930949	0.195623
Absent	*Trioceros jacksonii*	VTPE.LA.0191	1.284634	1.125384	0.896526	0.160168
Absent	*Trioceros jacksonii*	VTPE.LA.0192	1.300008	1.167642	0.922206	0.255996
Absent	*Trioceros jacksonii*	VTPE.LA.0193	1.288607	1.162833	0.927473	0.161967
Absent	*Trioceros jacksonii*	VTPE.LA.0194	1.320126	1.105374	0.949926	0.168497
Absent	*Trioceros jacksonii*	VTPE.LA.0196	1.272167	1.014268	0.879726	0.172019
Absent	*Trioceros jacksonii*	VTPE.LA.0195	1.219925	1.016657	0.871398	0.125806
Absent	*Trioceros jacksonii*	VTPE.LA.0210	1.414656	1.464594	1.002252	0.309843
Absent	*Trioceros jacksonii*	VTPE.LA.0187	1.313804	1.167849	0.891314	0.042182
Absent	*Trioceros jacksonii*	VTPE.LA.0179	1.294312	1.04501	0.904174	0.178689
Absent	*Trioceros jacksonii*	VTPE.LA.0180	1.273696	1.052694	0.855943	0.250664
Absent	*Trioceros jacksonii*	VTPE.LA.0181	1.197005	0.972851	0.856003	0.087781
Absent	*Trioceros jacksonii*	VTPE.LA.0182	1.179995	1.181415	0.976992	0.169086
Absent	*Trioceros jacksonii*	VTPE.LA.0183	1.406097	1.347154	0.916138	0.075912
Absent	*Trioceros jacksonii*	VTPE.LA.0184	1.292389	1.229118	0.913019	0.218273
Absent	*Trioceros jacksonii*	VTPE.LA.0186	1.287085	1.217642	0.93586	0.214844
Absent	*Trioceros jacksonii*	VTPE.LA.0185	1.314583	1.179667	0.966236	0.205746
Absent	*Trioceros jacksonii*	VTPE.LA.0188	1.3485	1.254621	0.97635	0.136086
Absent	*Trioceros jacksonii*	VTPE.LA.0177	1.311055	1.221284	0.905256	0.119256
Absent	*Trioceros jacksonii*	VTPE.LA.0178	1.211769	1.215796	0.925054	0.117271
Absent	*Trioceros jacksonii*	AMNH R-77033	1.406268	1.2876	1.030276	0.286456
Absent	*Trioceros jacksonii*	AMNH R-82120	1.31553	1.188591	0.950657	0.133219
Absent	*Trioceros jacksonii*	AMNH R-82121	1.331549	1.225774	0.941263	0.14145
Absent	*Trioceros jacksonii*	AMNH R-99984	1.499247	1.526598	1.081275	0.323458
Absent	*Trioceros jacksonii*	AMNH R-141099	1.494043	1.647833	1.142296	0.255514
Absent	*Trioceros jacksonii*	CM56087	1.437529	1.618174	1.04817	0.399328
Absent	*Trioceros jacksonii*	CM56088	1.525421	1.630814	1.038421	

Absent	*Trioceros jacksonii*	CM56090	1.467075	1.584591	0.957703	0.297542
Absent	*Trioceros jacksonii*	CM144855	1.348779	1.084076	0.852175	0.031408
Absent	*Trioceros jacksonii*	CM144878	1.274943	1.029262	0.948902	0.105169
Absent	*Trioceros jacksonii*	CM144880	1.35714	1.200166	0.937869	0.198657
Absent	*Trioceros jacksonii*	CM144882	1.378943	1.215188	0.935759	0.09482
Absent	*Trioceros jacksonii*	CM144884	1.405634	1.20085	0.968436	0.159266
Absent	*Trioceros jacksonii*	UF37283	1.557786	1.624519	1.034789	0.190332
Absent	*Trioceros jacksonii*	UF40630	1.47921	1.194431	0.964542	0.148603
Absent	*Trioceros jacksonii*	UF40631	1.342052	1.269396	0.874888	0.21801
Absent	*Trioceros jacksonii*	UF42438	1.325945	1.470616	1.017868	0.362859
Absent	*Trioceros jacksonii*	UF52736	1.465699	1.71174	1.125351	0.466126
Absent	*Trioceros jacksonii*	UF99050	1.463101	1.607273	1.076786	0.298198
Absent	*Trioceros jacksonii*	UF99051	1.441334	1.521935	1.001777	0.246991
Absent	*Trioceros jacksonii*	UF99052	1.557276	1.527694	1.059109	0.297104
Absent	*Trioceros jacksonii*	UF99155	1.502564	1.617399	1.107142	0.341435
Absent	*Trioceros jacksonii*	UF99229	1.513896	1.67554	1.055569	0.28892
Absent	*Trioceros jacksonii*	UF99230	1.472573	1.672578	1.146903	0.480582
Absent	*Trioceros jacksonii*	UF99236	1.440074	1.535889	0.958659	0.245759
Absent	*Trioceros jacksonii*	UF173156	1.485182	1.590931	1.063821	0.312812
Absent	*Trioceros jacksonii*	UF175439	1.319606	1.206394	0.883093	0.165838
Absent	*Trioceros jacksonii*	YPM HERR10816	1.36012	1.132804	0.967127	0.193403
Absent	*Trioceros jacksonii*	YPM HERR11093	1.397975	1.453441	0.963504	0.309417
Absent	*Trioceros jacksonii*	YPM HERR11096	1.379686	1.424718	0.9703	0.140508
Absent	*Trioceros jacksonii*	YPM HERR11489	1.241845	1.057514	0.837146	0.083503
Absent	*Trioceros jacksonii*	YPM HERR11770	1.340682	1.293495	0.912381	0.202488
Absent	*Trioceros jacksonii*	YPM HERR12115	1.347564	1.199837	0.892818	0.177248
Absent	*Trioceros jacksonii*	YPM HERR15898	1.399388	1.339789	0.968856	0.1827
Absent	*Trioceros jacksonii*	YPM HERR15900	1.42835	1.342561	0.984032	0.261976
Absent	*Trioceros jacksonii*	YPM HERR15904	1.283846	1.013217	0.908378	-0.00043
Absent	*Trioceros jacksonii*	YPM HERR16239	1.251898	1.005909	0.793651	0.097604

Absent	*Trioceros jacksonii*	YPM HERR16087	1.349191	1.114578	0.888741	0.17406
Absent	*Trioceros jacksonii*	YPM HERR16384	1.43559	1.501128	1.078674	0.265525
Absent	*Trioceros jacksonii*	YPM HERR16385	1.500977	1.657859	1.087284	0.344785
Absent	*Trioceros jacksonii*	YPM HERR17256	1.440657	1.541854	1.032417	0.312177
Absent	*Trioceros jacksonii*	YPM HERR19711	1.45591	1.515397	1.024075	0.365488
Absent	*Trioceros johnstoni*	AMNH R-143171	1.418053	1.35822	1.03274	0.170262
Absent	*Trioceros johnstoni*	CM144886	1.415187	1.203169	1.017659	0.056905
Absent	*Trioceros johnstoni*	CM144887	1.395712	1.335959	1.017826	0.109579
Absent	*Trioceros johnstoni*	CM144888	1.367933	1.202488	0.959518	0.137987
Absent	*Trioceros johnstoni*	CM144889	1.448461	1.34885	1.028409	0.137987
Absent	*Trioceros johnstoni*	CM144890	1.419027	1.308628	1.007876	0.07225
Absent	*Trioceros johnstoni*	CM144891A	1.39648	1.277105	1.021272	0.111263
Absent	*Trioceros johnstoni*	CM144891B	1.438707	1.29822	1.065094	0.097951
Absent	*Trioceros johnstoni*	CM144892	1.452035	1.359835	1.03531	0.178401
Absent	*Trioceros johnstoni*	CM144893	1.478747	1.430236	1.092826	0.188647
Absent	*Trioceros johnstoni*	CM144894	1.405493	1.363386	1.075766	0.167317
Absent	*Trioceros johnstoni*	CM144895	1.371421	1.166371	0.989005	0.053078
Absent	*Trioceros johnstoni*	CM144896	1.405211	1.281215	1.028978	0.204663
Absent	*Trioceros johnstoni*	CM144898	1.339744	1.278273	1.017993	0.257679
Absent	*Trioceros johnstoni*	MCZ R47274	1.428151	1.284047	1.026778	0.135769
Absent	*Trioceros johnstoni*	MCZ R47276	1.430961	1.3126	1.03539	0.228657
Absent	*Trioceros johnstoni*	MCZ R85542A	1.410541	1.264511	0.992023	
Absent	*Trioceros johnstoni*	MCZ R85542B	1.353493	1.212134	0.963788	
Absent	*Trioceros johnstoni*	MCZ R85542C	1.427875	1.300769	1.027227	
Absent	*Trioceros johnstoni*	UF61018	1.413402	1.344333	1.012922	0.180126
Absent	*Trioceros johnstoni*	UF76247	1.34771	1.23203	0.919392	0.147058
Absent	*Trioceros johnstoni*	UF76248	1.375343	1.26649	0.988604	0.200577
Absent	*Trioceros johnstoni*	UF76250	1.369303	1.31597	0.969183	0.206286
Absent	*Trioceros johnstoni*	UF76251	1.371177	1.206691	0.971601	0.136721
Absent	*Trioceros johnstoni*	UF76252	1.415646	1.45986	1.030073	0.232488

Absent	*Trioceros johnstoni*	UF76253	1.416544	1.2647	1.053808	0.137037
Absent	*Trioceros johnstoni*	UF76257	1.39317	1.330008	0.9861	0.142076
Absent	*Trioceros johnstoni*	UF76258	1.389074	1.212374	0.952308	0.184975
Absent	*Trioceros johnstoni*	UF76259	1.378492	1.228734		0.161667
Absent	*Trioceros johnstoni*	UF76260	1.401095	1.226033	0.983085	0.167908
Absent	*Trioceros johnstoni*	UF76261	1.373771	1.200002	0.894316	
Absent	*Trioceros johnstoni*	UF83526	1.435897	1.346412	1.023417	0.178401
Absent	*Trioceros johnstoni*	UF83527	1.420898	1.346431	1.003547	0.157154
Absent	*Trioceros johnstoni*	UF83530	1.36551	1.1782	0.969136	0.214314
Absent	*Trioceros johnstoni*	YPM HERR16455	1.400412	1.275334	0.990339	0.130655
Absent	*Trioceros johnstoni*	YPM HERR16456	1.386001	1.250371	0.96426	0.16465
Absent	*Trioceros johnstoni*	YPM HERR16457	1.3849	1.241472	0.941909	0.167613
Absent	*Trioceros johnstoni*	CM144900	1.301551	1.152991	0.933538	-0.02136
Absent	*Trioceros johnstoni*	CM144901	1.393645	1.295479	0.960471	
Present	*Chamaeleo calyptratus*	VTPE.LA.0265	1.541953	1.899049	1.055493	0.412964
Present	*Chamaeleo calyptratus*	VTPE.LA.0232	1.149096	0.725912	0.724522	
Present	*Chamaeleo calyptratus*	VTPE.LA.0233	1.13389	0.723702	0.705265	-0.05899
Present	*Chamaeleo calyptratus*	VTPE.LA.0234	1.089517	0.616476	0.694166	
Present	*Chamaeleo calyptratus*	VTPE.LA.0235	1.078674	0.674402	0.696968	-0.06905
Present	*Chamaeleo calyptratus*	VTPE.LA.0236	1.057362	0.489677	0.670802	-0.06601
Present	*Chamaeleo calyptratus*	VTPE.LA.0237	1.04708	0.624385	0.681332	-0.03292
Present	*Chamaeleo calyptratus*	VTPE.LA.0238	0.99127	0.567379	0.659916	
Present	*Chamaeleo calyptratus*	VTPE.LA.0239	1.114277	0.737987	0.715418	
Present	*Chamaeleo calyptratus*	VTPE.LA.0240	1.033665	0.639586	0.647676	-0.0348
Present	*Chamaeleo calyptratus*	VTPE.LA.0241	1.042221	0.774298	0.68744	-0.03152
Present	*Chamaeleo calyptratus*	VTPE.LA.0242	1.13088	0.844726	0.727623	
Present	*Chamaeleo calyptratus*	YPM HERR11105	1.522575	1.810891		0.068557
Present	*Chamaeleo calyptratus*	YPM HERR13719	1.532002	1.774568		0.118265
Present	*Chamaeleo calyptratus*	YPM HERR14949	1.412461	1.538247		0.251395
Present	*Chamaeleo calyptratus*	YPM HERR16156	1.51145	1.733983		0.174351

Present	*Chamaeleo calyptratus*	YPM HERR16554	1.487859	1.765035		0.067071
Present	*Chamaeleo calyptratus*	YPM HERR11750	1.692953	2.115561		0.313656
Present	*Chamaeleo calyptratus*	YPM HERR11772	1.531594	1.75621		0.273233
Present	*Chamaeleo chamaeleon*	UCMVZ 111574	1.516205	1.763391	1.134751	0.352375
Present	*Chamaeleo chamaeleon*	UCMVZ 111575	1.491516	1.649588	1.100336	0.321805
Present	*Chamaeleo chamaeleon*	UCMVZ 111576	1.520444	1.706897	1.170203	0.160769
Present	*Chamaeleo chamaeleon*	UCMVZ 111577	1.465294	1.600439	1.081779	0.210051
Present	*Chamaeleo chamaeleon*	UCMVZ 111578	1.503641	1.729473	1.109916	0.154424
Present	*Chamaeleo chamaeleon*	UCMVZ 111579	1.458184	1.592643	1.097604	0.166134
Present	*Chamaeleo chamaeleon*	UCMVZ 111580	1.493123	1.650745	1.108362	0.241546
Present	*Chamaeleo chamaeleon*	UCMVZ 111581	1.513351	1.747862	1.144419	0.172019
Present	*Chamaeleo chamaeleon*	UCMVZ 111582	1.496957	1.749211	1.139816	0.204391
Present	*Chamaeleo chamaeleon*	UCMVZ 111583	1.506884	1.689575	1.144512	0.349083
Present	*Chamaeleo chamaeleon*	UCMVZ 111584	1.491698	1.650026	1.125384	0.18949
Present	*Chamaeleo chamaeleon*	UCMVZ 111585	1.419675	1.48619	1.05854	0.056524
Present	*Chamaeleo chamaeleon*	UCMVZ 111586	1.429946	1.554659	1.052001	0.135769
Present	*Chamaeleo chamaeleon*	UCMVZ 111587	1.50458	1.732756	1.160679	0.174641
Present	*Chamaeleo chamaeleon*	UCMVZ 111588	1.431251	1.585517	1.053232	0.214049
Present	*Chamaeleo chamaeleon*	UCMVZ 111589	1.433818	1.55914	1.071698	0.193959
Present	*Chamaeleo chamaeleon*	UCMVZ 111591	1.417605	1.580708	1.046105	0.010724
Present	*Chamaeleo chamaeleon*	UCMVZ 111592	1.395414	1.468007	1.002468	0.159567
Present	*Chamaeleo chamaeleon*	UCMVZ 111593	1.422179	1.553568	1.115377	0.175802
Present	*Chamaeleo chamaeleon*	UCMVZ 111590	1.406676	1.546507	1.067443	0.035029
Present	*Chamaeleo chamaeleon*	AMNH R-73155	1.324138	1.228503	0.948462	0.083144
Present	*Chamaeleo chamaeleon*	AMNH R-73356	1.370439	1.338735	1.024157	0.12969
Present	*Chamaeleo chamaeleon*	AMNH R-141131	1.323066	1.253677	0.949146	0.092018
Present	*Chamaeleo chamaeleon*	AMNH R-147646	1.444275	1.574934	1.12156	0.294025
Present	*Chamaeleo chamaeleon*	UF99033	1.328583	1.24398	0.896912	
Present	*Chamaeleo chamaeleon*	YPM HERR10535	1.484328	1.663682	1.070518	0.332034
Present	*Chamaeleo chamaeleon*	YPM HERR10725	1.469999	1.585449	1.06487	0.339849

Present	*Chamaeleo chamaeleon*	YPM HERR11438	1.379522	1.106633	0.958898	0.139879
Present	*Chamaeleo dilepis*	MVZ 24607	1.361369	1.23175	1.012795	0.026125
Present	*Chamaeleo dilepis*	LACM 163860	1.357096	1.245389		-0.02457
Present	*Chamaeleo dilepis*	LACM 163861	1.360631	1.292721		-0.21042
Present	*Chamaeleo dilepis*	LACM 163862	1.348597	1.183241		0.040602
Present	*Chamaeleo dilepis*	LACM 163863	1.343842	1.372765		-0.04528
Present	*Chamaeleo dilepis*	LACM 164655	1.480711	1.624756	1.161817	0.139564
Present	*Chamaeleo dilepis*	LACM 164656	1.409138	1.31169	1.054345	0.037825
Present	*Chamaeleo dilepis*	LACM 164670	1.430562	1.411199	0.994405	0.142389
Present	*Chamaeleo dilepis*	LACM 164696	1.397308	1.438701	1.065019	0.189209
Present	*Chamaeleo dilepis*	LACM 164698	1.479158	1.543348	1.137607	0.068928
Present	*Chamaeleo dilepis*	LACM 165170	1.534323	1.680553	1.198052	0.378216
Present	*Chamaeleo dilepis*	LACM 189274	1.352819	1.371437	1.023499	0.110926
Present	*Chamaeleo dilepis*	AMNH R-47506	1.444342	1.483002	1.077767	0.062958
Present	*Chamaeleo dilepis*	AMNH R-47720	1.538716	1.783561	1.132676	0.130012
Present	*Chamaeleo dilepis*	AMNH R-73806	1.387425	1.472786	1.022841	0.174351
Present	*Chamaeleo dilepis*	AMNH R-74793	1.33163	1.501908	1.049722	0.206286
Present	*Chamaeleo dilepis*	AMNH R-74794	1.366628	1.596729	1.077441	0.245019
Present	*Chamaeleo dilepis*	AMNH R-74795	1.452706	1.518935	1.042103	0.151676
Present	*Chamaeleo dilepis*	AMNH R-74796	1.455819	1.587711	1.044736	0.163161
Present	*Chamaeleo dilepis*	AMNH R-77034	1.363462	1.362577	1.021272	0.151063
Present	*Chamaeleo dilepis*	AMNH R-175558	1.333931	1.267148	1.009876	0.143951
Present	*Chamaeleo dilepis*	CM112032	1.458094	1.504607	1.092299	0.11694
Present	*Chamaeleo dilepis*	CM114873	1.316641	1.234568	0.975386	0.040602
Present	*Chamaeleo dilepis*	CM144868	1.394487	1.499783	0.994493	0.15412
Present	*Chamaeleo dilepis*	CM144869	1.290652	1.199261	0.949244	-0.07779
Present	*Chamaeleo dilepis*	CM144870	1.364249	1.440909	0.992465	0.075547
Present	*Chamaeleo dilepis*	CM144871	1.504507	1.66483	1.062281	0.256237
Present	*Chamaeleo dilepis*	CM144872	1.355471	1.248243	1.012289	-0.01457
Present	*Chamaeleo dilepis*	MCZ R131519	1.4276	1.53447	0.991182	0.155336
Present	*Chamaeleo dilepis*	MCZ R50615	1.501744	1.675723	1.033263	0.180126
Present	*Chamaeleo dilepis*	MCZ R50618	1.044775	0.711892	0.679428	
Present	*Chamaeleo dilepis*	UF55351	1.500262	1.656108	1.073315	0.163161
Present	*Chamaeleo dilepis*	UF55901	1.431052	1.441852	1.020941	0.05423
Present	*Chamaeleo dilepis*	UF61140	1.463415	1.471512	1.077767	0.074451
Present	*Chamaeleo dilepis*	UF76255	1.438093	1.433866	1.081563	-0.0381
Present	*Chamaeleo dilepis*	UF76256	1.44557	1.51359	1.042969	0.128399
Present	*Chamaeleo dilepis*	UF76262	1.360774	1.309524	0.941064	0.080626
Present	*Chamaeleo dilepis*	UF76263	1.391196	1.253629	0.954869	0.037825
Present	*Chamaeleo dilepis*	UF99082	1.337782	1.35702	0.838156	0.198382
Present	*Chamaeleo dilepis*	YPM HERR10185	1.422688	1.437624	0.967408	0.024896
Present	*Chamaeleo dilepis*	YPM HERR11280	1.43998	1.551609	1.029587	0.051538
Present	*Chamaeleo dilepis*	YPM HERR18219	1.473589	1.535712	1.047703	0.284205
Present	*Chamaeleo gracilis*	MCZ uncatalogued	1.420616	1.394382	0.990428	-0.04964
Present	*Chamaeleo gracilis*	MCZ R41654	1.471878	1.50158	1.039573	0.031408

Present	*Chamaeleo gracilis*	MCZ R41666	1.374363	1.35957	0.942455	0.13258
Present	*Chamaeleo gracilis*	MCZ R7841	1.039612	0.469969	0.620656	-0.38722
Present	*Chamaeleo gracilis*	YPM HERR11049	1.426267	1.511629	0.971647	0.286007
Present	*Chamaeleo gracilis*	YPM HERR11050	1.427178	1.529135	0.963599	0.131298
Present	*Chamaeleo gracilis*	YPM HERR11113	1.359437	1.354032	0.938119	0.183839
Present	*Chamaeleo gracilis*	YPM HERR11123	1.264086	1.05534	0.855519	0.020775
Present	*Chamaeleo gracilis*	YPM HERR11125	1.274112	1.139501	0.878464	0.261025
Present	*Chamaeleo gracilis*	AMNH R-11608	1.498173	1.551974		0.259355
Present	*Chamaeleo senegalensis*	MCZ R173122	1.386998	1.594702	0.97211	0.270446
Present	*Chamaeleo senegalensis*	MCZ R173123	1.444326	1.472844	1.002598	0.291369
Present	*Chamaeleo senegalensis*	MCZ R173124	1.499371	1.528261	1.050534	0.203033
Present	*Chamaeleo senegalensis*	MCZ R173160	1.43236	1.347232	0.97635	0.171726
Present	*Chamaeleo senegalensis*	MCZ R173376	1.252805	1.071808	0.842422	0.136403
Present	*Chamaeleo senegalensis*	MCZ uncatalogued	1.433434	1.466022	0.972018	0.229426
Present	*Chamaeleo senegalensis*	UF40629	1.387426	1.338078	1.046612	0.160469
Present	*Chamaeleo senegalensis*	UF41281	1.39651	1.389609	0.935406	0.108903
Present	*Chamaeleo senegalensis*	UF42414	1.375304	1.351816	0.924538	0.164947
Present	*Chamaeleo senegalensis*	UF42415	1.475023	1.582132	1.110691	0.259833
Present	*Chamaeleo senegalensis*	UF54139	1.234414	1.064383	0.846275	-0.01278
Present	*Chamaeleo senegalensis*	UF54140	1.29682	1.165274	0.87093	0.012415
Present	*Chamaeleo senegalensis*	UF54141	1.254293	1.096841	0.869818	0.019116
Present	*Chamaeleo senegalensis*	UF54142	1.2957	1.172603	0.881099	-0.03574
Present	*Chamaeleo senegalensis*	UF55710	1.389391	1.361652	0.956216	0.131619
Present	*Chamaeleo senegalensis*	UF55716	1.248625	1.038024	0.849481	-0.03058
Present	*Chamaeleo senegalensis*	UF55717	1.236843	1.028449	0.829239	0.026125
Present	*Chamaeleo senegalensis*	UF55832	1.427215	1.439096	0.997954	0.197281
Present	*Chamaeleo senegalensis*	UF55833	1.423417	1.418202	1.018243	0.006894
Present	*Chamaeleo senegalensis*	UF55834	1.405441	1.430752	0.993172	0.102777
Present	*Chamaeleo senegalensis*	UF55835	1.371306	1.400452	1.001258	-0.07007
Present	*Chamaeleo senegalensis*	UF55836	1.373964	1.412377	0.981637	0.111934

Present	*Chamaeleo senegalensis*	UF56418	1.430865	1.460146	1.006338	0.225309
Present	*Chamaeleo senegalensis*	UF56419	1.454479	1.570216	0.994669	0.203305
Present	*Chamaeleo senegalensis*	UF56420	1.37623	1.364345	0.99158	0.175802
Present	*Chamaeleo senegalensis*	UF56591	1.377448	1.302482	1.000347	0.101403
Present	*Chamaeleo senegalensis*	UF56592	1.426621	1.448691	0.956216	0.220631
Present	*Chamaeleo senegalensis*	UF56593	1.383625	1.288473	0.993392	-0.00218
Present	*Chamaeleo senegalensis*	UF56594	1.399152	1.390317	0.960899	0.065953
Present	*Chamaeleo senegalensis*	UF56595	1.229465	1.007321	0.788734	-0.07058
Present	*Chamaeleo senegalensis*	UF56596	1.24436	1.032619	0.815711	0.024075
Present	*Chamaeleo senegalensis*	UF56597	1.212174	0.916822	0.834802	-0.10624
Present	*Chamaeleo senegalensis*	UF56598	1.19842	0.930542	0.750817	-0.03763
Present	*Chamaeleo senegalensis*	UF56599	1.323041	1.224222	0.855761	0.117934
Present	*Chamaeleo senegalensis*	UF56600	1.218991	0.996993	0.860038	-0.03668
Present	*Chamaeleo senegalensis*	UF56601	1.183533	0.883037	0.787815	-0.17263
Present	*Chamaeleo senegalensis*	UF56602	1.209499	0.978637	0.820399	-0.04144
Present	*Chamaeleo senegalensis*	UF56603	1.191107	0.924486	0.789581	-0.05208
Present	*Chamaeleo senegalensis*	UF56604	1.210143	0.936212	0.827886	-0.07058
Present	*Chamaeleo senegalensis*	UF56605	1.242068	1.002771	0.811441	-0.01818
Present	*Chamaeleo senegalensis*	UF56606	1.206963	1.015653	0.76923	-0.07058
Present	*Chamaeleo senegalensis*	UF56607	1.242858	1.128722	0.883093	-0.06399
Present	*Chamaeleo senegalensis*	UF56608	1.218815	1.002771	0.809156	-0.14146
Present	*Chamaeleo senegalensis*	UF56609	1.216612	0.978454	0.849911	-0.0716
Present	*Chamaeleo senegalensis*	UF56610	1.233878	0.929981	0.823865	0.051924
Present	*Chamaeleo senegalensis*	UF56611	1.388316	1.358449	0.971044	0.130012
Present	*Chamaeleo senegalensis*	UF56898	1.422541	1.554368	0.879096	0.274158
Present	*Chamaeleo senegalensis*	UF56899	1.37867	1.419658	0.964731	
Present	*Chamaeleo senegalensis*	YPM HERR17922	1.246277	1.014058	0.982226	0.201124
Present	*Chamaeleo senegalensis*	AMNH R-101366	1.504131	1.709007	1.074816	0.345766
Present	*Furcifer pardalis*	VTPE.LA.0219	1.420286	1.375151	1.029424	0.131619
Present	*Furcifer pardalis*	VTPE.LA.0218	1.402244	1.387657	0.963504	0.24403
Present	*Furcifer pardalis*	VTPE.LA.0217	1.396461	1.480381	1.012837	0.137671
Present	*Furcifer pardalis*	VTPE.LA.0216	1.462068	1.449	1.051461	0.097604
Present	*Furcifer pardalis*	VTPE.LA.0226	1.466363	1.559308	1.119751	0.199481

Present	*Furcifer pardalis*	VTPE.LA.0225	1.503246	1.7703	1.139155	0.243038
Present	*Furcifer pardalis*	VTPE.LA.0224	1.55717	1.934604	1.162594	0.408918
Present	*Furcifer pardalis*	VTPE.LA.0222	1.491208	1.663022	1.097674	0.224533
Present	*Furcifer pardalis*	VTPE.LA.0221	1.423246	1.399726	1.008643	0.188366
Present	*Furcifer pardalis*	VTPE.LA.0223	1.48548	1.623415	1.159958	0.04454
Present	*Furcifer pardalis*	VTPE.LA.0227	1.521073	1.680172	1.157789	0.248464
Present	*Furcifer pardalis*	VTPE.LA.0229	1.51195	1.723833	1.156822	0.303844
Present	*Furcifer pardalis*	AMNH R-131207	1.515675	1.559943	1.115677	0.170555
Present	*Furcifer pardalis*	CM144906	1.677105	1.987657	1.166549	0.343409
Present	*Furcifer pardalis*	CM157098	1.593087	1.848872	1.123133	0.285107
Present	*Furcifer pardalis*	YPM HERR10391	1.500319	1.632366	1.046027	0.328991
Present	*Furcifer pardalis*	YPM HERR11041	1.549396	1.708769	1.070629	0.230193
Present	*Furcifer pardalis*	YPM HERR11110	1.562994	1.701749	1.042733	0.282396
Present	*Furcifer pardalis*	YPM HERR11216	1.635906	1.927124	1.145662	0.313234
Present	*Furcifer pardalis*	YPM HERR11955	1.561614	1.727558	1.062168	0.266702
Present	*Furcifer pardalis*	YPM HERR12800	1.603502	1.910272	1.139722	0.22763
Present	*Furcifer pardalis*	YPM HERR13662	1.472947	1.502345	0.998564	0.177825
Present	*Furcifer pardalis*	YPM HERR16520	1.561484	1.671932	1.099266	0.103119
Present	*Trioceros cristatus*	VTPE.LA.0266	1.454159	1.592621	1.024814	0.100715
Present	*Trioceros cristatus*	VTPE.LA.0260	1.17196	0.766115	0.787956	-0.12494
Present	*Trioceros cristatus*	VTPE.LA.0261	1.256573	0.996074	0.894039	
Present	*Trioceros cristatus*	VTPE.LA.0262	1.152991	0.812847	0.8238	-0.05948
Present	*Trioceros cristatus*	VTPE.LA.0263	1.261358	1.144636	0.903904	0.040602
Present	*Trioceros cristatus*	VTPE.LA.0264	1.137607	0.786396	0.758533	-0.15552
Present	*Trioceros cristatus*	VTPE.LA.0248	1.412729	1.42794	1.074414	0.093071
Present	*Trioceros cristatus*	AMNH R-1801	1.329987	1.211681	0.970254	0.087071
Present	*Trioceros cristatus*	AMNH R-133811	1.45714	1.484186	1.067963	0.329398
Present	*Trioceros cristatus*	MCZ R162358	1.414806	1.422097	1.000564	0.049606
Present	*Trioceros melleri*	VTPE.LA.0257	1.716621	2.161802	1.244994	0.43072
Present	*Trioceros melleri*	VTPE.LA.0256	1.720821	2.130147	1.300921	0.625724
Present	*Trioceros melleri*	VTPE.LA.0228	1.683713	2.056436	1.262593	0.49693
Present	*Trioceros melleri*	VTPE.LA.0212	1.599883	1.829677	1.162564	0.203577
Present	*Trioceros melleri*	AMNH R-56487	1.708081	2.138498	1.275473	0.455606
Present	*Trioceros melleri*	AMNH R-74439	1.64368	1.896388	1.186165	0.334253
Present	*Trioceros melleri*	AMNH R-75166	1.661112	1.963561	1.23259	0.418633
Present	*Trioceros melleri*	CM114903	1.765192	2.198734	1.258565	0.477844
Present	*Trioceros melleri*	CM144902	1.717948	2.111568	1.197336	0.42586
Present	*Trioceros melleri*	CM144904	1.731632	2.126661	1.185712	0.434729
Present	*Trioceros melleri*	CM144905	1.772542	2.254413	1.206934	0.439806

Present	*Trioceros melleri*	UF52735	1.735779	2.12836	1.216746	0.45393
Present	*Trioceros melleri*	YPM HERR11155	1.68719	2.12258	1.229759	0.453624
Present	*Trioceros melleri*	YPM HERR11855	1.637199	1.984545	1.11032	0.293363
Present	*Trioceros melleri*	YPM HERR16383	1.737503	2.150904	1.227115	0.402605
Present	*Trioceros montium*	MCZ R38198	1.395711	1.361671	0.999565	0.045714
Present	*Trioceros montium*	UF68308	1.355432	1.236613	0.92947	-0.00877
Present	*Trioceros montium*	UF68488	1.341177	1.200467	0.90184	0.112605
Present	*Trioceros montium*	UF68503	1.360177	1.276669	0.966283	0.023664
Present	*Trioceros montium*	UF75004	1.404868	1.449895	0.983265	0.122871
Present	*Trioceros montium*	UF75005	1.369179	1.330069	0.979184	0.10721
Present	*Trioceros montium*	UF75032	1.261049	0.982769	0.839227	-0.02228
Present	*Trioceros montium*	UF75033	1.313509	1.197969	0.811776	0.019116
Present	*Trioceros montium*	UF75034	1.348422	1.194681	0.920384	0.042576
Present	*Trioceros montium*	UF71565	1.309304	1.166904	0.89137	-0.11295
Present	*Trioceros montium*	UF71719	1.289456	1.113308	0.83866	-0.08938
Present	*Trioceros montium*	UF74664	1.294731	1.064271	0.87204	-0.09637
Present	*Trioceros montium*	UF74665	1.342245	1.186504	0.908485	-0.02687
Present	*Trioceros montium*	UF74666	1.318314	1.109714	0.819544	0.068928
Present	*Trioceros montium*	YPM HERR13208	1.416141	1.410794	0.988425	0.127429
Present	*Trioceros montium*	YPM HERR13209	1.252902	1.067666	0.817631	0.062958

APPENDIX 7

Measurements of therapsid jaws

Group	Identification	Specimen #	Stratigraphic position	Measurement method	log mandible length (mm)	log AKRL area (mm^2)	log orbit diameter (mm)	log coronoid eminence/ process height (mm)
"pelycosaurs"	*Dimetrodon grandis*	MCZ VPRA-2029	Clear Fork Group, Baylor County, Texas, USA	Photograph	2.5958	3.2193		
"pelycosaurs"	*Dimetrodon limbatus*	FMNH UC1001	Briar Creek Bonebed, Nocona Formation, Archer County, Texas, USA	3D scan	2.5693	3.4891		
"pelycosaurs"	*Palaeohatteria longicaudata*	SS 13315 13317	Limestone Member, upper Niederhäslich Formation, Döhlen Basin, Germany	Photograph	1.8319	1.6977		
"pelycosaurs"	*Pantelosaurus saxonicus*	RS 14752	upper Döhlen Formation, Döhlen Basin, Germany	Photograph	2.2024	2.2556		
"pelycosaurs"	*Secodontosaurus obtusidens*	AMNH FR4091	Petrolia Formation, Archer County, Texas, USA	Caliper, photograph	2.5221	3.0778		
"pelycosaurs"	*Sphenacodon ferox*	UCMP83459	Anderson Quarry, Cutler Formation, New Mexico, USA	Photograph	2.4361	3.3563		
Biarmosuchia	*Biarmosuchus tener*	PIN1758/8	Ocher Subassemblage, Cis-Urals region, Russia	Photograph	2.3061	2.8157		
Biarmosuchia	*Herpetoskylax hopsoni*	CGP/1/67	*Cistecephalus* Assemblage Zone, Karoo Basin, South Africa	Photograph	2.1454	2.8430		
Biarmosuchia	*Hipposaurus boonstrai*	SAM-PK-8950	*Diictodon/Styracocephalus* Subzone, Karoo Basin, South Africa	Caliper, photograph	2.1846	2.8617		
Biarmosuchia	*Lemurosaurus pricei*	NMQR 1702	*Cistecephalus* Assemblage Zone, Karoo Basin, South Africa	3D scan	2.0906	2.3812		
Biarmosuchia	*Leucocephalus wewersi*	SAM-PK-11112	*Tropidostoma-Gorgonops* Subzone, Karoo Basin, South Africa	Photograph	2.0415	2.5830		
Biarmosuchia	*Paraburnetia sneeubergensis*	SAM-PK-K10037	Lowermost *Cistecephalus* Assemblage Zone, upper Teekloof Formation, Karoo Basin, South Africa	Caliper, photograph	2.2262	2.8162		
Biarmosuchia	*Proburnetia viatkensis*	PIN2416/1	Severodvinskian horizon, Vyatka River Basin, Kotel-nich District, Russia	Photograph	2.1661	2.5744		
Bidentalia	*Aulacephalodon bainii*	FMNH UC 1522	lower Cistecephalus Assemblage Zone,	3D scan	2.5443	3.1003		1.2043

			Murraysburg, Karoo Basin, South Africa					
Bidentalia	*Daptocephalus sp.*	NHCC LB218	Upper Madumabisa Mudstone Formation, Luangwa Basin, Zambia	3D scan	2.3328	3.0531		1.1277
Bidentalia	*Dicynodon lacerticeps*	BP/1/2098	upper *Cistecephalus* Assemblage Zone, Karoo Basin, South Africa	Caliper, 3D scan	2.4900	3.3407	1.9085	
Bidentalia	*?Euptychognathus sp.*	NHCC LB200	Upper Madumabisa Mudstone Formation, Luangwa Basin, Zambia	3D scan	2.2607	2.9264		0.7227
Bidentalia	*Kannemeyeria vanhoepeni*	UCMP42916	*Cynognathus* Assemblage Zone, Beaufort Group, Karoo Basin, South Africa	Photograph, 3D scan	2.4976	3.1565		1.0616
Bidentalia	*Lystrosaurus murrayi*	UCMP31360	*Lystrosaurus declivis* Assemblage Zone, Karoo Basin, South Africa	Caliper, photograph	1.9576	2.5252	1.6272	
Bidentalia	*Oudenodon bainii*	FMNH UC 2503	uppermost Hoedemaker to Steenkampsvlakte Member, Teekloof Formation, Karoo Basin, South Africa	3D scan	2.3474	2.9808		0.6408
Bidentalia	*Placerias hesternus*	UCMP137369	Placerias Quarry, Chinle Formation, Arizona, USA	Photograph, 3D scan	2.6454	3.6476	2.0063	
Bidentalia	*Rhachiocephalus magnus*	TM 4456	*Tropidostoma-Gorgonops* Subzone, Karoo Basin, South Africa	Caliper, 3D scan	2.5024	3.8766		
Bidentalia	*Stahleckeria potens*	AMNH FR3857	Upper Rio do Rasto Formation, Paraná Basin, Brazil	Caliper, 3D scan	2.6821	3.8114		1.2276
Bidentalia	*Tropidostoma microtrema*	CGP CM RS20	*Tropidostoma-Gorgonops* Subzone, Karoo Basin, South Africa	Caliper, 3D scan	2.2650	2.8436		0.7471
Cynodontia	*Galesaurus planiceps*	BP/1/5064	*Lystrosaurus declivis* Assemblage Zone, Karoo Basin, South Africa	Caliper, photograph	1.9494	2.1426	1.2553	1.0090
Cynodontia	*Nanictosaurus rubidgei*	TM279	*Daptocephalus* Assemblage Zone, Karoo Basin, South Africa	Caliper, photograph	1.6559	1.3638	0.8457	0.9613
Cynodontia	*Probainognathus jenseni*	PVSJ410	Ischigualasto Formation, San Juan Province, Argentina	3D scan	1.6622	0.4678		1.0069
Cynodontia	*Procynosuchus delaharpeae*	BP/1/226	*Cistecephalus* Assemblage Zone, Karoo Basin, South Africa	Caliper, photograph	1.8808	1.8353	1.2041	1.1544
Cynodontia	*Thrinaxodon liorhinus*	SAM-PK-K11034	*Lystrosaurus declivis* Assemblage Zone, Karoo Basin, South Africa	Caliper, photograph	1.8906	1.7537	1.1738	1.2202

Cynodontia	*Trirachodon berryi*	BP/1/4658	*Trirachodon-Kannemeyeria* Subzone, Karoo Basin, South Africa	Caliper, photograph	1.9395	1.0827	1.1761	1.4644
Dinocephalia	*Estemmenosuchus uralensis*	PIN1758/4	Ocher Subassemblage, Cis-Urals region, Russia	Photograph	2.7393	3.8391		
Dinocephalia	*Jonkeria truculenta*	AMNH FR 5633	*Tapinocephalus* Assemblage Zone, Karoo Basin, South Africa	Caliper, 3D scan	2.7529	3.9199		
Dinocephalia	*Moschops capensis*	AMNH FR 5550	*Tapinocephalus* Assemblage Zone, Karoo Basin, South Africa	Caliper, 3D scan	2.4150	3.5302		
Dinocephalia	*Sinophoneus yumenensis*	IVPP V 18120	Dashankou locality, Qingtoushan Formation	Caliper, 3D scan	2.0419	2.4781		
Dinocephalia	*Syodon biarmicum*	PIN157/2	Isheevo Subassemblage, Cis-Urals region, Russia	Photograph	2.3754	2.8122		
Dinocephalia	*Tapinocaninus pamelae*	NMQR 2986	*Eodicynodon* Assemblage Zone, Karoo Basin, South Africa	Caliper, photograph	2.6609	3.5811		
Dinocephalia	*Ulemosaurus svijagensis*	PIN2207/2	Isheevo Subassemblage, Cis-Urals region, Russia	Photograph	2.5398	3.4951		
Gorgonopsia	*Aelurognathus tigriceps*	NHCC LB350	Upper Madumabisa Mudstone Formation, Luangwa Basin, Zambia	Caliper, 3D scan	2.3927	3.2831		
Gorgonopsia	*Aloposaurus gracilis*	AMNH FR5317	*Cistecephalus* Assemblage Zone, Karoo Basin, South Africa	Caliper, 3D scan	2.0047	2.3578		
Gorgonopsia	*Arctops willistoni*	NHCC LB396	Upper Madumabisa Mudstone Formation, Luangwa Basin, Zambia	Caliper, 3D scan	2.3955	3.1220		
Gorgonopsia	*Cynariops robustus*	MB.R.999	*Tropidostoma/Gorgonops* Subzone, Biesiespoort locality, North Cape Province, Karoo Basin, South Africa	3D scan	2.0790	2.5240		
Gorgonopsia	*Cyonosaurus longiceps*	BP/1/2109	upper *Cistecephalus* Assemblage Zone, Karoo Basin, South Africa	Caliper, photograph	2.2253	3.1981		
Gorgonopsia	*Leontosaurus vanderhorsti*	BP/1/743	middle-upper *Cistecephalus* Assemblage Zone, Karoo Basin, South Africa	Caliper, photograph	2.4997	2.9028		
Gorgonopsia	*Lycaenops n. sp.*	NHCC LB178	Upper Madumabisa Mudstone Formation, Luangwa Basin, Zambia	Caliper, 3D scan	2.2861	2.6862		
Gorgonopsia	*Lycaenops ornatus*	BP/1/881	middle-upper *Cistecephalus* Assemblage Zone,	Caliper, photograph	2.3054	2.8520		

			Karoo Basin, South Africa					
Gorgonopsia	*Smilesaurus ferox*	BP/1/2465	lower-middle *Cistecephalus* Assemblage Zone, Karoo Basin, South Africa	Caliper, photograph	2.4594	3.3466		
non-bidentalians	*Cistecephaloides boonstrai*	SAM-PK-6243	*Cistecephalus* Assemblage Zone, Karoo Basin, South Africa	Caliper, photograph	1.6629	2.0119	0.8842	0.3507
non-bidentalians	*Cistecephalus microrhinus*	BP/1/253	lower-middle *Cistecephalus* Assemblage Zone, Karoo Basin, South Africa	Caliper, photograph	1.5798	2.0316	1.1139	
non-bidentalians	*Diictodon feliceps*	UCMP 41757	*Endothiodon* Assemblage Zone, Beaufort Formation, Karoo Basin, South Africa	Caliper, photograph	2.0023	2.6810	1.3775	0.7440
non-bidentalians	*Emydops arctatus*	BP/1/1307	*Endothiodon* Assemblage Zone, Karoo Basin, South Africa	Caliper, photograph	1.6990	2.1217	1.2041	0.4215
non-bidentalians	*Endothiodon bathystoma*	SAM-PK-K11131	*Endothiodon* Assemblage Zone, Karoo Basin, South Africa	Caliper, photograph	2.5250	3.3152	1.7559	0.9223
non-bidentalians	*"Eodicynodon" oosthuizeni*	BP/1/6230	*Eodicynodon* Assemblage Zone, Karoo Basin, South Africa	Caliper, 3D scan	1.7324	2.0622		0.4187
non-bidentalians	*Eosimops newtoni*	BP/1/6674	*Tapinocephalus* Assemblage Zone, Karoo Basin, South Africa	3D scan	1.8963	2.4240		0.8098
non-bidentalians	*Kembawacela kitchingi*	NHCC LB18	Upper Madumabisa Mudstone Formation, Luangwa Basin, Zambia	3D scan	1.5600	1.9444		0.2722
non-bidentalians	*Pristerodon mackayi*	BP/1/6685	*Cistecephalus* Assemblage Zone, Karoo Basin, South Africa	Caliper, photograph	1.7634	2.1811	1.2304	0.6899
non-bidentalians	*Robertia broomiana*	BP/1/7934	*Tapinocephalus* Assemblage Zone, Karoo Basin, South Africa	Caliper, photograph	1.8129	2.2454	1.3424	
non-bidentalians	*Ulemica invisa*	PIN 157/1112	Isheevo Subassemblage, Cis-Urals region, Russia	Photograph	2.2257	2.7859		
Therocephalia	*cf. Ictidostoma* sp.	BP/1/3155	*Endothiodon* Assemblage Zone, Karoo Basin, South Africa	Caliper, photograph	1.9590	2.4747	1.2553	1.1548
Therocephalia	*Choerosaurus dejageri*	SAM-PK-8797	*Cistecephalus* Assemblage Zone, Karoo Basin, South Africa	Caliper, photograph	1.9252	2.1732	1.2122	0.9229
Therocephalia	*Glanosuchus macrops*	AMNH FR5559	*Tapinocephalus* Assemblage Zone,	Caliper, 3D scan	2.4241	2.9683	1.5362	

			Karoo Basin, South Africa					
Therocephalia	*Hofmeyria atavus*	TM254	*Endothiodon* Assemblage Zone, Karoo Basin, South Africa	Caliper, photograph	1.8264	2.3533	1.1252	1.2867
Therocephalia	*Ictidosuchoides longiceps*	NMQR 385	"Katberg Formation", Karoo Basin, South Africa	Caliper, photograph	1.9802	2.3631	1.1688	1.0208
Therocephalia	*Mirotenthes digitipas*	UCMP 40467	*Cistecephalus* Assemblage Zone, Karoo Basin, South Africa	Caliper, photograph	2.0229	2.5786		1.2613
Therocephalia	*Moschorhinus kitchingi*	NMQR 3835	Palingkloof Member, Balfour Formation, Karoo Basin, South Africa	Caliper, photograph	2.3766	3.2616	1.5766	1.3455
Therocephalia	*Olivierosuchus parringtoni*	NMQR 3605	lowermost *Lystrosaurus declivis* Assemblage Zone, Balfour Formation, Karoo Basin, South Africa	Caliper, photograph	2.0649	2.6134	1.3111	1.1878
Therocephalia	*Pristerognathus polyodon*	SAM-PK-11942	*Diictodon/Styracocephalus* Subzone, Karoo Basin, South Africa	Caliper, photograph	2.4432	3.0722	1.7460	1.6012
Therocephalia	*Scaloposaurus constrictus*	SAM-PK-K11543	*Lystrosaurus declivis* Assemblage Zone, Karoo Basin, South Africa	Caliper, 3D scan	1.6784	1.6917	1.1268	
Therocephalia	*Tetracynodon darti*	BP/1/2710	*Lystrosaurus declivis* Assemblage Zone, Karoo Basin, South Africa	Caliper, photograph	1.8388	1.8035	1.1761	0.8721
Therocephalia	*Theriognathus microps*	BP/1/844	*Dicynodon/Theriognathus* subzone	Caliper, photograph	2.1430	2.6516	1.3802	1.4816
Therocephalia	*Zorillodontops gracilis*	SAM-PK-1392	*Lystrosaurus declivis* Assemblage Zone, Edonville, Karoo Basin, South Africa	Caliper, photograph	1.5767	1.5080	1.0481	0.8261